Motion Planning for the Two-Phase Stefan Problem in Level Set Formulation

$$\rho L \vec{V} \cdot n = [k \nabla y]_F^S \cdot n \text{ on } \Gamma_I(t)$$

$$\underline{u} \le u \le \overline{u} \text{ on } \Gamma_C$$

$$\phi_t + \vec{V} \cdot \nabla \phi = 0$$
$$\phi(0) = \phi_0$$

$$\min_{y,\phi,u} J(y,\phi,u)$$

$$y = y_M \text{ on } \Gamma_I(t)$$

$$D\left[\!\left[\int_{\Gamma_I(t)} g \, ds, \delta\phi \right]\!\right] = -\int_{\Gamma_I(t)} \frac{\delta_\phi}{|\nabla\phi|}\left(\frac{\partial g}{\partial n} + \kappa \, g\right) ds$$

$$\frac{\gamma}{2} \int_0^T \int_{\Gamma_I(t)} \max\{0, \phi_d - 0.02\}^2 \, ds \, dt$$

Dissertation submitted to the

Faculty of Mathematics

at

Chemnitz University of Technology

in accordance with the requirements for the degree Dr. rer. nat.

Author: Dipl.-Ing. Martin Bernauer

Advisor: Prof. Dr. Roland Herzog

Chemnitz, July 14, 2010

Für Veronika und Jonas

Contents

Statutory Declarations

These declarations refer to §6 of the doctoral degree regulations of the Faculty of Mathematics at Chemnitz University of Technology as of 2009-11-10.

- The candidate confirms that the work submitted is his own and that appropriate credit has been given where reference has been made to the work of others.
- The candidate declares that this thesis has not been submitted to any other institution as part of any PhD process.
- The candidate declares that he has not applied for any earlier or ongoing PhD graduation at any other institution.

(MARTIN BERNAUER)

Acknowledgments

The writing of this thesis would have been a much more difficult—if not impossible—task without the help and support of many people. First of all, I want to express my gratitude to my advisor, Prof. Roland Herzog, and to Prof. Karl Kunisch, not only for proposing such an interesting and challenging topic that matched my interests perfectly, but also for writing the successful project proposal on the basis of which this thesis emerged. In addition, I thank Prof. Roland Herzog for his enduring support and enthusiasm, and for all the new ideas he brought into my work.

Work on this thesis began during my time at the Radon Institute for Computational and Applied Mathematics (RICAM) in Linz, Austria. I thank all my former colleagues there for the nice and fruitful working environment they created. The smooth transition to the Chemnitz University of Technology was made possible by all the easy-going people at the faculty of mathematics. In particular, I express my thanks to the secretaries, to the people from the computing service, and to all members of the numerics group for all their guidance, technical help and comradeship. My "PhD brothers", Andreas Günnel, Frank Schmidt and Gerd Wachsmuth, and my advisor Roland Herzog deserve special mention here. They were always helpful with discussing mathematical problems and with answering one or the other question concerning LaTeX. Besides working next to each other, we enjoyed coffee breaks, concert visits, team races and musical jam sessions I will never forget.

In the mathematical world outside the Chemnitz University of Technology, I thank Prof. Gerd Dziuk, Prof. Karsten Eppler, Prof. Axel Voigt and, once more, Prof. Karl Kunisch for inspiring discussions at various occasions and for many helpful hints. Moreover, I acknowledge financial support from the "Fonds zur Förderung der wissenschaftlichen Forschung (FWF)[1]" under project grant P19918-N14.

Special heartfelt thanks go to all of my family. In particular, I express my gratitude to my parents for all their mental and financial support throughout my years of education. Finally, and most of all, I thank my wife Veronika and our son Jonas. Nothing in this world can outweigh all the patience they had during the last two years with a husband and a father who was not only physically absent too many times.

---

[1] http://www.fwf.ac.at

Abstract

This thesis is concerned with motion planning for the classical two-phase Stefan problem in level set formulation. The interface separating the fluid phases from the solid phases is represented as the zero level set of a continuous function whose evolution is described by the level set equation. Heat conduction in the two phases is modeled by the heat equation. A quadratic tracking-type cost functional that incorporates temperature tracking terms and a control cost term that expresses the desire to have the interface follow a prescribed trajectory by adjusting the heat flux through part of the boundary of the computational domain. The formal Lagrange approach is used to establish a first-order optimality system by applying shape calculus tools. For the numerical solution, the level set equation and its adjoint are discretized in space by discontinuous Galerkin methods that are combined with suitable explicit Runge-Kutta time stepping schemes, while the temperature and its adjoint are approximated in space by the extended finite element method (which accounts for the weak discontinuity of the temperature by a dynamic local modification of the underlying finite element spaces) combined with the implicit Euler method for the temporal discretization. The curvature of the interface which arises in the adjoint system is discretized by a finite element method as well. The projected gradient method, and, in the absence of control constraints, the limited memory BFGS method are used to solve the arising optimization problems. Several numerical examples highlight the potential of the proposed optimal control approach. In particular, they show that it inherits the geometric flexibility of the level set method. Thus, in addition to unidirectional solidification, closed interfaces and changes of topology can be tracked. Finally, the Moreau-Yosida regularization is applied to transform a state constraint on the position of the interface into a penalty term that is added to the cost functional. The optimality conditions for this penalized optimal control problem and its numerical solution are discussed. An example confirms the efficacy of the state constraint.

Zusammenfassung

Die vorliegende Arbeit beschäftigt sich mit einem Optimalsteuerungsproblem für das klassische Stefan-Problem in zwei Phasen. Die Phasengrenze wird als Niveaulinie einer stetigen Funktion modelliert, was die Lösung der so genannten Level-Set-Gleichung erfordert. Durch Anpassen des Wärmeflusses am Rand des betrachteten Gebiets soll ein gewünschter Verlauf der Phasengrenze angesteuert werden. Zusammen mit dem Wunsch, ein vorgegebenes Temperaturprofil zu approximieren, wird dieses Ziel in einem quadratischen Zielfunktional formuliert. Die notwendigen Optimalitätsbedingungen erster Ordnung werden formal mit Hilfe der entsprechenden Lagrange-Funktion und unter Benutzung von Techniken aus der Formoptimierung hergeleitet. Für die numerische Lösung müssen die auftretenden partiellen Differentialgleichungen diskretisiert werden. Dies geschieht im Falle der Level-Set-Gleichung und ihrer Adjungierten auf Basis von unstetigen Galerkin-Verfahren und expliziten Runge-Kutta-Methoden. Die Wärmeleitungsgleichung und die entsprechende Gleichung im adjungierten System werden mit einer erweiterten Finite-Elemente-Methode im Ort sowie dem impliziten Euler-Verfahren in der Zeit diskretisiert. Dieser Zugang umgeht die aufwändige Adaption des Gitters, die normalerweise bei der FE-Diskretisierung von Phasenübergangsproblemen unvermeidbar ist. Auch die Krümmung der Phasengrenze wird numerisch mit Hilfe der Methode der finiten Elemente angenähert. Zur Lösung der auftretenden Optimierungsprobleme werden ein Gradienten-Projektionsverfahren und, im Fall dass keine Kontrollschranken vorliegen, die BFGS-Methode mit beschränktem Speicherbedarf eingesetzt. Numerische Beispiele beleuchten die Stärken des vorgeschlagenen Zugangs. Es stellt sich insbesondere heraus, dass sich die geometrische Flexibilität der Level-Set-Methode auf den vorgeschlagenen Zugang zur optimalen Steuerung vererbt. Zusätzlich zur gerichteten Bewegung einer flachen Phasengrenze können somit auch geschlossene Phasengrenzen sowie topologische Veränderungen angesteuert werden. Exemplarisch, und zwar an Hand einer Beschränkung an die Lage der Phasengrenze, wird auch noch die Behandlung von Zustandsbeschränkungen mittels der Moreau-Yosida-Regularisierung diskutiert. Ein numerisches Beispiel demonstriert die Wirkung der Zustandsbeschränkung.

1 Introduction

1.1 Motivation

Free and moving boundary problems are of significant importance in science and technology. Due to the strong coupling between unknown geometric quantities (e.g., a certain part of the domain boundary), and unknown physical quantities (e.g., the temperature distribution in the interior of the domain), these problems are non-linear by nature. Thus, the analysis, the numerical solution and, in particular, the optimal control of such problems are challenging tasks.

The two-phase Stefan problem is a model for phase change problems that arise, for instance, in the continuous casting of steel or in crystal growth. Concerning the geometric setup, the model involves a solid phase and a fluid phase that are separated by a moving interface describing the solidification front. The temperature distribution in each of the phases is characterized by the heat equation. Due to state-dependent material properties, the coefficients in these equations are typically discontinuous across the interface. The coupling between the moving interface and the temperature is modeled as the so called Stefan condition that relates the normal velocity of the interface to the jump of the temperature gradient across the interface.

It is known that certain shapes of the interface are preferable over others. For instance, in crystal growth, a convex or, in the best case, flat interface improves the quality of the outcoming crystal. In addition to product quality, the length of a production cycle or the amount of energy consumed during the production process might depend on the shape of the interface. Thus, the optimal control of the two-phase Stefan problem and related problems, in particular the control of the moving interface, is highly desirable.

Previous work on the optimal control of the Stefan problem mainly focused on one-dimensional problems, on formulations of the forward problem in which

the moving interface is described as the graph of a function, or on weak formulations that completely avoid the explicit description of the interface. While the latter problem class admits a thorough analysis of the resulting optimal control problems, including their numerical approximation, the fact that an explicit interface representation is not available makes them less attractive for motion planning tasks where the goal is to track a desired interface motion. This is of course remedied by describing the interface as the graph of a function, but the applicability of this representation is limited. In particular, more complex interface geometries can not be handled easily. An example of a casting model in which closed interfaces and even changes of topology arise can be found in [**30**]. Existing optimal control approaches for the two-phase Stefan problem are expected to have difficulties handling this situation. An additional motivation for extending the interface description from the graph approach to a more general framework is the fact that during the iterative solution of optimal control problems for Stefan-type problems, the interface may be severely deformed, resulting in situations that can not be handled by the graph approach.

This thesis presents an optimal control approach to motion planning for the two-phase Stefan problem in level set formulation. The level set representation of the moving interface provides enough flexibility for handling closed interfaces and changes of topology. In the considered setup, a fixed domain, the so called hold-all, is decomposed into the solid and the fluid phases that are separated by the moving interface. As mentioned above, the temperature distribution in each of the two phases is described by the heat equation with constant coefficients that are allowed to jump across the interface, modeling state-dependent material behavior. The coupling between the temperature and the motion of the interface is described by the Stefan condition that relates the normal velocity of the interface to the jump of the temperature gradients across the interface. Control of this process is administered by adjusting the heat flux through part of the boundary of the computational domain. In addition to the tracking of a desired interface motion, temperature tracking terms are included in the cost functional. The proposed optimal control approach is based on the "optimize-then-discretize" paradigm in which first-order necessary optimality conditions are established in a continuous framework. A discretization is applied only afterwards for the numerical solution of the arising partial differential equation systems.

An adjoint system that allows for the efficient evaluation of the gradient of the cost functional is derived formally by a Lagrange approach, using tools from shape calculus to account for the geometric variations. At first, only control constraints are considered. The resulting optimality system is then extended to a penalized control problem resulting from applying the Moreau-Yosida

regularization to a constraint on the position of the interface. As usual, the optimality system consists of two coupled partial differential equation systems, describing the forward and the adjoint problems, respectively, and a variational inequality which, in the absence of control constraints, simplifies to the gradient equation. The level set representation of the interface necessitates the solution of the so called level set equation which is in the proposed framework a linear first-order Hamilton-Jacobi equation. Thus, the state which is adjoint to the level set function is described by a linear first-order equation of conservation type. The temperature and its adjoint quantity are described by time-dependent second-order diffusion equations. An additional condition that enforces the coupling between the involved states arises in both the forward and the adjoint systems. This structural similarity is exploited advantageously in the discretization of these PDE systems that is required for the numerical solution of the considered optimal control problems.

The level set equation and its adjoint are discretized in space by discontinuous Galerkin schemes which provide a modern and powerful framework for discretizing first-order hyperbolic partial differential equations. Explicit Runge-Kutta methods of appropriate order are used for the time stepping. While the level set solver is adapted from an existing approach on rectangular grids to the triangular grids used in this thesis, the solver for the adjoint level set equation requires the development of a novel strategy. To account for the weak discontinuity of the temperature in the two-phase Stefan problem and the adjoint temperature in the corresponding adjoint system, an extended finite element method is built upon the level set solver to discretize the forward and the adjoint heat equations in space. This extended finite element approach avoids the remeshing that is required with standard finite element methods for phase change problems by a dynamic local enrichment of the underlying finite element spaces. The implicit Euler method is implemented for the time stepping. The optimal control problems are solved by the projected gradient method and, in the absence of control constraints, by the limited memory BFGS method.

The potential of the proposed optimal control approach to motion planning for the moving interface in the two-phase Stefan problem is highlighted by several numerical examples. We show in particular that this approach allows for the tracking of closed interfaces and changes of topology. This geometric flexibility is inherited from the level set method and significantly extends previous approaches. In addition, we demonstrate the efficacy of the Moreau-Yosida regularization applied to the constraint on the position of the interface.

1.2 Outline

Chapter 2 – The Two-Phase Stefan Problem. This chapter sets the scene for the optimal control of the two-phase Stefan problem. Based on energy balance principles, the mathematical model is introduced by deriving the heat equation and the Stefan condition. Some background on the level set method which is used for capturing the moving interface is provided. Extensions of the Stefan problem are discussed, and we review the existence of weak and strong solutions. An overview of existing optimal control approaches to Stefan-type problems closes this introductory chapter.

Chapter 3 – Motion Planning Subject to Control Constraints. An introduction to the optimal control of partial differential equations subject to control constraints opens this chapter. We then formulate the motion planning problem for the moving interface in the two-phase Stefan problem as an optimal control problem. The adjoint system which is needed for the efficient evaluation of gradients is derived formally using tools from shape calculus and transport theorems which are summarized in Appendix A. A discussion of the optimization methods that are used to solve the given optimal control problems is included.

Chapter 4 – Discretization. The discretization of the forward and the adjoint systems is the content of this chapter. The level set equation and its adjoint equation are discretized in space using discontinuous Galerkin schemes that are combined with an explicit Runge-Kutta time stepping method. The extended finite element method (X-FEM) is utilized to discretize the heat equation and its adjoint equation in space. The time stepping is realized by the implicit Euler method. We also comment on the finite element approximation of the curvature of the interface.

Chapter 5 – Numerical Examples. To highlight the potential and to discuss the limitations of the proposed optimal control approach, five numerical examples are contained in this chapter. The configurations in these examples are chosen to show typical features of the level set method. Tracking of closed interfaces and of changes of topology is presented. A unidirectional solidification problem provides the motivation for using state constraints.

Chapter 6 – Motion Planning Subject to a State Constraint. As in Chapter 3, we start with a general introduction to state constrained optimal control of partial differential equations and a review of regularization techniques. The Moreau-Yosida regularization is then applied to a constraint on the interface position. The optimality conditions of the resulting unconstrained optimal control problem are derived and the approximation of these conditions is discussed. A numerical example closes this chapter.

2 The Two-Phase Stefan Problem

Contents

The aim of this chapter is to provide some theoretical background on Stefan-type problems. We first devise the basic ingredients of the classical two-phase Stefan problem, namely, the heat equation and the so called Stefan condition. Different interface representation techniques are discussed. Due to its flexibility, and because it provides a sharp interface representation, the level set method is used in this work. Important properties and distinguishing features of this interface capturing technique are outlined. We then turn to several extensions of the Stefan problem and highlight the importance of such problems by touching on several applications. A short introduction to the solution theory of Stefan problems with a focus on the two-phase case precedes the review of existing approaches to the optimal control of Stefan-type problems that closes this chapter.

2.1 Mathematical Modeling

The goal of this section is to establish the model equations of the two-phase Stefan problem. As we shall see in the course of this section, the Stefan problem is a model for phase change phenomena that describes the temperature distribution in the considered domain by the heat equation with coefficients that are typically discontinuous across the moving interface that separates the fluid and the solid phases. Therefore, we start the modeling with deriving the standard heat equation. We then include the phase change by

adding the so called Stefan condition to the model. Finally, we comment on different interface representation techniques. The exposition in Section 2.1.1 and Section 2.1.2 closely follows [51, Sections 5.4–5.6] and [72, Sections 1.4.1 and 2.1.3].

> **Remark 2.1** (Basic Setup). Throughout this text, we assume that the *hold-all* $D \subset \mathbb{R}^2$ is a given bounded set whose boundary we denote by ∂D. This hold-all represents the domain in which a certain material undergoes the phase change in the finite time interval $[t_0, T]$. At the same time, D also serves as the computational domain in which all arising equations are discretized for the numerical solution, see Chapter 4. Unless otherwise stated, $t_0 = 0$.

2.1.1. The Heat Equation

Let $G(t) \subset D$ be an arbitrary control volume that moves in the velocity field $\mathbf{v}$. Moreover, let ρ denote the density of the material contained in D, $\mathbf{y}(x, t)$ the density of the internal energy, $q(x, t)$ the heat flux, and $f(x, t)$ the heat source density. The first law of thermodynamics states that the energy balance equation

$$\frac{d}{dt} \int_{G(t)} \rho \left(\tfrac{1}{2} |\mathbf{v}|^2 + \mathbf{y} \right) dx = \int_{G(t)} \rho \vec{f} \cdot \mathbf{v} \, dx + \int_{\partial G(t)} \sigma \, n \cdot \mathbf{v} \, ds$$
$$- \int_{\partial G(t)} q \cdot n \, ds + \int_{G(t)} \rho f \, dx \tag{2.1}$$

must hold. The left hand side of (2.1) accounts for the change of energy with respect to time, where the total energy is given as the sum of the kinetic energy $\int_{G(t)} \tfrac{1}{2} \rho \, |\mathbf{v}|^2 \, dx$ and the internal energy $\int_{G(t)} \rho \, \mathbf{y} \, dx$. The first two terms on the right hand side of (2.1) represent the power added by volume and by surface forces. The third term describes the loss of heat energy caused by the flux q across the boundary of the control volume. The last term summarizes the amount of heat produced by external sources f.

We apply the Reynolds Transport Theorem (Theorem A.10) and Green's formula to rewrite (2.1) as

$$\int_{G(t)} \frac{\partial}{\partial t} \left(\rho \left(\tfrac{1}{2} |\mathbf{v}|^2 + \mathbf{y} \right) \right) + \operatorname{div} \left(\rho \left(\tfrac{1}{2} |\mathbf{v}|^2 + \mathbf{y} \right) \mathbf{v} \right) dx$$
$$= \int_{G(t)} \rho \vec{f} \cdot \mathbf{v} \, dx + \int_{G(t)} \operatorname{div} (\sigma^\top \mathbf{v}) \, dx - \int_{G(t)} \operatorname{div} q \, dx + \int_{G(t)} \rho f \, dx.$$

Since the control volume $G(t)$ is arbitrary, this integral identity is equivalent to the differential equation

$$\frac{\partial}{\partial t}\left(\rho\left(\tfrac{1}{2}|\mathbf{v}|^2 + \mathbf{y}\right)\right) + \operatorname{div}\left(\rho\left(\tfrac{1}{2}|\mathbf{v}|^2 + \mathbf{y}\right)\mathbf{v}\right)$$
$$= \rho\,\vec{f}\cdot\mathbf{v} + \operatorname{div}\left(\sigma^\top\mathbf{v}\right) - \operatorname{div}q + \rho\,f.$$

In our model, we neglect heat convection, i.e., we set $\mathbf{v} = 0$. By the equation of continuity,

$$\rho_t + \operatorname{div}\left(\rho\,\mathbf{v}\right) = 0,$$

an immediate consequence of this simplification is that the density ρ is constant, resulting in the energy balance equation

$$\rho\,\mathbf{y}_t + \operatorname{div}q = \rho\,f.$$

The constitutive law for the heat flux q is Fourier's law, which reads

$$q = -k\,\nabla y, \tag{2.2}$$

for isotropic materials, where k is the scalar heat conductivity and y denotes the temperature. Finally, we use the relation

$$\mathbf{y}_t = c\,y_t,$$

where c is the heat capacity, to obtain the *heat equation*

$$\rho\,c\,y_t - \operatorname{div}\left(k\,\nabla y\right) = \rho\,c\,y_t - k\,\Delta y = \rho\,f \tag{2.3}$$

that describes the heat conduction in D by a time-dependent diffusion process.

Remark 2.2. (1) Equation (2.3) has to be equipped with proper initial and boundary conditions. We mainly use the conditions $y(t_0) = y_0$ and the Neumann boundary condition

$$k\frac{\partial y}{\partial n} = g,$$

where g is a given heat flux acting on ∂D.
(2) From now on, we assume that the heat source f is properly scaled so that we can drop the ρ in front of it.

2.1.2. Modeling the Phase Change

Motivation. In phase change problems as, for instance, the melting of ice in a basin of water, the continuous casting of steel or dendritic solidification, a free boundary separating the phases occurs. This free boundary is a priori unknown and is thus, in addition to the unknown temperature distribution,

part of the solution of a phase change problem. As a consequence, the heat
equation alone does not provide a complete description of the phase change.
Rather, it must be coupled with an equation that determines the interface
motion. The goal of this section is to derive the so called Stefan condition
that is an example of such an additional condition at the free boundary.

Latent Heat. Gupta [**72**, Section 2.1.3] provides the following motivation of
the latent heat that arises in phase change phenomena: If metal (initially in
solid state) is heated, the temperature rises up to the *equilibrium temperature*
y_M. At this point, a certain amount of additional heat is absorbed without
raising the temperature of the metal. This heat is called *latent heat*. It
accounts for the energy that is required to pull atoms from a closely packed
structure (as in solid metals) to a more freely packed structure (as in liquid
metals). When the liquid solidifies again, this latent heat is released.

Geometric Setup. To describe a change of phase from fluid to solid (or,
equivalently, in the reverse direction) mathematically, we subdivide the do-
main D into the two time-dependent domains $\Omega_S(t)$, occupied by the *solid
phase*, and $\Omega_F(t)$, occupied by the *fluid phase*. The *interface* separating
these two phases is denoted by $\Gamma_I(t)$. As mentioned in [**51**, Section 7.3], the
heat equation (2.3) is still valid in each of the phases. Note that the con-
stants c and k may be different in the two phases due to different material
properties. This is accounted for by using the notation c_S, c_F, k_S and k_F to
denote the material constants in the two phases from now on.

The Stefan Condition. A mathematically rigorous derivation of the Stefan
condition can be found in [**51**, Section 7.3]. For the sake of brevity, we rather
follow Gupta [**72**, Section 1.4.1], who derives the Stefan condition in the case
of a solidification process. Let P be a point on $\Gamma_I(t)$ and let Q be a point on
$\Gamma_I(t + \Delta t)$, lying on the line that is defined by P and the normal vector n to
$\Gamma_I(t)$ at P. We consider a rectangle $\mathcal{R}$ with side lengths Δw and $|\vec{PQ}|$, see
Figure 2.1. As the solidification takes place, the latent heat $\rho\, L\, \Delta w\, |\vec{PQ}|$ is
released at the rate

$$\lim_{\Delta t \to 0} \rho\, L\, \frac{|\vec{PQ}|}{\Delta t}\, \Delta w = \rho\, L\, \left(\vec{V} \cdot n\right) \Delta w,$$

where $\vec{V}$ is the velocity of the interface. The amount of heat that flows
through a surface element with normal vector n and area Δw during the
time interval Δt is in the limit ($\Delta t \to 0$) given by $-k\, \nabla y \cdot n\, \Delta w$, see (2.2).
Thus, the energy conservation principle applied to $\mathcal{R}$ implies that

$$-\left(-k_S\, \nabla y_S \cdot n_P\, \Delta w\right) - \left(-k_F\, \nabla y_F \cdot n_Q\, \Delta w\right) + \rho\, L\, \left(\vec{V} \cdot n\right) \Delta w = 0,$$
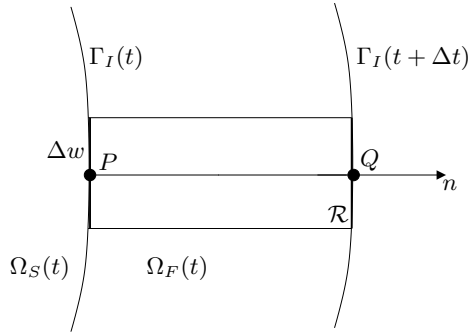
FIGURE 2.1. Derivation of the Stefan condition.

where the first and the second term account for the amount of heat that is lost across the left and right boundary of $\mathcal{R}$. Since the outer normal to $\mathcal{R}$ at P satisfies $n_P = -n_Q = -n$, we conclude that the *Stefan condition*

$$\rho\, L\, \vec{V} \cdot n = k_S\, \nabla y_S \cdot n - k_F\, \nabla y_F \cdot n \tag{2.4}$$

must hold at the interface $\Gamma_I(t)$.

Remark 2.3. The jump of the temperature gradient across the interface will also be denoted by

$$k_S\, \nabla y_S \cdot n - k_F\, \nabla y_F \cdot n = \left[k\, \nabla y \right]_F^S \cdot n.$$

The Classical Two-Phase Stefan Problem. We now summarize the results of the last two sections and come up with the *classical two-phase Stefan problem* [**72**, Section 1.4.1] with Neumann boundary conditions:

Find a function $y : D \times [0, T] \to \mathbb{R}$ (the temperature) and the interface $\Gamma_I(t)$ such that:

$$\rho\, c_S\, y_t - k_S\, \Delta y = f \qquad\qquad \text{in } \Omega_S(t) \tag{2.5a}$$

$$\rho\, c_F\, y_t - k_F\, \Delta y = f \qquad\qquad \text{in } \Omega_F(t) \tag{2.5b}$$

$$y(x, 0) = y_0(x) \qquad\qquad \text{in } \Omega_S(0) \cup \Omega_F(0) \tag{2.5c}$$

$$y(x, t) = y_M \qquad\qquad \text{on } \Gamma_I(t) \tag{2.5d}$$

$$k_S \tfrac{\partial y_S}{\partial n} = g \qquad\qquad \text{on } \partial\Omega_S(t) \cap \partial D \tag{2.5e}$$

$$k_F \frac{\partial y_F}{\partial n} = g \qquad\qquad\qquad \text{on } \partial\Omega_F(t) \cap \partial D \qquad\qquad (2.5\text{f})$$

$$\rho L \vec{V} \cdot n = \left[k \nabla y \right]_F^S \cdot n \qquad\qquad\qquad \text{on } \Gamma_I(t) \qquad\qquad (2.5\text{g})$$

on a given time horizon $[0, T]$.

Remark 2.4.   (1) Due to the so called *isothermal interface condition* (2.5d) that prescribes the equilibrium temperature at the interface, this form of the Stefan problem is only a reasonable model of solidification (or, equivalently, melting) processes if we require the conditions

$$y \geq y_M \text{ in } \Omega_F(t) \quad\text{and}\quad y \leq y_M \text{ in } \Omega_S(t). \qquad\qquad (2.6)$$

This means in particular that, as soon as the temperature y is known, the moving interface $\Gamma_I(t)$ and the solid and the fluid phases can be determined in an a-posteriori step. A disadvantage of this formulation is that supercooling effects (see Section 2.3) can not be dealt with.
(2) As the moving interface $\Gamma_I(t)$ is unknown, (2.5) is a highly non-linear problem. Note that this non-linearity is purely geometric rather than algebraic. In fact, all equations in (2.5), considered independently of each other, are linear.
(3) An interpretation of the Stefan condition (2.5g) is that it prescribes the velocity field $\vec{V}$ on the interface via

$$\vec{V} = \frac{1}{\rho L} \left[k \nabla y \right]_F^S \qquad\qquad\qquad \text{on } \Gamma_I(t). \qquad\qquad (2.7)$$

A constant extension in normal direction can be used to extend $\vec{V}$ to all of D, see Section 4.2.3.

It remains to either reformulate the two-phase Stefan problem (2.5) in a weak sense that avoids the explicit representation of the interface $\Gamma_I(t)$, or to choose a specific representation of $\Gamma_I(t)$ to make (2.5) amenable to numerical computations.

2.1.3. Representing the Moving Interface

The burden of representing the interface can be completely avoided by rewriting the two-phase Stefan problem (2.5) in terms of the enthalpy, as a variational inequality or by using a phase field model, see Section 2.4. In all of these reformulations, the interface can only be obtained a posteriori as the y_M-level set of the temperature. In particular, so called mushy regions in which $y = y_M$ may evolve. A sharp interface is not uniquely defined there.

(a) Embedding of two circles into a surface.   (b) Merging of the two circles.
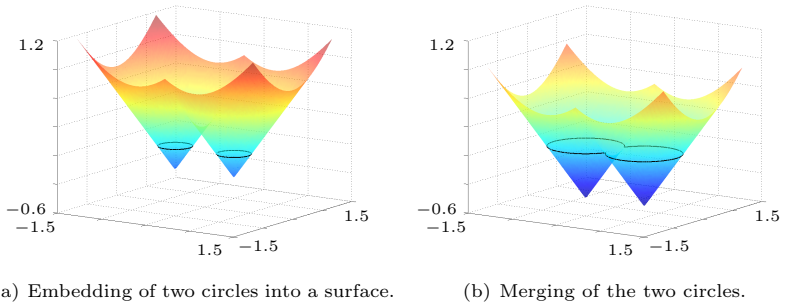
FIGURE 2.2. Illustration of the level set method.

Thus, for the optimal control of the interface motion in the two-phase Stefan problem, we prefer formulations that provide a more explicit representation of the interface.

Probably the most direct way to represent $\Gamma_I(t)$ explicitly is to describe it as the *graph of a function*. This classical approach has already been successfully applied to the optimal control of the Stefan problem [79, 80]. The obvious limitation of this approach is that closed interfaces can not be handled easily. A *parameterization* of $\Gamma_I(t)$ can be used to improve the interface representation in this direction. Schmidt [146] apparently was the first one to use such a parameterization to compute three-dimensional dendrites with finite elements. Still, changes of topology cause problems with parameterizations. *Phase field approaches* and the *level set method* are implicit interface capturing techniques that avoid the problems of the explicit representations just mentioned. Phase field equations typically have smooth solutions, the resulting interface representation is diffuse. In contrast, solutions of the level set equation are usually non-smooth (see Theorem 2.6), the resulting interface representation is sharp. This is more adequate for control purposes than a diffuse interface and, therefore, we model $\Gamma_I(t)$ by the level set method. This representation has already been used for the simulation of Stefan-type problems, see, e.g., [25, 26, 30, 67, 86, 168]. For optimal control purposes, this is a novel approach.

2.2   The Level Set Method

The *level set method* provides a framework for interface capturing by embedding the moving interface $\Gamma_I(t)$ into a higher-dimensional object. For

example, in two spatial dimensions, $\Gamma_I(t)$ is a moving curve in $\mathbb{R}^2$ and $\phi : \mathbb{R}^2 \times [0, T] \to \mathbb{R}$ is a function describing a surface such that at any time $\Gamma_I(t) = \{x : \phi(x, t) = 0\}$, see Figure 2.2(a). Since its introduction by Osher and Sethian [131], the level set method has successfully been applied in quite different areas such as mathematical imaging [158], inverse problems [19], shape optimization [4], state-constrained optimal control [77], and, in particular, in many branches of computational physics, see, e.g., [26, 71, 116] and [130, Chapter IV] and the references in these sources. The reason for this popularity is that the level set method is very flexible. It naturally handles closed interfaces and topological changes, see Figure 2.2.

The Level Set Equation. The level set method can be devised as follows [147, Section 1.2]. At any time, the moving interface $\Gamma_I(t)$ is determined by the zero level set of a higher-dimensional moving surface ϕ. Thus, the path $x(t)$ of a particle on the moving interface is required to satisfy the equation

$$\phi\big(x(t), t\big) = 0 \quad \text{for all } t \in [0, T].$$

Total differentiation with respect to t yields

$$\nabla\phi\big(x(t), t\big) \cdot \dot{x}(t) + \phi_t\big(x(t), t\big) = 0 \quad \text{for all } t \in [0, T],$$

where $\dot{x}(t) = \vec{V}(x, t)$ is the velocity of the particle at time t. This gives rise to the *level set equation*

$$\phi_t + \vec{V} \cdot \nabla\phi = 0 \qquad\qquad \text{in } \mathbb{R}^2, \qquad (2.8a)$$

$$\phi(x, 0) = \phi_0(x) \qquad\qquad \text{in } \mathbb{R}^2, \qquad (2.8b)$$

which is a linear advection equation for the level set function ϕ under the velocity field $\vec{V}$. The initial condition (2.8b) is usually defined using the signed distance function ϕ_0 to the initial position of the interface.

Geometric Properties. The sign of ϕ can be used to distinguish the interior of the domain that the interface encloses from its surrounding area. We choose ϕ to be negative in the interior (which will later represent the solid phase $\Omega_S(t)$) and positive in the exterior (the fluid phase $\Omega_F(t)$). Several other important geometric properties of $\Gamma_I(t)$ and the enclosed domain can be easily described using the level set function ϕ:

- The *outward unit normal* to $\Gamma_I(t)$ is given by [130, Section 1.4]

$$n = \frac{\nabla\phi}{|\nabla\phi|}. \qquad (2.9)$$

- The *curvature* of $\Gamma_I(t)$ is given by [130, Section 1.4]

$$\kappa = \text{div}\, \frac{\nabla\phi}{|\nabla\phi|}, \qquad (2.10)$$
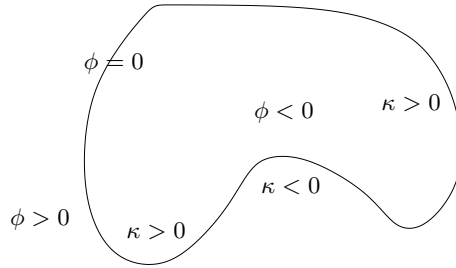
FIGURE 2.3. Sign of the curvature of $\Gamma_I(t)$.

where $\kappa > 0$ for convex regions and $\kappa < 0$ for concave regions, see Figure 2.3.

- The *volume* of the enclosed domain can be expressed as

$$\int_{\{\phi<0\}} 1\, dx = \frac{1}{2} \int_{\{\phi<0\}} \operatorname{div} \begin{pmatrix} x_1 \\ x_2 \end{pmatrix} dx = \frac{1}{2} \int_{\{\phi=0\}} \begin{pmatrix} x_1 \\ x_2 \end{pmatrix} \cdot n\, ds.$$

- The *length* of the interface can also be computed as a domain integral according to

$$\int_{\{\phi=0\}} 1\, ds = \int_{\{\phi=0\}} \frac{\nabla\phi}{|\nabla\phi|} \cdot \frac{\nabla\phi}{|\nabla\phi|}\, ds \stackrel{(2.9)}{=} \int_{\{\phi<0\}} \operatorname{div} \frac{\nabla\phi}{|\nabla\phi|}\, dx.$$

The Stefan Condition in Level Set Formulation. Following Gupta [72, Section 1.4.1], we can also express the Stefan condition (2.5g) in terms of the level set function ϕ. The representation (2.9) of the normal vector yields

$$\rho\, L\, \vec{V} \frac{\nabla\phi}{|\nabla\phi|} = \rho\, L\, \vec{V} \cdot n \stackrel{(2.5g)}{=} \left[k\, \nabla y\right]_F^S \cdot n = \left[k\, \nabla y\right]_F^S \cdot \frac{\nabla\phi}{|\nabla\phi|},$$

or, equivalently,

$$\rho\, L\, \vec{V} \cdot \nabla\phi = \left[k\, \nabla y\right]_F^S \cdot \nabla\phi.$$

It follows from the level set equation (2.8), that

$$-\rho\, L\, \phi_t = \left[k\, \nabla y\right]_F^S \cdot \nabla\phi$$

must hold. We do not state the complete two-phase Stefan problem in level set formulation here but refer to Section 3.2 (p. 29).

Solutions of the Level Set Equation. By virtue of (2.9), (2.8a) can be recast as the non-linear equation

$$\phi_t + \vec{V} \cdot n \, |\nabla\phi| = 0 \qquad \text{in } \mathbb{R}^2, \qquad (2.11)$$

which is also called the level set equation. This non-linear formulation is useful in situations, in which only the normal velocity $\vec{V} \cdot n$ is given and $\vec{V}$ is not known explicitly. An obvious advantage of (2.8) is its linear structure which in general makes the implementation of numerical methods for solving the level set equation much easier.

Remark 2.5. Actually, the non-linear equation (2.11) appears more often in the literature than its linear counterpart (2.8), but whenever we use the term level set equation, we refer to (2.8).

Each of the two forms of the level set equation can be recast as a *Hamilton-Jacobi equation*

$$\phi_t + H(\nabla\phi) = 0. \qquad (2.12)$$

In case of (2.8a), the *Hamiltonian*

$$H_L(\nabla\phi) := \vec{V} \cdot \nabla\phi$$

is linear, whereas the Hamiltonian corresponding to (2.11) is non-linear:

$$H_N(\nabla\phi) := \vec{V} \cdot n \, |\nabla\phi|.$$

The proper notion of solutions to first-order Hamilton-Jacobi equations of the type (2.12) was introduced by Crandall and Lions in 1983 [35] (see also [36]) using the space $\text{BUC}\left(\mathbb{R}^2\right)$ of bounded and uniformly continuous functions on $\mathbb{R}^2$.

Theorem 2.6 (Existence and Uniqueness of Viscosity Solutions). *Let $H \in C(\mathbb{R}^2)$ and $\phi_0 \in \text{BUC}\left(\mathbb{R}^2\right)$. Then there is exactly one function $\phi \in \text{BUC}\left(\mathbb{R}^2 \times [0,T]\right)$ for all $T > 0$ such that $\phi(x,0) = \phi_0(x)$ and for every $\eta \in C^1\left(\mathbb{R}^2 \times (0,\infty)\right)$ and $T > 0$:*

If (x_0, t_0) is a local maximum of $\phi - \eta$ on $\mathbb{R}^2 \times (0,T]$, then

$$\eta_t(x_0, t_0) + H\left(\nabla\eta(x_0, t_0)\right) \leq 0;$$

and

If (x_0, t_0) is a local minimum of $\phi - \eta$ on $\mathbb{R}^2 \times (0,T]$, then

$$\eta_t(x_0, t_0) + H\left(\nabla\eta(x_0, t_0)\right) \geq 0.$$

ϕ is called the viscosity solution of (2.12).

Remark 2.7 (Properties of Viscosity Solutions)**.**

(1) Viscosity solutions are weak solutions to Hamilton-Jacobi equations in the sense that the differential operator is shifted from the unknown ϕ to the test function η pointwise in local extrema, see [**35**, Definition I.1].

(2) Viscosity solutions depend on the problem data, i.e., on the Hamiltonian H, in a stable way [**35**, Theorem I.2].

(3) In addition, this concept is consistent: At those points at which a viscosity solution is differentiable, it also satisfies the Hamilton-Jacobi equation in a classical sense [**35**, Corollary I.6].

Numerical Issues. When solving Hamilton-Jacobi equations of the type (2.12) numerically, the discretization has to be carried out with care to make sure that the correct solution, the viscosity solution, is approximated. This property of the discretization can be enforced by using so called monotone schemes [**36**]. We discuss this issue in more detail in Section 4.2.1.

Concerning the level set equation, several challenges arise in addition to choosing a proper discretization. As mentioned above, an obvious choice for the initial level set function ϕ_0 in (2.8b) is the signed distance function to the initial interface position. Often, an explicit representation of this signed distance function is not available and it has to be constructed numerically. For various reasons, it is desirable to keep the level set function close to a signed distance function during the computation. This goal requires a reinitialization of the level set function. In case of the Stefan problem, the velocity field in (2.8a) must be extended to at least a neighborhood of the current interface position. We elaborate on these issues in Section 4.2.3.

2.3 Extensions and Applications of the Stefan Problem

The Stefan problem (2.5) can be extended and modified in several ways to broaden the range of real world problems for which it can serve as a model. Some of these extensions and potential applications of the Stefan problem are discussed in this section.

The Gibbs-Thomson Correction. Gupta [**72**, Section 2.2.2] explains that, due to the interface curvature, particles at the interface are on average less surrounded by neighboring particles of the same state and, thus, their tendency to change the state, either from solid to liquid or in the reverse direction, increases. Depending on the setup, the new equilibrium temperature y_M^c might be higher or lower than y_M. The isothermal interface condition (2.5d) is a

model for the ideal equilibrium temperature that does not take these curvature effects into account. In situations in which such effects are important the Gibbs-Thomson correction

$$y_M^c = y_M + \epsilon_s\, \kappa \tag{2.13}$$

can be used. Here, κ is the interface curvature and ϵ_s is a constant depending on the surface energy. The Gibbs-Thomson correction also provides a way to include supercooling effects in the Stefan problem (2.5), i.e., the requirements (2.6) can be dropped. A more general form of (2.13) is the modified Gibbs-Thomson correction [**72**, Sections 2.2.3 and 4.1] which incorporates interface kinetics.

Flow in the Fluid Phase. The model (2.5) was devised assuming that flow in the fluid phase can be neglected. In certain applications, this assumption is too restrictive, e.g., if the densities of the solid and the fluid phases differ too much. In this case, the Stefan problem (2.5) must be extended by a flow in the fluid phase [**72**, Sections 1.3 and 1.4.7], modeled, for instance, by the Navier-Stokes equations [**51**, Chapter 5]. The flow is coupled to the heat conduction equation by adding a convective term in the fluid phase.

Non-Linear Stefan Problems. As mentioned in Remark 2.4, the Stefan problem (2.5) is geometrically non-linear by nature. In addition, it is often necessary to consider algebraic non-linearities:

- The heat capacities c_S and c_F, and the heat conductivities k_S and k_F in (2.5) are assumed to be constant. In many applications, these are in fact highly temperature dependent, leading to the heat equation
  $$\rho\, c(y)\, y_t - \mathrm{div}\big(k(y)\, \nabla y\big) = f.$$
  As a consequence, (2.5a) and (2.5b) have to be modified as well.
- We assume that the density ρ is constant and, in particular, equal in both phases, which is certainly not true in general. One rather has to consider a density that depends on the phase (which does not introduce additional non-linearities) or even a temperature dependent density $\rho = \rho(y)$.
- The Neumann boundary conditions (2.5e)–(2.5f) might have to be replaced by radiation boundary conditions of Stefan-Boltzmann type [**72**, Section 1.4.4].

Multiphase Stefan Problems. Historically, the Stefan problem was first formulated as a one-phase problem to model the formation of ice in the polar sea [**153**]. It is straightforward to obtain such a one-phase formulation from the two-phase problem (2.5) by setting the temperature in one of the

phases equal to the equilibrium temperature y_M. The Stefan condition is still valid but it can be simplified as one of the temperature gradients vanishes. Stefan problems with more than two phases can be formulated as well [**72**, Section 3.2.3]. Obviously, their structure is much more complicated as phase boundaries might intersect, generating so called triple junction points. Nonetheless, such problems have been studied analytically and numerically, see, e.g., [**28**, **59**, **68**, **164**]. For a recent interesting application in the modeling of one-dimensional cell-to-cell adhesion and diffusion we refer to [**6**].

Applications Free and moving boundary problems are ubiquitous in applications. This is confirmed by the statement

> *"Around one third of all the differential equation models arising in industrial applications are free boundary problems."*

from the OCIAM[1] website. Friedman [**60**] offers a brief review of free boundary problems arising in science and technology, while Tarzia [**155**] provides an impressive bibliography on the analysis, the numerical treatment and applications of free and moving boundary problems.

As mentioned above, the Stefan problem was formulated as a one-phase problem related to the formation of ice in the polar sea [**153**]. A similar problem had already been studied quite some time earlier by Lamé and Clapeyron [**102**]. Typical situations in which the Stefan problem or related problems serve as a model are phase change problems in physics and technology. Two prominent examples of industrially relevant application areas are the continuous casting of steel [**75**, **119**, **140**] and crystal growth [**65**, **100**, **159**, **160**]. Stefan-type problems can also be used to model welding processes [**161**] and biofilm growth [**45**]. An application of the Stefan problem in biology has already been mentioned above [**6**].

2.4 Weak and Strong Solutions

This section contains a brief review of different formulations of the Stefan problem and the corresponding existence and uniqueness results, with a focus on the multidimensional case. The discussion does not aim for completeness. It is rather included to give an overview and to justify the purely formal approach to the optimal control problem discussed in this text.

The Enthalpy Formulation. Assume for the sake of simplicity that

$$k_S = k_F = k, \quad c_S = c_F = \rho = 1.$$

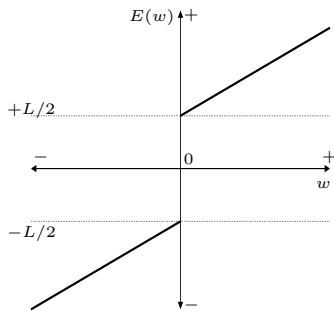[1]http://www2.maths.ox.ac.uk/ociam/research/methods/freebdrys.shtml

FIGURE 2.4. Enthalpy $E(w)$ vs. normalized temperature w.

Then the two-phase Stefan problem for the normalized temperature $w = y - y_M$ with Dirichlet boundary conditions and in the absence of heat sources reads

$$\left.\begin{aligned}
w_t &= k\,\Delta w && \text{in } D \\
L\,\vec{V}\cdot n &= k\,[\nabla w]_F^S \cdot n && \text{on } \Gamma_I(t) \\
w(x,0) &= w_0(x) && \text{in } D \\
w(x,t) &= w_\partial(x,t) && \text{on } \partial D.
\end{aligned}\right\} \qquad (2.14)$$

After introducing the enthalpy (see Figure 2.4)

$$E(w) := w + \frac{L}{2}\,\varphi$$

with the discontinuous phase field function (see Figure 2.5(a))

$$\varphi := \begin{cases} 1 & w > 0, \\ -1 & w < 0, \end{cases} \qquad (2.15)$$

problem (2.14) can be equivalently expressed in the *enthalpy formulation* [129]

$$\left.\begin{aligned}
\frac{\partial}{\partial t}E(w) &= k\,\Delta w && \text{in } D \\
w(x,0) &= w_0(x) && \text{in } D \\
w(x,t) &= w_\partial(x,t) && \text{in } D
\end{aligned}\right\} \qquad (2.16)$$

which avoids the explicit tracking of $\Gamma_I(t)$. By locating the discontinuity of the enthalpy E, a sharp interface representation can be obtained a posteriori. In the one-dimensional case, Oleĭnik [129] transforms the enthalpy formulation into an integral identity, and proves existence and uniqueness of a

weak solution in the sense of a bounded measurable function. Kamenomost-skaja [88] uses a similar approach to establish existence and uniqueness for a three-dimensional multiphase Stefan problem in the same class of functions.

The Phase Field Formulation. Caginalp [21] replaces the discontinuous phase field function (2.15) by a continuous function that attains the same values in the solid and in the fluid regions but has a smooth transition in a symmetric interval around the origin, see Figure 2.5(b). Consequently, the resulting interface representation is no longer sharp, and an equation that describes the evolution of the phase field function is needed. Caginalp proposes to use the Ginzberg-Landau free energy

$$\mathcal{F}_w(\varphi) = \int_D \frac{\xi^2}{2} \left(\nabla \varphi \right)^2 + \frac{1}{8} \left(\varphi^2 - 1 \right)^2 - 2\, w\, \varphi\, dx,$$

where ξ is a length-scale parameter that determines the width of the transition region of φ from -1 to 1, and $\frac{1}{8} \left(\varphi^2 - 1 \right)^2$ is a so called double well potential that ensures that the energy attained in the solid and fluid phases is smaller than outside. Minimizing this Ginzberg-Landau free energy functional leads to the coupled *phase field system*

$$\left. \begin{array}{ll} \tau\, \varphi_t = \xi^2\, \Delta\varphi + \dfrac{1}{2} \left(\varphi - \varphi^3 \right) + 2\, w & \text{in } D \\[2mm] w_t + \dfrac{L}{2}\, \varphi_t = k\, \Delta w & \text{in } D \end{array} \right\} \tag{2.17}$$

with the boundary and initial conditions on w as in (2.16) and suitable boundary and initial conditions on φ. Caginalp [21] proves that (2.17) has a unique solution

$$\begin{pmatrix} w \\ \varphi \end{pmatrix} \in C\big([0,T]; \mathrm{BUC}\,(D)\big)$$

globally in time under certain smoothness assumptions on the data. In collaboration with Chen, he also proves convergence of this phase field model to the sharp interface limit as $\xi \to 0$ [22].

The Variational Inequality Formulation. Duvaut [47] introduces the first variational inequality formulation for one-phase Stefan problems by defining the so called freezing index [57]

$$\widehat{y} = \begin{cases} \int_{\phi(x)}^t y(x,\tau)\, d\tau & \text{in } \Omega_S(t), \\ 0 & \text{in } \Omega_F(t), \end{cases}$$

assuming that $y = 0$ in $\Omega_F(t)$, $\Omega_F(0) = D$ and that the interface is determined by the equation $t = \phi(x)$. Friedman and Kinderlehrer [61] consider a

(a) Discontinuous phase field function.   (b) Continuous phase field function.
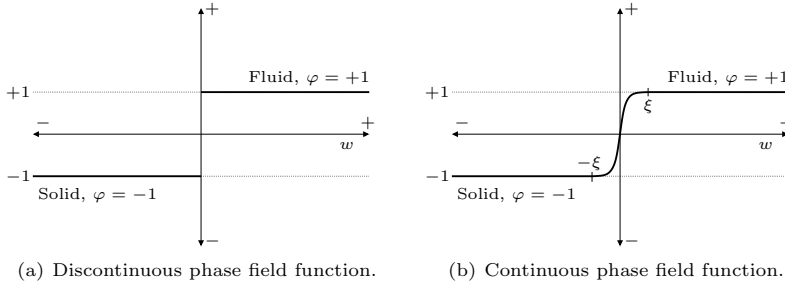
FIGURE 2.5. Phase field functions.

slightly more general setup and use an extension of Duvaut's freezing index to prove existence and uniqueness of a solution

$$y \in L^\infty\big([0,T]; H^{2,p}(D)\big) \ (1 \le p \le \infty), \quad y_t \in L^\infty\big([0,T]; L^\infty(D)\big)$$

to the one-phase Stefan problem in *parabolic variational inequality formulation*. Duvaut extends his approach to two-phase problems [48], see also [72, Section 7.4.3].

Pawłow and Niezgódka [126] apply the Kirchhoff transformation

$$\theta = \mathfrak{K}(y), \quad \big(\mathfrak{K}(y)\big)(x,t) = \int_{y_M}^{y} k(x,t,\xi)\,d\xi, \quad (x,t) \in D \times [0,T],$$

to the classical formulation of the two-phase Stefan problem and establish existence and uniqueness, as well as continuous dependence on the data, of a weak solution of the two-phase Stefan problem with $L^\infty\big([0,T]; V_0\big)$ regularity, where

$$V_0 = \big\{v \in H^1(D) \ : \ v\big|_{\partial D} = 0\big\}.$$

We refer to [126] for the details. Pawłow [133] uses the transformed problem as a starting point to formulate the two-phase Stefan problem as a parabolic variational inequality. As in the previously mentioned paper [126], Pawłow shows existence, uniqueness and continuous dependence on the data of a weak solution with the same $L^\infty\big([0,T]; V_0\big)$ regularity. The main improvement of this formulation compared to the approach of Duvaut [48] is the inclusion of non-linearities in the problem data.

Classical Solutions. Weak solutions to the two-phase Stefan problem can be obtained by the methods discussed above. However, in all of these approaches, the explicit tracking of the interface is avoided and, thus, such weak formulations are not the natural choice for optimal control approaches

to planning the motion of the interface. Classical solutions to Stefan problems that allow for an explicit representation of the interface, e.g., as the graph of a function, have also been investigated.

Budak and Moskal [18] formulate theorems on uniqueness and existence of classical solutions and continuous dependence of these on the data. The authors remark that their results generalize to the multidimensional case, and to non-linearities in the equations and in the boundary conditions. None of the results in this paper are proved and Rubinstein [143] classifies them as "undoubtedly wrong". Caffarelli [20] investigates the regularity of the free boundary in a one-phase Stefan problem.

In his book on the Stefan problem [109], Meĭrmanov collects local-in-time results on the existence of classical solutions to the one-phase Stefan problem (Section II.1) and the two-phase Stefan problem (Section II.5) in the multidimensional case. He also establishes a global-in-time result for classical solutions to the one-phase Stefan problem in multiple dimensions (Section III.1). The crucial point is that none of the techniques that are applicable to the one-phase problem can be adapted to the two-phase case and, thus, so far no general global-in-time results for the two-phase Stefan problem are known (Section III.2).

Borodin [16,17] proves a global-in-time existence result that implies that the free boundary can be written as the graph of a function. Escher et al. [53] establish a global-in-time result for classical solutions to the two-phase Stefan problem with Gibbs-Thomson correction. However, their analysis relies on the fact that the moving interface can be represented as the graph of a function at any time. Prüss et al. [138] consider the two-phase Stefan problem with isothermal interface condition and prove the existence of analytic solutions on arbitrary time intervals. As in the previously mentioned approaches, the moving interface is represented as the graph of a function.

In summary, we find that for the classical two-phase Stefan problem in the general level set formulation (3.2), no global-in-time existence results are available. As a consequence, any approach to the optimal control of the classical two-phase Stefan problem (2.5) can only be formal if the moving phase boundary is described by the level set method.

2.5 Overview of Existing Optimal Control Approaches

We close this chapter with a—mostly chronological and by far incomplete—review of existing approaches to the optimal control of the Stefan problem and related free boundary problems. Contributions including constraints are commented on at the end of this section.

Hoffmann and Sprekels [83] consider a one-dimensional inverse two-phase Stefan problem. Their goal is to approximate an ideal interface motion by using a non-optimal feedback control law. The authors show the existence of a solution and provide numerical experiments. Niezgódka and Pawlow [126] provide results on weak solutions of multidimensional Stefan problems in enthalpy formulation. In the companion paper [125], they use these results to prove existence of optimal controls. Moreover, they analyze approximations of the optimal control problems under consideration. These approximation results are the basis for computing numerical solutions in [134]. Hoffmann et al. [82] treat the problem of a feedback control via thermostats for a multidimensional Stefan problem in enthalpy formulation. They do not present any numerical calculations.

Knabner [93] uses a linearization technique for the control of one-dimensional Stefan problems. He carries out the minimization over a finite-dimensional subspace only, but is able to derive estimates of the order of convergence. After a discretization, the problem boils down to solving a least squares problem. The author presents several numerical examples.

Kunisch et al. [98, 99] consider the inverse problem of estimating the time-dependent heat conductivity in a one-dimensional one-phase Stefan problem. The authors use an equivalent integral equation to show the existence of a solution of the forward problem. Based on this result, the solvability of the parameter identification problem is established. Moreover, the convergence of the method is investigated. A discussion of the discretization of the integral equations is included and numerical examples are provided.

Zabaras and coworkers [169] discuss a design problem for two-dimensional Stefan problems. Their approach is based on a deforming finite element formulation. The authors assume that the desired interface location is known in the form of coordinates of nodes on the interface at distinct instances of time only. The boundary heat flux serves as the design variable. Kang and Zabaras [89] consider a similar design problem. Their goal is to find a boundary heat flux, which realizes the desired interface motion, by minimizing the defect between the reference temperature at the interface and the temperature at the actual interface. They derive a sensitivity problem and the corresponding adjoint problem. For the numerical solution of the optimization problem, a deforming finite element method and a conjugate gradient algorithm are used. In their examples section, the authors present a unidirectional solidification problem and the problem of solidification in a corner.

Yang [167] examines the inverse design of unidirectional solidification problems with natural convection by minimizing a similar cost functional as Kang

and Zabaras [89]. However, this approach relies on the restrictive assumption that the heat flux into the free boundary is known. Yang also uses a deforming finite element approach and an adjoint calculus for the solution of the optimization problem.

Barbu et al. [10] study the identification of the boundary heat flux in a multi-dimensional one-phase Stefan problem. They interpret the forward problem as a closed loop system in a non-cylindrical domain, and carry out the analysis of this problem in a Hilbert space setting. The solvability of the identification problem is shown, and its approximation by a family of optimal control problems is analyzed using convex analysis tools. Numerical experiments are provided for one-dimensional problems.

Dunbar et al. [46] use a series representation of the solution of a one-dimensional non-linear one-phase Stefan problem to study motion planning by a boundary control. A weak maximum principle for the forward problem is discussed and numerical simulations are provided.

Hinze and Ziegenbalg [79] represent the interface in a two-phase Stefan problem as the graph of a function over a rectangular domain, which allows for the direct control of the interface motion. They use the temperature at the boundary of the container as the control variable and aim to track the desired interface motion by minimizing an appropriate cost functional including an observation at terminal time. An adjoint system is derived in a formal way. This adjoint system is the basis for a gradient method with line search to solve the optimization problem. The discretization of the infinite-dimensional problems is carried out by a finite difference approach. The authors present a numerical example to verify their theoretical results. Later, the same authors extend this approach and include convection-driven flow in the fluid phase [80]. More details concerning this approach can be found in [172].

Protas and Liao [137] consider a one-dimensional optimization problem for a PDE system in a moving domain. The authors map the moving domain into a fixed domain and then derive an adjoint system. Alternatively, they show how to derive an adjoint system directly in the moving domain using methods of non-cylindrical calculus. These two approaches do not commute. The numerical examples given in this paper are based on a spectral discretization. The authors also discuss the consistency of their gradient approximation.

Repke et al. [139] discuss an optimal control problem for a stationary free surface Stokes flow which models a film casting process. The goal is to have the free boundaries that are described as the graphs of functions follow a prescribed trajectory by adjusting the ambient aerodynamic pressure. The authors present two different approaches. The natural choice is to include the free boundaries as state variables in the problem. Alternatively, the

additional kinematic condition at the free boundaries is added to the cost functional as a penalty term as suggested in [161]. In each of these two cases, an adjoint system and a gradient equation are derived using the Lagrange formalism. The BFGS method is used to solve the optimization problems. The forward and the adjoint systems are solved by a fixed-point method using finite elements.

Control and State Constraints

Hoffmann and Jiang [81] show the well-posedness of a phase field model for a three-dimensional solidification problem in which the heat source acts as a distributed control. Fréchet-differentiability of the control-to-state operator is proved. The authors establish the existence of an optimal control in the presence of control constraints, and they provide an optimality system which consists of the forward problem, an adjoint system and a variational inequality.

Heinkenschloss and Sachs [73] use these results as a starting point to set up a projected Newton method. They discuss the implementation of the proposed algorithm and present numerical results. Later, Heinkenschloss and Tröltzsch [74] extend this approach and prove convergence of an SQP method for the solution of the proposed control problem subject to control constraints.

Roubíček [142] studies a multidimensional Stefan problem in enthalpy formulation with a radiation boundary condition. The boundary temperature acts as the control in the corresponding optimal control problem which includes state-space constraints for observations of the state in the interior of the domain or on the boundary. The existence of a solution is argued. For the numerical solution of the optimal control problem, the state constraint is removed by a penalty method and an approximation result is established. A finite element discretization in space is combined with the implicit Euler method in time to solve the unconstrained optimal control problem numerically. Roubíček and Verdi [141] study a continuous casting model in enthalpy formulation that includes the Stefan problem as a special case. A cooling intensity coefficient acts as the control on the boundary of the domain. The goal is to minimize a tracking functional for the temperature subject to control constraints of box type and a general state constraint. As in the previously mentioned approach [142], the state constraint is dealt with by a penalty method. The authors prove convergence of the finite element approximation under a stability condition linking the penalty parameter for the state constraint with the spatial discretization parameter and the time step of the implicit Euler method.

In a series of papers [**121**–**124**], Neittaanmäki and Tiba study the optimal control of the two-phase Stefan problem in enthalpy formulation by the heat flux through the domain boundary. The temperature is subject to a box-constraint, which is treated by a regularization approach proposed in [**156**]. The authors prove the solvability of the state-constrained optimal control problem, but do not give numerical results.

3 Motion Planning Subject to Control Constraints

This chapter is mainly devoted to the formal derivation of the first-order optimality system for a control-constrained motion planning problem for the classical two-phase Stefan problem. To set the scene, we first review principles of PDE-constrained optimization problems with control constraints in an abstract setting. We then formulate the motion planning problem as an optimal control problem for a free boundary and proceed by formally deriving first-order necessary optimality conditions using the associated Lagrange functional. The shape calculus tools and transport theorems on which this derivation relies are provided in Appendix A. A brief discussion of the adjoint-based projected gradient method and the limited memory BFGS method that are used to solve the control-constrained optimal control problems closes this chapter.

3.1 Principles of PDE-Constrained Optimization

In this introductory section, we consider an abstract optimal control problem to demonstrate the principles of PDE-constrained optimization problems subject to control constraints. We use the Lagrange formalism to establish

an optimality system on the basis of which the numerical solution of the optimal control problem can be obtained by a suitable algorithm. For more details on this subject, we refer to the extensive literature, in particular to the books by Lions [**107**], Tröltzsch [**157**] and Neittaanmäki et al. [**120**].

Let us focus here on the problem

$$\min_{y \in \mathcal{Y}, u \in \mathcal{U}} J(y, u)$$

s. t.

$$e(y, u) = 0,$$
$$u \in \mathcal{U}_{\text{ad}} \subset \mathcal{U}. \tag{OCPCC}$$

The *state* (*state variable*) y belongs to the state space $\mathcal{Y}$, and the *control* u is an element of the control space $\mathcal{U}$. Typically, $\mathcal{Y}$ and $\mathcal{U}$ are Banach spaces or even Hilbert spaces, depending on the actual problem at hand. The *control constraint* $u \in \mathcal{U}_{\text{ad}}$ restricts the controls to a set of *admissible controls*, $\mathcal{U}_{\text{ad}}$, which is assumed to be a convex subset of the control space $\mathcal{U}$. The state and the control are related by the *state equation* $e(y, u) = 0$, where usually $e : \mathcal{Y} \times \mathcal{U} \to \mathcal{Z}^*$, and $\mathcal{Z}^*$ is the dual of (a Banach space) $\mathcal{Z}$. While the state equation is determined by the specific application under consideration, the *cost functional* $J : \mathcal{Y} \times \mathcal{U} \to \mathbb{R}$ can be chosen to fit the needs of the user. Frequently, this functional is of tracking type, i.e., it aims to bring y as close to a *desired state* y_d as possible.

As in finite-dimensional optimization problems, *first-order necessary optimality conditions* are the basis for solving (OCPCC). An extremely useful tool to obtain these optimality conditions formally is the *Lagrange functional* $\mathcal{L} : \mathcal{Y} \times \mathcal{U} \times \mathcal{Z} \to \mathbb{R}$ which is defined as

$$\mathcal{L}(y, u, p) := J(y, u) - \langle e(y, u), p \rangle_{\mathcal{Z}^*, \mathcal{Z}} \, .$$

The choice of the sign in front of the duality pairing in this definition is not consistent in the literature, some authors prefer a plus sign over the minus. The *adjoint state* p serves as a *Lagrange multiplier* for the state equation. Setting $\mathcal{L}_y \, \delta y = 0$ for all admissible directions of variation δy yields the *adjoint equation*

$$e_y^*(y, u) \, p = J_y(y, u).$$

Note that this equation is always linear in p, even if the state equation is non-linear. The optimality of a control u and a state y is characterized by the variational inequality

$$\langle \mathcal{L}_u, v - u \rangle = \langle J_u(y, u) - e_u^*(y, u) \, p, v - u \rangle \geq 0 \quad \text{for all } v \in \mathcal{U}_{\text{ad}}.$$

The complete first-order optimality system that solutions $\bar{y}, \bar{u}$ of (OCPCC) and the corresponding adjoint state $\bar{p}$ must satisfy is thus given by the nonlinear system

$$e(\bar{y}, \bar{u}) = 0,$$
$$e_y^*(\bar{y}, \bar{u})\,\bar{p} = J_y(\bar{y}, \bar{u}),$$
$$\bar{u} \in \mathcal{U}_{\mathrm{ad}},$$
$$\langle J_u(\bar{y}, \bar{u}) - e_u^*(\bar{y}, \bar{u})\,\bar{p}, v - \bar{u}\rangle \geq 0 \quad \text{for all } v \in \mathcal{U}_{\mathrm{ad}}.$$

Function space oriented optimization methods for the numerical solution of (OCPCC) can be built upon this first-order optimality system, for instance, a projected gradient method or a quasi-Newton method such as the limited memory BFGS method, see Section 3.4.1.

Remark 3.1. (1) If $\mathcal{U}_{\mathrm{ad}} = \mathcal{U}$, i.e., in the absence of control constraints, the above variational inequality is replaced by the *gradient equation*

$$J_u(\bar{y}, \bar{u}) - e_u^*(\bar{y}, \bar{u})\,\bar{p} = 0,$$

and the requirement $\bar{u} \in \mathcal{U}_{\mathrm{ad}}$ is dropped.

(2) As an alternative to the explicit treatment of the control constraint described above, one can (formally) introduce Lagrange multipliers also for the control constraint and solve the resulting Karush-Kuhn-Tucker system, e.g., by an active set strategy [14], see also [157, Sections 2.8 and 2.12.4].

3.2 Motion Planning as an Optimal Control Problem

Motivation. As indicated by Hinze and Ziegenbalg [79], the shape—and consequently the motion—of the interface $\Gamma_I(t)$ strongly influences the outcome of many industrial production processes involving phase change phenomena, as well as the length of a production cycle of such processes. Thus, it is desirable to control the motion of the interface, for instance, by tracking a prescribed trajectory. In addition, it might be important to have the temperature distribution close to a desired temperature profile, e.g., to prevent steel from cooling too slowly or too rapidly.

Problem Setup. We subdivide the boundary of our given hold-all D into two parts, $\partial D = \Gamma_C \cup \Gamma_N$, $\Gamma_C \cap \Gamma_N = \emptyset$. We assume that a certain prescribed heat flux g acts on Γ_N, which might be empty, and that we can control the heat flux u on Γ_C, which we require to be nonempty. For reasons that are
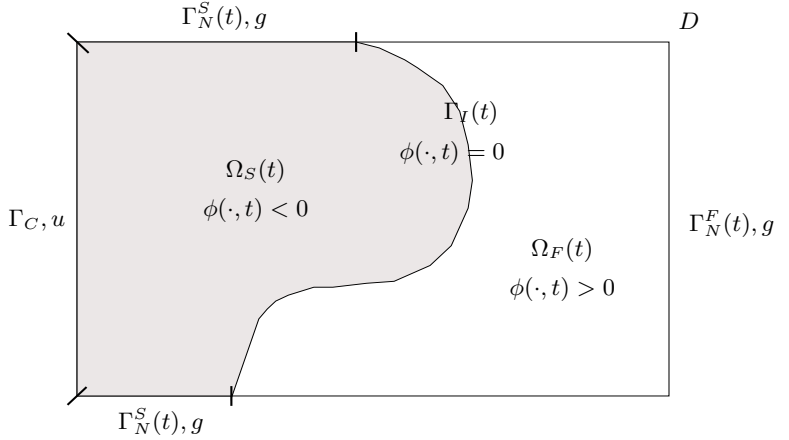
FIGURE 3.1. Setup of geometry for the motion planning problem for the two-phase Stefan problem.

explained in Remark 3.2 below, $\Gamma_I(t)$ must not touch Γ_C, while contact with Γ_N is allowed. Thus, the decomposition of ∂D induces the sets

$$\left.\begin{aligned} \Gamma_C^S := \Gamma_C \cap \partial\Omega_S(t), \quad \Gamma_C^F := \Gamma_C \cap \partial\Omega_F(t), \\ \Gamma_N^S(t) := \Gamma_N \cap \partial\Omega_S(t), \quad \Gamma_N^F(t) := \Gamma_N \cap \partial\Omega_F(t), \end{aligned}\right\} \tag{3.1}$$

see Figure 3.1. The two-phase Stefan problem in level set formulation using the decomposition (3.1) of ∂D reads:

Find a function $y : D \times [0, T] \to \mathbb{R}$ (the temperature) and a function $\phi : D \times [0, T] \to \mathbb{R}$ (the level set function) such that (see Figure 3.1)

$$\rho\, c_S\, y_t - k_S\, \Delta y = f \qquad\qquad \text{in } \Omega_S(t) \tag{3.2a}$$

$$\rho\, c_F\, y_t - k_F\, \Delta y = f \qquad\qquad \text{in } \Omega_F(t) \tag{3.2b}$$

$$y(x, 0) = y_0(x) \qquad\qquad \text{in } D \tag{3.2c}$$

$$k_S\, \tfrac{\partial y}{\partial n} = u \qquad\qquad \text{on } \Gamma_C^S \tag{3.2d}$$

$$k_F\, \tfrac{\partial y}{\partial n} = u \qquad\qquad \text{on } \Gamma_C^F \tag{3.2e}$$

$$k_S\, \tfrac{\partial y}{\partial n} = g \qquad\qquad \text{on } \Gamma_N^S(t) \tag{3.2f}$$

$$k_F\, \tfrac{\partial y}{\partial n} = g \qquad\qquad \text{on } \Gamma_N^F(t) \tag{3.2g}$$

$$y(x, t) = y_M \qquad\qquad \text{on } \Gamma_I(t) \tag{3.2h}$$

$$-\rho\, L\, \phi_t = \left[k\, \nabla y\right]_F^S \cdot \nabla\phi \qquad\qquad \text{on } \Gamma_I(t) \tag{3.2i}$$

$$\phi(x, 0) = \phi_0(x) \qquad\qquad \text{in } D \qquad\qquad (3.2\text{j})$$

on a certain time horizon $[0, T]$.

Throughout this text, we will also refer to (3.2) as the *forward system*.

Remark 3.2. Due to the structure of the adjoint system that is to be devised in Section 3.3, the control u will show a lot of activity at contact points between $\Gamma_I(t)$ and Γ_C. This control behavior might result in the physically meaningless situation that $y < y_M$ in parts of $\Omega_F(t)$ and $y > y_M$ in parts of $\Omega_S(t)$, a contradiction to (2.6). Therefore, we do not allow $\Gamma_I(t)$ to touch Γ_C.

The Optimal Control Problem. In the terminology of Section 3.1, the system (3.2) represents the state equation. The two state variables of (3.2) are the temperature y and the level set function ϕ. As already mentioned, the heat flux u through part of the boundary ∂D acts as the control. The tracking-type cost functional

$$\begin{aligned}
J(y, \phi, u) = {} & \frac{\gamma_1}{2} \int_0^T \int_D |y - y_d|^2 \, dx \, dt + \frac{\gamma_2}{2} \int_0^T \int_{\Gamma_I(t)} |\phi_d|^2 \, ds \, dt \\
& + \frac{\gamma_3}{2} \int_D |y(T) - y_T|^2 \, dx + \frac{\gamma_4}{2} \int_{\Gamma_I(T)} |\phi_T|^2 \, ds \qquad (3.3) \\
& + \frac{\gamma_5}{2} \int_0^T \int_{\Gamma_C} |u|^2 \, ds \, dt
\end{aligned}$$

provides a mathematical description of the control goals stated above. The first two terms aim to control the temperature distribution and the motion of the interface over the control horizon $[0, T]$, while the third and the fourth term monitor the final temperature distribution and the final interface position at terminal time T. The variables $y_d = y_d(x, t)$, $y_T = y_T(x)$, $\phi_d = \phi_d(x, t)$ and $\phi_T = \phi_T(x)$ are referred to as the desired states. Note that ϕ_d and ϕ_T must be functions whose zero level sets represent the desired interface positions. The last term in (3.3) has two meanings. From an application point of view, this term models control costs, while the mathematical reason for adding this term is the regularizing effect it has. We discuss this cost functional in a little more detail at the end of this section.

The motion planning problem we consider is

$$\min_{y, \phi, u} J(y, \phi, u) \quad \text{subject to} \quad (3.2). \qquad\qquad (\text{MPP})$$
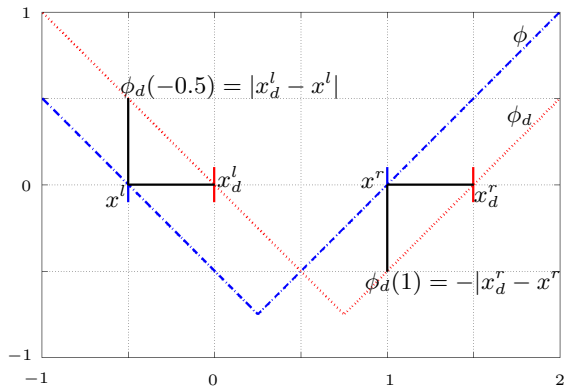
FIGURE 3.2. One-dimensional illustration of the cost functional (3.3).

Remark 3.3. (1) Note that the level set function ϕ carrying the geometric information is a state variable. Thus, (MPP) is an optimal control problem for a free boundary problem, rather than a shape optimization problem.

(2) Obviously, (MPP) has the structure of (OCPCC). This admits the application of the Lagrange formalism introduced in Section 3.1 to derive first-order necessary optimality conditions.

(3) (MPP) does not contain any control constraints. We comment on the inclusion of these in Remark 3.9 at the end of Section 3.3.4.

We treat the optimal control problem (MPP) by an "optimize-then-discretize" approach, meaning that we derive the first-order necessary optimality conditions in a continuous framework (Section 3.3). The coupled partial differential equations in the forward and the adjoint systems that are part of these optimality conditions are discretized afterwards (Chapter 4).

How to Choose the Desired States ϕ_d and ϕ_T? The description of the desired interface motion via the desired states ϕ_d and ϕ_T is of course not unique. Any function whose zero level sets reproduce the desired interface motion can be used in the cost functional (3.3). However, there are specific choices of ϕ_d and ϕ_T with a natural meaning, namely, the signed distance

functions to the desired interface positions. In this case, the terms

$$\int_{\Gamma_I(t)} |\phi_d|^2 \, ds \quad \text{and} \quad \int_{\Gamma_I(T)} |\phi_T|^2 \, ds$$

express the accumulated squared distance of the current interface from the desired interface at time $t \in [0, T]$, see Figure 3.2 for a one-dimensional illustration. Note that this is independent of the choice of ϕ away from $\Gamma_I(t)$.

Potential Reformulations of the Cost Functional. Following ideas of Dziuk and Elliott [50], a potential reformulation of the cost functional (3.3) is devised as follows. Since $\phi = 0$ on $\Gamma_I(t)$, we have

$$\int_{\Gamma_I(t)} |\phi_d|^2 \, ds = \int_{\Gamma_I(t)} |\phi - \phi_d|^2 \, ds.$$

Moreover,

$$\int_{\inf_D \phi}^{\sup_D \phi} \int_{\{\phi=r\}} |\phi - \phi_d|^2 \, ds \, dr = \int_D |\phi - \phi_d|^2 \, |\nabla \phi| \, dx$$

by the coarea formula [50]. To restrict the observations to a neighborhood of the current interface, the integrand $|\phi - \phi_d|^2 \, |\nabla \phi|$ is multiplied by a proper density function, e.g., $\delta(\phi)$, see [130, Section 1.5]. The resulting contribution to the cost functional (3.3) is then given by

$$\int_D \delta(\phi) \, |\phi - \phi_d|^2 \, |\nabla \phi| \, dx,$$

and a similar formula can be established for the interface tracking term at final time T. Thus, the cost functional (3.3) can be rewritten as a functional involving only tracking terms that are defined on all of the hold-all D. As we shall see in the next section, cost functionals of this type are not suitable for motion planning in the level set formulation. The reason is that the resulting forcing terms that these reformulated cost functionals contribute to the adjoint level set equation are defined also away from the interface.

Another conceivable reformulation of the cost functional (3.3) includes terms that relate the length—or some other geometric quantity—of the current interface to the same quantity of the desired interface. The motivation for including such terms is that (3.3) can also be decreased by forcing $\Gamma_I(t)$ to disappear. Numerical experiments with several different cost functionals incorporating the length of $\Gamma_I(t)$ have indicated that these modifications do not have the desired effect. Rather, a proper choice of the weights in (3.3) prevents $\Gamma_I(t)$ from disappearing and paves the way for the desired interface tracking. The Mumford-Shah functional [118] which is used in image segmentation is based on a regularization idea that is, in a certain sense,

complementary to the discussed modifications of the cost functional (3.3). In this functional, the length of the curve representing edges in the image is used as a penalty term to prevent this curve from getting too long and from developing fractal structures.

3.3 Derivation of the Optimality System

In this section, we derive first-order optimality conditions for (MPP) in the absence of control constraints. As argued in Section 2.4, no global-in-time existence results for classical solutions of the two-phase Stefan problem in level set formulation are available. As a consequence, the subsequent treatment of the optimal control problem (MPP) is only formal. In particular, the existence of solutions of (MPP) is assumed and can not currently be proved.

We assume that each choice of the control u induces unique states $y(u)$ and $\phi(u)$. Plugging these new quantities into the cost functional of (MPP) leads us to the unconstrained problem

$$\min_{u} \widehat{J}(u)$$

for the reduced cost functional $\widehat{J}(u) := J(y(u), \phi(u), u)$. To compute the gradient of $\widehat{J}(u)$, we introduce the Lagrange functional to (MPP). (Here and in Sections 3.3.1–3.3.4, we omit the ds, dx and dt for the sake of brevity.)

$$
\begin{aligned}
\mathcal{L}(y, \, \phi, \, u, \, p, \, p_S^C, \, p_F^C, \, p_S^N, \, p_F^N, \, p_I, \, \psi) = {} & J(y, \phi, u) - \int_0^T \int_D (-f)\, p \\
& - \int_0^T \int_{\Omega_S(t)} \left(\rho\, c_S\, y_t - k_S\, \Delta y\right) p - \int_0^T \int_{\Omega_F(t)} \left(\rho\, c_F\, y_t - k_F\, \Delta y\right) p \\
& - \int_0^T \int_{\Gamma_N^S(t)} \left(k_S\, \tfrac{\partial y}{\partial n} - g\right) p_S^N - \int_0^T \int_{\Gamma_C^S} \left(k_S\, \tfrac{\partial y}{\partial n} - u\right) p_S^C \\
& - \int_0^T \int_{\Gamma_N^F(t)} \left(k_F\, \tfrac{\partial y}{\partial n} - g\right) p_F^N - \int_0^T \int_{\Gamma_C^F} \left(k_F\, \tfrac{\partial y}{\partial n} - u\right) p_F^C \\
& - \int_0^T \int_{\Gamma_I(t)} (y - y_M)\, p_I - \int_0^T \int_{\Gamma_I(t)} \left(\rho\, L\, \phi_t + \left[k\, \nabla y\right]_F^S \cdot \nabla \phi\right) \psi.
\end{aligned}
\tag{3.4}
$$

The adjoint system is obtained by setting $\mathcal{L}_y(\cdot) = \mathcal{L}_\phi(\cdot) = 0$, as explained in Section 3.1. Note that we demand the conditions

$$y(x, 0) = y_0(x), \tag{3.2c}$$

$$\phi(x, 0) = \phi_0(x) \tag{3.2j}$$

explicitly. This means that when calculating the derivatives $\mathcal{L}_y \, \delta y$ (in Section 3.3.1) and $\mathcal{L}_\phi \, \delta \phi$ (in Section 3.3.2), we have to require

$$\delta y(x,0) = \delta \phi(x,0) = 0$$

for the directions of variation.

3.3.1. The Adjoint Temperature

The derivation of the adjoint heat equation is rather straightforward. We apply the chain rule to the quadratic contributions of the cost functional and replace y by δy in those parts that the temperature enters linearly:

$$
\begin{aligned}
\mathcal{L}_y \, \delta y = {}& \int_0^T \int_D \gamma_1 \, (y - y_d) \, \delta y + \int_D \gamma_3 \, (y(T) - y_T) \, \delta y(T) \\
& - \int_0^T \int_{\Omega_S(t)} \left(\rho \, c_S \, \delta y_t - k_S \, \Delta \delta y \right) p - \int_0^T \int_{\Omega_F(t)} \left(\rho \, c_F \, \delta y_t - k_F \, \Delta \delta y \right) p \\
& - \int_0^T \int_{\Gamma_N^S(t)} k_S \, \frac{\partial \delta y}{\partial n} \, p_S^N - \int_0^T \int_{\Gamma_C^S} k_S \, \frac{\partial \delta y}{\partial n} \, p_S^C \\
& - \int_0^T \int_{\Gamma_N^F(t)} k_F \, \frac{\partial \delta y}{\partial n} \, p_F^N - \int_0^T \int_{\Gamma_C^F} k_F \, \frac{\partial \delta y}{\partial n} \, p_F^C \\
& - \int_0^T \int_{\Gamma_I(t)} \delta y \, p_I - \int_0^T \int_{\Gamma_I(t)} \psi \, \left[k \, \nabla \delta y \right]_F^S \cdot \nabla \phi.
\end{aligned}
$$

To obtain the adjoint heat equation in strong form, we have to move the spatial and the temporal derivatives from the direction of variation δy to the adjoint state p. To this end, we apply integration by parts in each of the phases, once with respect to time (see Corollary A.11) and twice with respect to space (by using Green's formula):

$$
\begin{aligned}
\mathcal{L}_y \, \delta y = {}& \int_0^T \int_D \gamma_1 \, (y - y_d) \, \delta y + \int_D \gamma_3 \, (y(T) - y_T) \, \delta y(T) \\
& - \int_{\Omega_S(T)} \rho \, c_S \, \delta y(T) \, p(T) + \int_{\Omega_S(0)} \rho \, c_S \, \delta y(0) \, p(0) \\
& + \int_0^T \int_{\Omega_S(t)} \rho \, c_S \, p_t \, \delta y + \int_0^T \int_{\partial \Omega_S(t)} \rho \, c_S \, \delta y \, p \, v_S \\
& + \int_0^T \int_{\partial \Omega_S(t)} k_S \, \frac{\partial \delta y}{\partial n} \, p - \int_0^T \int_{\Omega_S(t)} k_S \, \nabla \delta y \nabla p \\
& - \int_{\Omega_F(T)} \rho \, c_F \, \delta y(T) \, p(T) + \int_{\Omega_F(0)} \rho \, c_F \, \delta y(0) \, p(0)
\end{aligned}
$$

$$+ \int_0^T \int_{\Omega_F(t)} \rho\, c_F\, p_t\, \delta y + \int_0^T \int_{\partial\Omega_F(t)} \rho\, c_F\, \delta y\, p\, v_F$$

$$+ \int_0^T \int_{\partial\Omega_F(t)} k_F \frac{\partial \delta y}{\partial n}\, p - \int_0^T \int_{\Omega_F(t)} k_F\, \nabla\delta y \nabla p$$

$$- \int_0^T \int_{\Gamma_N^S(t)} k_S \frac{\partial \delta y}{\partial n}\, p_S^N - \int_0^T \int_{\Gamma_C^S} k_S \frac{\partial \delta y}{\partial n}\, p_S^C$$

$$- \int_0^T \int_{\Gamma_N^F(t)} k_F \frac{\partial \delta y}{\partial n}\, p_F^N - \int_0^T \int_{\Gamma_C^F} k_F \frac{\partial \delta y}{\partial n}\, p_F^C$$

$$- \int_0^T \int_{\Gamma_I(t)} \delta y\, p_I - \int_0^T \int_{\Gamma_I(t)} \psi\, \big[k\, \nabla\delta y\big]_F^S \cdot \nabla\phi$$

$$= \int_0^T \int_D \gamma_1\, (y - y_d)\, \delta y + \int_D \gamma_3\, (y(T) - y_T)\, \delta y(T)$$

$$- \int_{\Omega_S(T)} \rho\, c_S\, \delta y(T)\, p(T) + \int_{\Omega_S(0)} \rho\, c_S\, \delta y(0)\, p(0)$$

$$+ \int_0^T \int_{\Omega_S(t)} \rho\, c_S\, p_t\, \delta y + \int_0^T \int_{\Gamma_I(t)} \rho\, c_S\, \delta y\, p\, \vec{V} \cdot n$$

$$+ \int_0^T \int_{\partial\Omega_S(t)} k_S \frac{\partial \delta y}{\partial n}\, p - \int_0^T \int_{\partial\Omega_S(t)} k_S \frac{\partial p}{\partial n}\, \delta y$$

$$+ \int_0^T \int_{\Omega_S(t)} k_S\, \Delta p\, \delta y - \int_{\Omega_F(T)} \rho\, c_F\, \delta y(T)\, p(T)$$

$$+ \int_{\Omega_F(0)} \rho\, c_F\, \delta y(0)\, p(0) + \int_0^T \int_{\Omega_F(t)} \rho\, c_F\, p_t\, \delta y$$

$$- \int_0^T \int_{\Gamma_I(t)} \rho\, c_F\, \delta y\, p\, \vec{V} \cdot n + \int_0^T \int_{\partial\Omega_F(t)} k_F \frac{\partial \delta y}{\partial n}\, p$$

$$- \int_0^T \int_{\partial\Omega_F(t)} k_F \frac{\partial p}{\partial n}\, \delta y + \int_0^T \int_{\Omega_F(t)} k_F\, \Delta p\, \delta y$$

$$- \int_0^T \int_{\Gamma_N^S(t)} k_S \frac{\partial \delta y}{\partial n}\, p_S^N - \int_0^T \int_{\Gamma_C^S} k_S \frac{\partial \delta y}{\partial n}\, p_S^C$$

$$- \int_0^T \int_{\Gamma_N^F(t)} k_F \frac{\partial \delta y}{\partial n}\, p_F^N - \int_0^T \int_{\Gamma_C^F} k_F \frac{\partial \delta y}{\partial n}\, p_F^C$$

$$- \int_0^T \int_{\Gamma_I(t)} \delta y\, p_I - \int_0^T \int_{\Gamma_I(t)} \psi\, \big[k\, \nabla\delta y\big]_F^S \cdot \nabla\phi.$$

Here, v_S and v_F denote the normal velocities that arise in Corollary A.11 applied to integration in $\Omega_S(t)$ and $\Omega_F(t)$, respectively. Note that we have used the properties

$$v_S = v_F = 0 \quad \text{on } \partial D \quad \text{and} \quad v_S = \vec{V} \cdot n, \ v_F = -\vec{V} \cdot n \quad \text{on } \Gamma_I(t),$$

which state that the boundary of the hold-all D is fixed and, thus, does not move, and that the velocity fields in Corollary A.11 are determined by the Stefan condition (2.4) on the moving interface $\Gamma_I(t)$.

Sorting the terms in the last formula for $\mathcal{L}_y \, \delta y$ corresponding to their domain of integration and using $\delta y(x,0) = 0$ and $n \overset{(2.9)}{=} \frac{\nabla \phi}{|\nabla \phi|}$ on $\Gamma_I(t)$, we find the following condition for the adjoint temperature p:

$$
\begin{aligned}
0 = &\int_0^T \int_{\Omega_S(t)} \left(\rho \, c_S \, p_t + k_S \, \Delta p + \gamma_1 \, (y - y_d) \right) \delta y \\
&+ \int_0^T \int_{\Omega_F(t)} \left(\rho \, c_F \, p_t + k_F \, \Delta p + \gamma_1 \, (y - y_d) \right) \delta y \\
&- \int_{\Omega_S(T)} \left(\rho \, c_S \, p(T) - \gamma_3 \, (y(T) - y_T) \right) \delta y(T) \\
&- \int_{\Omega_F(T)} \left(\rho \, c_F \, p(T) - \gamma_3 \, (y(T) - y_T) \right) \delta y(T) \\
&+ \int_0^T \int_{\Gamma_N^S(t)} \left(-k_S \tfrac{\partial p}{\partial n} \right) \delta y + k_S \tfrac{\partial \delta y}{\partial n} (p - p_S^N) \\
&+ \int_0^T \int_{\Gamma_C^S} \left(-k_S \tfrac{\partial p}{\partial n} \right) \delta y + k_S \tfrac{\partial \delta y}{\partial n} (p - p_S^C) \\
&+ \int_0^T \int_{\Gamma_N^F(t)} \left(-k_F \tfrac{\partial p}{\partial n} \right) \delta y + k_F \tfrac{\partial \delta y}{\partial n} (p - p_F^N) \\
&+ \int_0^T \int_{\Gamma_C^F} \left(-k_F \tfrac{\partial p}{\partial n} \right) \delta y + k_F \tfrac{\partial \delta y}{\partial n} (p - p_F^C) \\
&+ \int_0^T \int_{\Gamma_I(t)} \left(\rho \, c_S \, p \, \vec{V} \cdot n - \rho \, c_F \, p \, \vec{V} \cdot n - k_S \tfrac{\partial p}{\partial n} + k_F \tfrac{\partial p}{\partial n} - p_I \right) \delta y \\
&+ \int_0^T \int_{\Gamma_I(t)} \left(p - \psi \, |\nabla \phi| \right) \left[k \, \nabla \delta y \right]_F^S \cdot n \qquad \text{for all } \delta y.
\end{aligned}
$$

By altering the directions of variation δy properly, we eliminate certain terms from this last equation step by step. This process finally yields the equations

$$-\rho\,c_S\,p_t - k_S\,\Delta p = \gamma_1\,(y - y_d) \qquad \text{in } \Omega_S(t)$$

$$-\rho\,c_F\,p_t - k_F\,\Delta p = \gamma_1\,(y - y_d) \qquad \text{in } \Omega_F(t)$$

$$\rho\,c_S\,p(T) = \gamma_3(y(T) - y_T) \qquad \text{in } \Omega_S(T)$$

$$\rho\,c_F\,p(T) = \gamma_3(y(T) - y_T) \qquad \text{in } \Omega_F(T)$$

$$p_S^C = p, \quad k_S\,\tfrac{\partial p}{\partial n} = 0 \qquad \text{on } \Gamma_C^S$$

$$p_F^C = p, \quad k_F\,\tfrac{\partial p}{\partial n} = 0 \qquad \text{on } \Gamma_C^F$$

$$p_S^N = p, \quad k_S\,\tfrac{\partial p}{\partial n} = 0 \qquad \text{on } \Gamma_N^S(t)$$

$$p_F^N = p, \quad k_F\,\tfrac{\partial p}{\partial n} = 0 \qquad \text{on } \Gamma_N^F(t)$$

$$p_I = \rho\,(c_S - c_F)\,p\,\vec{V}\cdot n - \left[k\,\nabla p\right]_F^S \cdot n \qquad \text{on } \Gamma_I(t)$$

$$p = \psi\,|\nabla\phi| \qquad \text{on } \Gamma_I(t)$$

that characterize the *adjoint temperature* p and the multipliers p_S^C, p_F^C, p_S^N, p_F^N and p_I. Apparently, an equation for the adjoint state ψ is needed to make this system complete.

3.3.2. The Adjoint Level Set Function

The derivation of the adjoint equation to the Stefan condition (3.2i) is by far more involved than the derivation of the adjoint heat equation. This is due to the geometric non-linearity that ϕ introduces into the coupled problem (3.2). In particular, the domains of integration in the Lagrange functional (3.4) depend on ϕ. As a consequence, taking the derivative of this functional with respect to the level set function ϕ requires shape calculus tools. Appendix A provides the necessary background and collects formulæ for taking derivatives of domain and boundary integrals in a level set context.

We denote by $D\,[\![H(\phi); \delta\phi]\!]$ the variation of the functional $H(\cdot)$ in direction $\delta\phi$. Using this notation, the derivative of the Lagrange functional $\mathcal{L}$ in direction $\delta\phi$ is given by

$$\mathcal{L}_\phi\,\delta\phi =$$

$$D\,[\![J(y,\phi,u); \delta\phi]\!] - \tag{3.5a}$$

$$D\left[\!\!\left[\int_0^T \int_D (-f)\,p;\ \delta\phi\right]\!\!\right] - \tag{3.5b}$$

$$D\left[\!\!\left[\int_0^T \int_{\Omega_S(t)} \left(\rho\,c_S\,y_t - k_S\,\Delta y\right)p;\ \delta\phi\right]\!\!\right] - \tag{3.5c}$$

$$D \left[\!\!\left[\int_0^T \int_{\Omega_F(t)} \left(\rho \, c_F \, y_t - k_F \, \Delta y \right) p; \, \delta\phi \right]\!\!\right] - \tag{3.5d}$$

$$D \left[\!\!\left[\int_0^T \int_{\Gamma_N^S(t)} \left(k_S \tfrac{\partial y}{\partial n} - g \right) p + \int_0^T \int_{\Gamma_N^F(t)} \left(k_F \tfrac{\partial y}{\partial n} - g \right) p; \, \delta\phi \right]\!\!\right] - \tag{3.5e}$$

$$D \left[\!\!\left[\int_0^T \int_{\Gamma_C^S} \left(k_S \tfrac{\partial y}{\partial n} - u \right) p + \int_0^T \int_{\Gamma_C^F} \left(k_F \tfrac{\partial y}{\partial n} - u \right) p; \, \delta\phi \right]\!\!\right] - \tag{3.5f}$$

$$D \left[\!\!\left[\int_0^T \int_{\Gamma_I(t)} \left(y - y_M \right) p_I; \, \delta\phi \right]\!\!\right] - \tag{3.5g}$$

$$D \left[\!\!\left[\int_0^T \int_{\Gamma_I(t)} \left(\rho \, L \, \phi_t + \left[k \, \nabla y \right]_F^S \cdot \nabla\phi \right) \psi; \, \delta\phi \right]\!\!\right]. \tag{3.5h}$$

We now analyze the contributions (3.5a)–(3.5h) step by step.

$\boxed{(3.5\text{a})}$ In the cost functional J, the domain integrals for tracking a desired temperature profile and the control cost term do not depend on ϕ. The remaining two terms are of boundary integral type, calling for an application of (A.13). Consequently, the contributions of the cost functional are

$$D \left[\!\!\left[\frac{\gamma_1}{2} \int_0^T \int_D |y - y_d|^2 + \frac{\gamma_3}{2} \int_D |y(T) - y_T|^2; \, \delta\phi \right]\!\!\right]$$

$$+ D \left[\!\!\left[\frac{\gamma_2}{2} \int_0^T \int_{\Gamma_I(t)} |\phi_d|^2 + \frac{\gamma_4}{2} \int_{\Gamma_I(T)} |\phi_T|^2 + \frac{\gamma_5}{2} \int_0^T \int_{\Gamma_C} |u|^2; \, \delta\phi \right]\!\!\right]$$

$$= D \left[\!\!\left[\frac{\gamma_2}{2} \int_0^T \int_{\Gamma_I(t)} |\phi_d|^2 + \frac{\gamma_4}{2} \int_{\Gamma_I(T)} |\phi_T|^2; \, \delta\phi \right]\!\!\right]$$

$$= -\frac{\gamma_2}{2} \int_0^T \int_{\Gamma_I(t)} \frac{\delta\phi}{|\nabla\phi|} \left(\frac{\partial}{\partial n} \left(|\phi_d|^2 \right) + \kappa \, |\phi_d|^2 \right)$$

$$- \frac{\gamma_4}{2} \int_{\Gamma_I(T)} \frac{\delta\phi(T)}{|\nabla\phi|} \left(\frac{\partial}{\partial n} \left(|\phi_T|^2 \right) + \kappa \, |\phi_T|^2 \right). \qquad \diamond$$

$\boxed{(3.5\text{b})}$ The heat source f is integrated against the adjoint temperature p over all of the hold-all. Obviously, this term is independent of ϕ and, thus, does not contribute to the variation of the Lagrange functional with ϕ.

$\diamond$

$\boxed{(3.5c)}$ The heat balance in the solid phase enters the Lagrange functional as a domain integral. According to (A.10), its variation evaluates to

$$(3.5c) = -\int_0^T \int_{\partial\Omega_S(t)} \frac{\delta\phi}{|\nabla\phi|} \left(\rho\, c_S\, y_t - k_S\, \Delta y\right) p$$

$$= -\int_0^T \int_{\Gamma_I(t)} \frac{\delta\phi}{|\nabla\phi|} \left(\rho\, c_S\, y_t - k_S\, \Delta y\right) p = -\int_0^T \int_{\Gamma_I(t)} \frac{\delta\phi}{|\nabla\phi|} f\, p,$$

where we have used that $\delta\phi = 0$ on ∂D in the second equality, and the last equality holds in the sense of a trace because of (3.2a). $\diamond$

$\boxed{(3.5d)}$ Along the same lines as for (3.5c), we derive an expression for the variation of the heat balance in the fluid phase. Note that there is a change of sign because the geometric variation introduced by $\delta\phi$ is just in the opposite direction compared to the solid phase.

$$(3.5d) = \int_0^T \int_{\Omega_F(t)} \frac{\delta\phi}{|\nabla\phi|} \left(\rho\, c_F\, y_t - k_F\, \Delta y\right) p$$

$$= \int_0^T \int_{\Gamma_I(t)} \frac{\delta\phi}{|\nabla\phi|} \left(\rho\, c_F\, y_t - k_F\, \Delta y\right) p = \int_0^T \int_{\Gamma_I(t)} \frac{\delta\phi}{|\nabla\phi|} f\, p,$$

where the last equality holds in the sense of a trace because of (3.2b). $\diamond$

$\boxed{(3.5e) \text{ and } (3.5f)}$ To have an admissible velocity field for the speed method, we require $\delta\phi = 0$ on ∂D in accordance with Remark A.6. Thus, (3.5e) is identically zero. In addition, the integrands and the domains of integration in (3.5f) are independent of ϕ. Similarly to (3.5b), (3.5f) does not contribute to the variation of the Lagrange functional with ϕ. $\diamond$

$\boxed{(3.5g) \text{ and } (3.5h)}$ To evaluate (3.5g) and (3.5h), we have to assume that the multiplier p_I, the adjoint state ψ and the jump of the temperature gradient $\left[k\,\nabla y\right]_F^S$ are defined on all of D, i.e., we interpret these terms as restrictions of globally defined quantities to $\Gamma_I(t)$. Otherwise the standard shape calculus tools from Appendix A are not applicable.

Based on this assumption it is straightforward to compute the contribution of the interface condition (3.2h) by (A.13):

$$(3.5g) = -\int_0^T \int_{\Gamma_I(t)} \frac{\delta\phi}{|\nabla\phi|} \left(\frac{\partial\big((y - y_M)\, p_I\big)}{\partial n} + \kappa\,(y - y_M)\, p_I \right)$$

$$\overset{\text{by (3.2h)}}{=} -\int_0^T \int_{\Gamma_I(t)} \frac{\delta\phi}{|\nabla\phi|} \frac{\partial}{\partial n}\big((y - y_M)\, p_I\big)$$

$$\overset{\text{by (3.2h)}}{=} -\int_0^T \int_{\Gamma_I(t)} \frac{\delta\phi}{|\nabla\phi|} \frac{\partial(y - y_M)}{\partial n} p_I = -\int_0^T \int_{\Gamma_I(t)} \frac{\delta\phi}{|\nabla\phi|} \frac{\partial y}{\partial n} p_I.$$

Remark 3.4 (Including the Gibbs-Thomson Correction). If the isothermal interface condition (3.2h) is replaced by the Gibbs-Thomson correction (2.13), differentiation of the corresponding term in the Lagrange functional with respect to ϕ requires differentiating the curvature κ. The relation (2.10) can be used as a starting point in this case.

We now apply the chain rule (A.14) to (3.5h). Since the integrand is of the form $\psi\, A(\phi + \delta\phi)$ with a linear operator A, we infer:

$$\begin{aligned}
(3.5\text{h}) = {}& -\int_0^T \int_{\Gamma_I(t)} \frac{\delta\phi}{|\nabla\phi|} \left(\frac{\partial}{\partial n}\big((\rho\,L\,\phi_t + \big[k\,\nabla y\big]_F^S \cdot \nabla\phi)\,\psi\big) \right. \\
& \left. + \kappa\,(\rho\,L\,\phi_t + \big[k\,\nabla y\big]_F^S \cdot \nabla\phi)\,\psi \right) \\
& + \int_0^T \int_{\Gamma_I(t)} (\rho\,L\,\delta\phi_t + k_S\nabla y \cdot \nabla\delta\phi - k_F\,\nabla y \cdot \nabla\delta\phi)\,\psi \\
\overset{\text{by (3.2i)}}{=} {}& -\int_0^T \int_{\Gamma_I(t)} \frac{\delta\phi}{|\nabla\phi|} \frac{\partial}{\partial n}(\rho\,L\,\phi_t + \big[k\,\nabla y\big]_F^S \cdot \nabla\phi)\,\psi \\
& + \int_0^T \int_{\Gamma_I(t)} (\rho\,L\,\delta\phi_t + \big[k\,\nabla y\big]_F^S \cdot \nabla\delta\phi)\,\psi. \qquad (3.6)
\end{aligned}$$

Remark 3.5. Note that if we use a constant extension of the velocity $\vec{V}$ to all of D, (3.6) can be further simplified. In this case, the level set equation (2.8) holds and, therefore, the normal derivative of its restriction to $\Gamma_I(t)$ vanishes:

$$\frac{\partial}{\partial n}(\rho\,L\,\phi_t + \big[k\,\nabla y\big]_F^S \cdot \nabla\phi) = 0.$$

As a consequence, we have

$$(3.5\text{h}) = \int_0^T \int_{\Gamma_I(t)} (\rho\,L\,\delta\phi_t + \big[k\,\nabla y\big]_F^S \cdot \nabla\delta\phi)\,\psi.$$

To obtain the adjoint Stefan condition, we have to move the derivatives in (3.6) from the direction of variation $\delta\phi$ to the adjoint state ψ. Because we assume ψ to be globally defined, the integrand in (3.6) is globally defined as well. Thus, Corollary A.13 is applicable, and in conjunction with (2.7) it

implies

$$
\int_0^T \int_{\Gamma_I(t)} \rho\, L\, \delta\phi_t\, \psi = \int_{\Gamma_I(T)} \rho\, L\, \delta\phi\, \psi - \int_{\Gamma_I(0)} \rho\, L\, \delta\phi\, \psi
$$

$$
- \int_0^T \int_{\Gamma_I(t)} \rho\, L\, \delta\phi\, \psi_t + \nabla(\rho\, L\, \delta\phi\, \psi)\cdot \vec{V} + \rho\, L\, \delta\phi\, \psi\, \mathrm{div}_{\Gamma_I(t)}\, \vec{V}
$$

$$
= \int_{\Gamma_I(T)} \rho\, L\, \delta\phi\, \psi - \int_{\Gamma_I(0)} \rho\, L\, \delta\phi\, \psi - \int_0^T \int_{\Gamma_I(t)} \rho\, L\, \delta\phi\, \psi_t
$$

$$
- \int_0^T \int_{\Gamma_I(t)} \delta\phi\, \rho\, L\, \left(\nabla\psi\cdot\vec{V} + \psi\, \mathrm{div}_{\Gamma_I(t)}\, \vec{V} \right)
$$

$$
- \int_0^T \int_{\Gamma_I(t)} \rho\, L\, \psi\, \nabla\delta\phi \cdot \vec{V}.
$$

Fortunately, the last term in this equation cancels with those parts of (3.6) that contain $\nabla\delta\phi$:

$$
-\rho\, L\, \psi\, \nabla\delta\phi\cdot\vec{V} + \psi\left[k\,\nabla y\right]_F^S \cdot \nabla\delta\phi
$$

$$
\overset{\text{by (2.7)}}{=} \psi\left(-\left[k\,\nabla y\right]_F^S \cdot \nabla\delta\phi + \left[k\,\nabla y\right]_F^S \cdot \nabla\delta\phi \right) = 0. \qquad \diamond
$$

Finally, we collect all contributions (3.5a)–(3.5h). Using $\delta\phi(x,0)=0$, we end up with the following expression for the derivative of the Lagrange functional $\mathcal{L}$ in direction $\delta\phi$:

$$
\mathcal{L}_\phi\, \delta\phi = -\frac{\gamma_2}{2} \int_0^T \int_{\Gamma_I(t)} \frac{\delta\phi}{|\nabla\phi|} \left(\frac{\partial}{\partial n}\left(|\phi_d|^2\right) + \kappa\,|\phi_d|^2 \right)
$$

$$
- \frac{\gamma_4}{2} \int_{\Gamma_I(T)} \frac{\delta\phi(T)}{|\nabla\phi|} \left(\frac{\partial}{\partial n}\left(|\phi_d(T)|^2\right) + \kappa\,|\phi_d(T)|^2 \right)
$$

$$
+ \int_0^T \int_{\Gamma_I(t)} \frac{\delta\phi}{|\nabla\phi|} f\, p - \int_0^T \int_{\Gamma_I(t)} \frac{\delta\phi}{|\nabla\phi|} f\, p + \int_0^T \int_{\Gamma_I(t)} \frac{\delta\phi}{|\nabla\phi|} \frac{\partial y}{\partial n}\, p_I
$$

$$
+ \int_0^T \int_{\Gamma_I(t)} \frac{\delta\phi}{|\nabla\phi|} \frac{\partial}{\partial n}(\rho\, L\, \phi_t + \left[k\,\nabla y\right]_F^S \cdot \nabla\phi)\, \psi
$$

$$
- \left\{ \int_{\Gamma_I(T)} \rho\, L\, \delta\phi\, \psi - \int_{\Gamma_I(0)} \rho\, L\, \delta\phi\, \psi - \int_0^T \int_{\Gamma_I(t)} \rho\, L\, \delta\phi\, \psi_t \right.
$$

$$
\left. - \int_0^T \int_{\Gamma_I(t)} \delta\phi\, \rho\, L\, \left(\nabla\psi\cdot\vec{V} + \psi\, \mathrm{div}_{\Gamma_I(t)}\, \vec{V} \right) \right\}
$$

$$
= -\frac{\gamma_2}{2} \int_0^T \int_{\Gamma_I(t)} \frac{\delta\phi}{|\nabla\phi|} \left(\frac{\partial}{\partial n}\left(|\phi_d|^2\right) + \kappa\,|\phi_d|^2 \right) + \int_0^T \int_{\Gamma_I(t)} \frac{\delta\phi}{|\nabla\phi|} \frac{\partial y}{\partial n}\, p_I
$$

$$+ \int_0^T \int_{\Gamma_I(t)} \frac{\delta\phi}{|\nabla\phi|} \frac{\partial}{\partial n} \left(\rho\, L\, \phi_t + \left[k\, \nabla y\right]_F^S \cdot \nabla\phi\right) \psi$$

$$+ \int_0^T \int_{\Gamma_I(t)} \rho\, L\, \delta\phi\, \psi_t + \int_0^T \int_{\Gamma_I(t)} \delta\phi\, \rho\, L\, \left(\nabla\psi \cdot \vec{V} + \psi\, \mathrm{div}_{\Gamma_I(t)}\, \vec{V}\right)$$

$$- \frac{\gamma_4}{2} \int_{\Gamma_I(T)} \frac{\delta\phi(T)}{|\nabla\phi|} \left(\frac{\partial}{\partial n}\left(|\phi_d(T)|^2\right) + \kappa\, |\phi_d(T)|^2\right) - \int_{\Gamma_I(T)} \rho\, L\, \delta\phi\, \psi.$$

Requiring $\mathcal{L}_\phi\, \delta\phi = 0$ for all admissible directions $\delta\phi$ results in the *adjoint Stefan condition*:

$$-\rho\, L\, |\nabla\phi|\, \psi_t = -\frac{\gamma_2}{2} \left(\frac{\partial}{\partial n}\left(|\phi_d|^2\right) + \kappa\, |\phi_d|^2\right) + \frac{\partial y}{\partial n}\, p_I + |\nabla\phi|\, \rho\, L\, \nabla\psi \cdot \vec{V}$$

$$+ \psi\left[\frac{\partial}{\partial n}(\rho\, L\, \phi_t + \left[k\, \nabla y\right]_F^S \cdot \nabla\phi) + |\nabla\phi|\, \rho\, L\, \mathrm{div}_{\Gamma_I(t)}\, \vec{V}\right],$$

$$\psi(T) = -\frac{1}{\rho\, L\, |\nabla\phi|} \frac{\gamma_4}{2} \left(\frac{\partial}{\partial n}\left(|\phi_T|^2\right) + \kappa\, |\phi_T|^2\right).$$

Note that $\vec{V}$ is constant in normal direction by construction. This implies

$$\mathrm{div}_{\Gamma_I(t)}\, \vec{V} = \mathrm{div}\, \vec{V} \tag{3.7}$$

by Definition A.8. In combination with Remark 3.5, (3.7) can be used to further simplify this adjoint Stefan condition, and to rewrite it as

$$-\rho\, L\, |\nabla\phi|\, \left(\psi_t + \mathrm{div}(\psi\, \vec{V})\right) = -\frac{\gamma_2}{2} \left(\frac{\partial}{\partial n}\left(|\phi_d|^2\right) + \kappa\, |\phi_d|^2\right) + \frac{\partial y}{\partial n}\, p_I, \quad (3.8\mathrm{a})$$

$$\rho\, L\, |\nabla\phi|\, \psi(T) = -\frac{\gamma_4}{2} \left(\frac{\partial}{\partial n}\left(|\phi_T|^2\right) + \kappa\, |\phi_T|^2\right). \tag{3.8b}$$

Remark 3.6. If we reverse the time direction by setting $t = T - s$, $s \in [0, T]$, and introduce the new variables

$$\Psi(x, s) := \psi(x, T - s), \quad \vec{W} := -\vec{V},$$

the PDE (3.8) can be rewritten as

$$\rho\, L\, |\nabla\phi|\, \left(\dot{\Psi} + \Psi\, \mathrm{div}_{\Gamma_I(t)}\, \vec{W}\right) = -\frac{\gamma_2}{2} \left(\frac{\partial}{\partial n}\left(|\phi_d|^2\right) + \kappa\, |\phi_d|^2\right) + \frac{\partial y}{\partial n}\, p_I,$$

$$\rho\, L\, |\nabla\phi|\, \Psi(0) = -\frac{\gamma_4}{2} \left(\frac{\partial}{\partial n}\left(|\phi_T|^2\right) + \kappa\, |\phi_T|^2\right), \tag{3.9}$$

where $\dot{\Psi} = \Psi_t + \nabla\Psi \cdot \vec{W}$ is the material derivative of Ψ. Equation (3.9) constitutes a first-order PDE on the moving surface $\Gamma_I(t)$.

Note that all derivatives in the first-order conservation law (3.8) on $\Gamma_I(t)$ are globally defined. Moreover, the motion in this equation is purely tangential because of (3.7). Thus, as in the level set method, (3.8) can be directly extended to all of D, or at least to a neighborhood of $\Gamma_I(t)$, by using a constant extension of the terminal condition (3.8b) and the forcing term on the right hand side of (3.8a). We return to this point in Section 4.5.

3.3.3. Summary and Interpretation of the Adjoint Stefan Problem

In summary, the following adjoint system results from setting $\mathcal{L}_y(\cdot) = \mathcal{L}_\phi(\cdot) = 0$.

$$-\rho\,c_S\,p_t - k_S\,\Delta p = \gamma_1\,(y - y_d) \qquad \text{in } \Omega_S(t) \quad (3.10\text{a})$$

$$-\rho\,c_F\,p_t - k_F\,\Delta p = \gamma_1\,(y - y_d) \qquad \text{in } \Omega_F(t) \quad (3.10\text{b})$$

$$\rho\,c_S\,p(T) = \gamma_3(y(T) - y_T) \qquad \text{in } \Omega_S(T) \quad (3.10\text{c})$$

$$\rho\,c_F\,p(T) = \gamma_3(y(T) - y_T) \qquad \text{in } \Omega_F(T) \quad (3.10\text{d})$$

$$p_S^C = p, \quad k_S\,\tfrac{\partial p}{\partial n} = 0 \qquad \text{on } \Gamma_C^S \quad (3.10\text{e})$$

$$p_F^C = p, \quad k_F\,\tfrac{\partial p}{\partial n} = 0 \qquad \text{on } \Gamma_C^F \quad (3.10\text{f})$$

$$p_S^N = p, \quad k_S\,\tfrac{\partial p}{\partial n} = 0 \qquad \text{on } \Gamma_N^S(t) \quad (3.10\text{g})$$

$$p_F^N = p, \quad k_F\,\tfrac{\partial p}{\partial n} = 0 \qquad \text{on } \Gamma_N^F(t) \quad (3.10\text{h})$$

$$p_I = \rho\,[c]_F^S\,p\,\vec{V}\cdot n - [k\,\nabla p]_F^S\cdot n \qquad \text{on } \Gamma_I(t) \quad (3.10\text{i})$$

$$p = \psi\,|\nabla\phi| \qquad \text{on } \Gamma_I(t) \quad (3.10\text{j})$$

$$-\hat{L}\left(\psi_t + \operatorname{div}(\psi\,\vec{V})\right) = \tfrac{\partial y}{\partial n}\,p_I - \tfrac{\gamma_2}{2}\left(\tfrac{\partial}{\partial n}|\phi_d|^2 + \kappa\,|\phi_d|^2\right) \qquad \text{on } \Gamma_I(t) \quad (3.10\text{k})$$

$$\hat{L}\,\psi(T) = -\tfrac{\gamma_4}{2}\left(\tfrac{\partial}{\partial n}|\phi_T|^2 + \kappa\,|\phi_T|^2\right) \qquad \text{on } \Gamma_I(T) \quad (3.10\text{l})$$

$$\hat{L} := \rho\,L\,|\nabla\phi|. \qquad (3.10\text{m})$$

We refer to p and ψ as the *adjoint temperature* and the *adjoint level set function*, respectively. Equations (3.10a)–(3.10h) have a similar structure as the corresponding equations (3.2a)–(3.2g) in the forward system. The only difference is that source terms appear on the right hand sides of (3.10a)–(3.10d). These represent the contributions of the temperature tracking terms in the cost functional. The boundary conditions for p are homogeneous and of Neumann type on all of ∂D. Equation (3.10i) is of Stefan type and states that the multiplier p_I can be expressed in terms of p. $\vec{V}$ is the velocity field with which the interface moves as defined in (2.4). The coupling between the two adjoint states p and ψ is enforced by the adjoint interface condition (3.10j) that completes the adjoint heat equation. Note that this equation plays the

same role as (3.2h) in the forward system. Finally, equations (3.10k)–(3.10l) constitute the adjoint Stefan condition. The forcing terms on the right hand sides of these equations are the contributions of the interface tracking terms in the cost functional J. As expected, the time direction is reversed in the adjoint system.

Remark 3.7. As mentioned above, we call the adjoint state ψ the *adjoint level set function*. The terms *adjoint Stefan condition* and *adjoint level set equation* are used equivalently for the equations (3.10k)–(3.10l) characterizing this adjoint quantity.

3.3.4. The First-Order Optimality System

Now that we have the adjoint system (3.10) at hand, the only missing ingredient of the desired optimality system is the gradient equation which is established by setting $\mathcal{L}_u \, \delta u = 0$. Using the same notation as in Section 3.3.2, we obtain

$$\mathcal{L}_u \, \delta u = D\left[\!\!\left[\frac{\gamma_5}{2} \int_0^T \int_{\Gamma_C} |u|^2; \delta u \right]\!\!\right] - \left(D\left[\!\!\left[\int_0^T \int_{\Gamma_C^S} \left(k_S \frac{\partial y}{\partial n} - u \right) p_S^C; \delta u \right]\!\!\right] \right.$$
$$\left. + D\left[\!\!\left[\int_0^T \int_{\Gamma_C^F} \left(k_F \frac{\partial y}{\partial n} - u \right) p_F^C; \delta u \right]\!\!\right] \right).$$

The first term is the only contribution of the cost functional and evaluates to

$$D\left[\!\!\left[\frac{\gamma_5}{2} \int_0^T \int_{\Gamma_C} |u|^2; \delta u \right]\!\!\right] = \frac{\gamma_5}{2} \int_0^T \int_{\Gamma_C} 2\, u \, \delta u = \int_0^T \int_{\Gamma_C} \gamma_5 \, u \, \delta u.$$

The remaining two terms are the contributions of the corresponding Neumann boundary conditions (3.2d)–(3.2e). By (3.10e)–(3.10f), they can be simplified to

$$D\left[\!\!\left[\int_0^T \int_{\Gamma_C^S} \left(k_S \frac{\partial y}{\partial n} - u \right) p_S^C; \delta u \right]\!\!\right] + D\left[\!\!\left[\int_0^T \int_{\Gamma_C^F} \left(k_F \frac{\partial y}{\partial n} - u \right) p_F^C; \delta u \right]\!\!\right]$$
$$= \int_0^T \int_{\Gamma_C^S} -\delta u \, p_S^C + \int_0^T \int_{\Gamma_C^F} -\delta u \, p_F^C = -\int_0^T \int_{\Gamma_C} \delta u \, p.$$

Thus, we arrive at the gradient equation

$$0 = \gamma_5 \, u + p \qquad\qquad \text{on } \Gamma_C. \qquad\qquad (3.11)$$

In summary, the optimality system of the optimal control problem (MPP) in the absence of control and state constraints is given by

- the forward system (3.2),
- the adjoint system (3.10) and
- the gradient equation (3.11).

Remark 3.8 (A Property of the Optimal Control). If the cost functional does not involve temperature tracking terms at terminal time, i.e., if $\gamma_3 = 0$, the adjoint temperature vanishes at $t = T$. Owing to (3.11), this is true also for the control u.

Remark 3.9 (Including Control Constraints). If the control u is restricted to belong to a convex set $\mathcal{U}_{\mathrm{ad}}$ of admissible controls, the gradient equation (3.11) must be replaced by a variational inequality as described in Section 3.1. In our particular setup this variational inequality has the form

$$\mathcal{L}_u(v - u) = \int_0^T \int_{\Gamma_C} (\gamma_5\, u + p)\,(v - u)\, ds\, dt \geq 0 \quad \forall v \in \mathcal{U}_{\mathrm{ad}}.$$

The adjoint system (3.10) remains unchanged.

3.4   Optimization Methods

In the presence of pointwise control constraints of the form

$$\mathcal{U}_{\mathrm{ad}} = \{\underline{u} \leq u \leq \overline{u}\}, \tag{3.12}$$

we use the *projected gradient method* (see Algorithm 1) to solve (MPP). If there are no control constraints present, (MPP) is solved using the *limited memory BFGS method* (see Algorithm 2). It is well known that gradient-based algorithms exhibit slow convergence. Nonetheless, they are the method of choice to numerically verify that the proposed optimal control approach is reasonable, due to their straightforward implementation. The limited memory BFGS method tries to improve the speed of convergence by preconditioning the gradient direction with a symmetric positive definite matrix which is usually an approximation to (the inverse of) the Hessian. This approximation is updated during the iteration. Thanks to this update strategy, no second order derivatives are needed. For more details on the BFGS method and, in particular, on the application of higher order methods in optimal control, we refer to [127, Chapter 6], [91, Chapter 4] and [78], respectively.

Algorithm 1 Adjoint-Based Projected Gradient Method

Input: u^0
Output: $\widehat{u}, \widehat{y}, \widehat{\phi}, \widehat{p}, \widehat{\psi}$

1: $j = 0$
2: **while** the convergence condition is not fulfilled **do**
3:    Solve the forward problem (3.2) for y^j and ϕ^j.
4:    Solve the adjoint problem (3.10) for p^j and ψ^j.
5:    Construct the descent direction from (3.11)

$$v^j = -(\gamma_5\, u^j + p^j).$$

6:    Determine σ^j from

$$\sigma^j := \arg\min \widehat{J}\big(\mathcal{P}_{[\underline{u},\overline{u}]}\left(u^j + \sigma\, v^j\right)\big).$$

7:    Set $u^{j+1} = \mathcal{P}_{[\underline{u},\overline{u}]}\left(u^j + \sigma^j\, v^j\right)$, $j \to j+1$.
8: **end while**

3.4.1. The Adjoint-Based Projected Gradient Method

Discretization. In each iteration of Algorithm 1, steps 3 and 4 require the solution of the coupled equation systems (3.2) and (3.10). Obviously, these solutions can only be obtained numerically after a suitable discretization. This is discussed in detail in Chapter 4.

The Descent Direction. The choice of the descent direction v^j in step 5 corresponds to the negative gradient, i.e., the direction of steepest descent.

Ensuring Admissibility. The projection $\mathcal{P}_{[\underline{u},\overline{u}]}\left(\cdot\right)$ in steps 6 and 7 ensures that the computed controls are admissible with respect to the pointwise constraint (3.12). The projection is defined as

$$\mathcal{P}_{[\underline{u},\overline{u}]}\left(u\right) = \min\{\overline{u}, \max\{\underline{u}, u\}\}, \tag{3.13}$$

and, as the control constraint, it has to be interpreted in a pointwise sense.

Line Search. Determining the step size σ^j in step 6 is too complicated a task to be solved exactly. Instead, a line search procedure, the Armijo rule with backtracking, is used to determine an approximation to σ^j, see, e.g., [127, Chapter 3].

Initial Guess. Owing to the non-linearity of the two-phase Stefan problem (3.2), the optimal control problem (MPP) is non-convex. Thus we can only expect convergence of Algorithm 1 to stationary points. The initial guess u^0 determines which of these stationary points Algorithm 1 approximates. In all of the numerical examples in Chapter 5, we use the initial guess $u^0 \equiv 0$.

Termination of the Iteration. In addition, the performance of Algorithm 1 is controled by the convergence condition in step 2. We propose to stop the iteration if one of the following criteria is fulfilled:

(1) The control increment is small compared to the initial increment [**91**, p. 93]:

$$\|u^j - u^j_+\| \leq \tau^u_a + \tau^u_r \|u^0 - u^0_+\|. \tag{T1}$$

Here, u^j_+ denotes the update of the control u^j, potentially after applying the projection (3.13). τ^u_a and τ^u_r are absolute and relative tolerances for which we use the default values $\tau^u_a = 10^{-8}, \tau^u_r = 10^{-8}$.

(2) The gradient has been decreased sufficiently [**91**, p. 16]:

$$\|\nabla \widehat{J}(u^j)\| \leq \tau^\nabla_a + \tau^\nabla_r \|\nabla \widehat{J}(u^0)\|. \tag{T2}$$

As in (T1), τ^∇_a and τ^∇_r are absolute and relative tolerances. Here, we use the moderate default values $\tau^\nabla_a = 10^{-4}, \tau^\nabla_r = 10^{-4}$.

(3) The number of iterations exceeds MAXITER:

$$j \geq \text{MAXITER}. \tag{T3}$$

By default, we set MAXITER $= 100$.

(4) The accepted step length is below a predefined tolerance:

$$\sigma^j < \tau^\sigma. \tag{T4}$$

The default value is chosen as $\tau^\sigma = 10^{-7}$.

The last criterion, (T4), implements the advice of Nocedal and Wright [**127**, p. 62] that the line search procedure should include a stopping test if it can not find a better function value after a certain number of trial steps.

3.4.2. The Limited Memory BFGS Method

Algorithm 2 summarizes the limited memory BFGS method we use. The remarks in Section 3.4.1 concerning the discretization, the choice of the initial guess and the termination of the iteration apply to the limited memory BFGS method as well. Some additional issues related to the implementation of Algorithm 2 are the following:

- Step 19 can be implemented with the help of a recursive procedure that computes the matrix vector product $H^j \nabla \widehat{J}^j$ given an initial guess of the inverse of the Hessian chosen in step 18 and the pairs $\{s^j, g^j\}^m_{j=1}$, see [**127**, Algorithm 7.4, p. 178].

Algorithm 2 Limited Memory BFGS Method

Input: u^0, m
Output: $\widehat{u}, \widehat{y}, \widehat{\phi}, \widehat{p}, \widehat{\psi}$

1: $j = 0, l = 0$.
2: Solve the forward problem (3.2) for y^j and ϕ^j.
3: **while** the convergence condition is not fulfilled **do**
4:     Solve the adjoint problem (3.10) for p^j and ψ^j.
5:     Compute the gradient from (3.11)
$$\nabla \widehat{J}^j = \gamma_5\, u^j + p^j.$$
6:     **if** $j \geq 1$ **then**
7:       Compute
$$s^{j-1} := \sigma^{j-1}\, d^{j-1}, \quad g^{j-1} := \nabla \widehat{J}^j - \nabla \widehat{J}^{j-1}.$$
8:       **if** $(s^{j-1})^\top g^{j-1} > 0$ **then**
9:         $l \to l + 1$.
10:         **if** $l > m$ **then**
11:           Discard $\{s^{l-m}, g^{l-m}\}$ from the storage.
12:         **end if**
13:         Add $\{s^{j-1}, g^{j-1}\}$ to the storage.
14:       **else**
15:         Empty the storage, $l \to 0$.
16:       **end if**
17:     **end if**
18:     Choose an initial approximation to the inverse of the Hessian, H_0^j.
19:     Construct the direction
$$d^j := -H^j\, \nabla \widehat{J}^j.$$
20:     Determine σ^j by the Armijo rule with backtracking.
21:     Set $u^{j+1} = u^j + \sigma^j\, d^j$.
22:     $j \to j + 1$.
23: **end while**

- As the initial choice of the inverse of the Hessian in step 18, we use
$$H_0^j = \frac{(s^{j-1})^\top g^{j-1}}{(g^{j-1})^\top g^{j-1}}\, I,$$
where I is the identity matrix of suitable dimensions, see [**127**, p. 178].
- The condition $(s^{j-1})^\top g^{j-1} > 0$ is checked in step 8 to ensure that the updated approximation to the inverse of the Hessian is positive definite assuming that its predecessor is also positive definite. If

this condition is violated, we follow the advice of Kelley [**91**, Section 4.2.2] and forget the iteration history as it can be seen as being suspect in this case. This strategy admits the Armijo rule in step 20 instead of a line search procedure that ensures that the Wolfe conditions are satisfied.

4 Discretization

Contents

A brief review of existing approaches to the numerical solution of Stefan problems in level set formulation sets the scene in this chapter. We proceed with the development of a discontinuous Galerkin (DG) scheme that is used in combination with an explicit Runge-Kutta method to discretize the level set equation. The reinitialization of the level set function and the construction of extension velocities by the fast marching method are discussed. An extended finite element method (X-FEM) is built upon the level set solver to discretize the heat equation in space. For the time stepping, the standard implicit (backward) Euler scheme is used. An algorithm for the solution of the two-phase Stefan problem in which these two components are combined is presented (Algorithm 3, p. 76) and validated on two benchmark examples. While the equation for the adjoint level set function is discretized in space

using a different discontinuous Galerkin scheme, the same Runge-Kutta time stepping method as for the level set equation is applied. The adjoint heat equation is discretized by the X-FEM and the implicit Euler scheme as indicated above. Again, these two building blocks are combined in an algorithm for the solution of the adjoint Stefan problem (Algorithm 4, p. 94).

4.1   Solving the Stefan Problem in Level Set Formulation

Sethian and Strain [148] propose the first level set approach to the solution of Stefan problems. They transform the energy balance equations into *boundary integral equations* on the moving interface which is represented by the level set method. Chen et al. [26] develop a *finite difference-based* approach to solving the two-phase Stefan problem in two spatial dimensions. Fried [58] extends the *finite element method* of Schmidt [146] who uses a parameterization of the moving interface to a level set framework. This approach assumes that the motion of the interface is characterized by a mean curvature flow. It is applicable in three spatial dimensions. Müller [117] develops a finite-element based approach that extends the previously mentioned methods of Schmidt and Fried to the general case that the interface motion is directly governed by the Stefan condition. Gibou et al. [67] extend the approach of [26] to a *higher-order approximation* of the interface and to three spatial dimensions. In collaboration with Fedkiw, Gibou designs a fourth order accurate finite difference scheme for the Laplace equation that is applicable to the Stefan problem, as demonstrated by the authors [66]. Gibou et al. [25] discuss an *adaptive method* with supralinear convergence properties that builds upon previous work of the authors. The most recent technique for solving Stefan problems in level set formulation probably is the *extended finite element method* (X-FEM). In 2002, Chessa and coworkers [30] and Ji et al. [86] present the first such methods. Zabaras et al. [168] extend these approaches by including convection in the fluid phase. Cheng and Fries [27] investigate higher-order methods.

This work uses the X-FEM for various reasons:

- The X-FEM operates on a fixed grid, avoiding moving the mesh and repeated remeshing.
- In addition, such a fixed grid structure has the advantage that the number of optimization variables is also fixed. This is in contrast to moving mesh methods in which the number of optimization variables may not be known a priori.
- There has been some interest in using the X-FEM for shape and topology optimization, see, e.g., [113,114,163] and the references

in these papers. However, using the X-FEM for optimal control purposes is a novel approach.

Some Alternative Approaches. Depending on the formulation of the Stefan problem, other solution strategies are more suitable than the level set method. Without aiming for completeness, we list here some alternatives. As mentioned above, Schmidt [146] uses a *parameterization* of the interface, while, e.g., Hinze and Ziegenbalg [79] describe the moving boundary as the *graph of a function*. The latter approach is also a representative of the class of *moving mesh methods*. Other approaches in this direction are the works of Albert and O'Neill [3], Sullivan et al. [154], Beckett and coworkers [12, 13], and Baines et al. [9]. The latter method features *adaptivity*, as do the approaches by Gibou et al. [25], and Nochetto and collaborators [128]. For the *enthalpy formulation* of the two-phase Stefan problem (see Chapter 2.4), the literature on numerical methods is rich. As representatives of this direction, we mention here the approaches by Crowley [37], Chorin [32], Hoppe [84], Caldwell and Chan [23], Esen and Kutluay [54], and the review article by Voller et al. [162]. The last class of methods we refer to are based on *phase field* formulations, see, e.g., the articles by Kobayashi [94], Elliott and Gardiner [52], and Karma and Rappel [90].

4.2   Discretization of the Level Set Equation

In Section 2.2, we classified the level set equation (2.8) as a first-order Hamilton-Jacobi equation. Thus, its spatial and temporal discretizations have to be undertaken with care to obtain the viscosity solution introduced in Theorem 2.6. A popular approach is to use a rectangular grid and to discretize the level set equation in space by special *finite difference schemes*, so called essentially non-oscillatory (ENO) schemes, possibly of high order [132]. An extension to triangular grids can be found, e.g., in [170]. This spatial discretization has to be combined with total variation diminishing (TVD) Runge-Kutta methods [69]. *Finite volume schemes* for Hamilton-Jacobi equations are applicable to level set equations as well, see, e.g., [64, 95] and the book by LeVeque [106]. Finally, the level set equation can also be discretized in space by *finite elements*. However, standard Galerkin finite element approaches can not be used directly. One either has to apply a remeshing technique as in [11] or to resort to GLS stabilization and shock-capturing operators as in [30, 168]. *Discontinuous Galerkin* (DG) *methods* provide a modern and powerful framework for the spatial approximation of hyperbolic conservation laws [34]. Marchandise et al. [108] discuss a quadrature-free discontinuous Galerkin method for the level set equation, but as for the mass preserving finite element method of Di Pietro et al. [41], the velocity field

is assumed to be divergence free. Cheng and Shu propose a DG scheme for Hamilton-Jacobi equations on rectangular grids that does not rely on special assumptions on the velocity field [29]. We extend this approach to triangular meshes which offer more flexibility for complicated geometries. The DG spatial approximation is combined with a *strong stability preserving* (SSP) *Runge-Kutta method* in time [70].

Remark 4.1. The method of Yan and Osher [166] is an attractive alternative to the DG scheme we use because it handles non-convex Hamiltonians as well. Thus it is applicable directly to the non-linear version (2.11) of the level set equation. Unfortunately, this approach appeared too late to be used within this work.

4.2.1. Spatial Discretization

Throughout this section, we denote by ∂_t, ∂_x and ∂_y the partial derivatives with respect to time and the x- and y-coordinates, respectively.

For discretizing the Hamilton-Jacobi equation

$$0 = \phi_t + H(x, y, \partial_x \phi, \partial_y \phi)$$

with a convex Hamiltonian H on the domain $\Omega = [a, b] \times [c, d] \subset \mathbb{R}^2$ in space, Cheng and Shu [29] first subdivide the coordinate axes according to

$$a = x_{\frac{1}{2}} < x_{\frac{3}{2}} < \cdots < x_{N_x + \frac{1}{2}} = b,$$
$$c = y_{\frac{1}{2}} < y_{\frac{3}{2}} < \cdots < y_{N_y + \frac{1}{2}} = d,$$

resulting in a discretized domain

$$\Omega = \Omega_h = \bigcup_{i=1}^{N_x} \bigcup_{j=1}^{N_y} I_{ij}, \quad I_{ij} = \left[x_{i-\frac{1}{2}}, x_{i+\frac{1}{2}} \right] \times \left[y_{j-\frac{1}{2}}, y_{j+\frac{1}{2}} \right],$$

see Figure 4.1. Moreover, they introduce the sets

$$J_i = \left[x_{i-\frac{1}{2}}, x_{i+\frac{1}{2}} \right], \qquad\qquad J_{i+\frac{1}{2}} = [x_i, x_{i+1}],$$
$$K_j = \left[y_{j-\frac{1}{2}}, y_{j+\frac{1}{2}} \right], \qquad\qquad K_{j+\frac{1}{2}} = [y_j, y_{j+1}],$$

where $i = 1, \ldots, N_x$ and $j = 1, \ldots, N_y$.

Finally, they define the discontinuous finite element space

$$V_h^k = \left\{ v \ : \ v|_{I_{ij}} \in P^k(I_{ij}), \ i = 1, \ldots, N_x, \ j = 1, \ldots, N_y \right\} \tag{4.1}$$

of piecewise polynomials and formulate the scheme:

Find $\phi_h(x, y, t) \in V_h^k$ such that
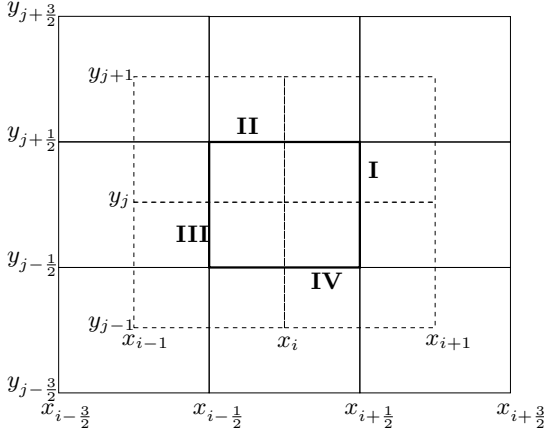
FIGURE 4.1. Part of a rectangular mesh. The bold edges belong to the cell I_{ij}.

$$0 = \int_{I_{ij}} \left(\partial_t \phi_h(x,y,t) + H\big(x,y,\partial_x\phi_h,\partial_y\phi_h\big) \right) v_h(x,y)\, dx\, dy \qquad (4.2)$$

$$+ \int_{K_j} \left(\min_{x \in J_{i+\frac{1}{2}}} H_1(x_{i+\frac{1}{2}},y,\partial_x\phi_h,\overline{\partial_y\phi_h}) \right)^{-} [\phi_h]\,(x_{i+\frac{1}{2}},y)\, v_h(x_{i+\frac{1}{2}}^{-},y)\, dy$$

$$+ \int_{K_j} \left(\min_{x \in J_{i-\frac{1}{2}}} H_1(x_{i-\frac{1}{2}},y,\partial_x\phi_h,\overline{\partial_y\phi_h}) \right)^{+} [\phi_h]\,(x_{i-\frac{1}{2}},y)\, v_h(x_{i-\frac{1}{2}}^{+},y)\, dy$$

$$+ \int_{J_i} \left(\min_{y \in K_{j+\frac{1}{2}}} H_2(x,y_{j+\frac{1}{2}},\overline{\partial_x\phi_h},\partial_y\phi_h) \right)^{-} [\phi_h]\,(x,y_{j+\frac{1}{2}})\, v_h(x,y_{j+\frac{1}{2}}^{-})\, dx$$

$$+ \int_{J_i} \left(\min_{x \in K_{j-\frac{1}{2}}} H_2(x,y_{j-\frac{1}{2}}\overline{\partial_x\phi_h},\partial_y\phi_h) \right)^{+} [\phi_h]\,(x,y_{j-\frac{1}{2}})\, v_h(x,y_{j-\frac{1}{2}}^{+})\, dx,$$

where the partial derivatives of H with respect to $\partial_x\phi$ and $\partial_y\phi$ are denoted by H_1 and H_2, respectively, and

$$\overline{\partial_x\phi_h} = \frac{1}{2}\big((\partial_x\phi_h)^{+} + (\partial_x\phi_h)^{-}\big), \quad \overline{\partial_y\phi_h} = \frac{1}{2}\big((\partial_y\phi_h)^{+} + (\partial_y\phi_h)^{-}\big)$$

denote the average jumps of the gradient of the solution in x- and y-direction. Moreover,

$$(\cdot)^{-} := \min(\cdot,0) \quad \text{and} \quad (\cdot)^{+} := \max(\cdot,0).$$

This scheme is monotone for convex Hamiltonians. Note that, due to the linear structure of the level set equation (2.8), the Hamiltonian of this equation is also linear and, in particular, convex. This is in contrast to the non-linear level set equation (2.11) whose Hamiltonian is not convex. In the latter case, the DG scheme of Cheng and Shu does in general not approximate the correct viscosity solution.

To translate the idea of [29] to triangular grids, we obviously have to replace the special rectangular grid by a general triangulation $\mathcal{T}_h$ of Ω. The first integral in (4.2) naturally translates into an integral over an element $K \in \mathcal{T}_h$, while the boundary integral terms in (4.2) require a little more work. Consider, e.g., the second integral in (4.2). If we denote by ∇H the gradient of H with respect to $\partial_x \phi$ and $\partial_y \phi$, we have

$$H_1(x_{i+\frac{1}{2}}, y, \partial_x \phi_h, \overline{\partial_y \phi_h}) = \nabla H(x_{i+\frac{1}{2}}, y, \partial_x \phi_h, \overline{\partial_y \phi_h}) \cdot n_{\mathbf{I}},$$

where $n_{\mathbf{I}} = (1, 0)^\top$ is the outward unit normal to the edge $\mathbf{I}$ of the cell I_{ij}, see Figure 4.1. Similar relations obviously hold for the remaining three integrals. In addition, we observe that for the linear level set equation (2.8)

$$\nabla H(x, y, \partial_x \phi, \partial_y \phi) = \begin{pmatrix} H_1(x, y, \partial_x \phi, \partial_y \phi) \\ H_2(x, y, \partial_x \phi, \partial_y \phi) \end{pmatrix} = \vec{V}(x, y),$$

so that the interior minimization problems in (4.2) drop out. Consequently, all terms involving derivatives of the Hamiltonian can be replaced by terms of the form $\vec{V} \cdot n_i$, where $i \in \{\mathbf{I}, \mathbf{II}, \mathbf{III}, \mathbf{IV}\}$.

We are now in the position to formulate the discontinuous Galerkin scheme for the spatial discretization of the level set equation (2.8). Given a triangulation $\mathcal{T}_h$ of the domain Ω, we define the discontinuous finite element space

$$\mathcal{P}_{\mathrm{pw}}^k := \left\{ v \mid v \in P^k(K) \text{ for all } K \in \mathcal{T}_h \right\} \tag{4.3}$$

as a generalization of (4.1). The scheme then reads:

Find $\phi_h \in \mathcal{P}_{\mathrm{pw}}^k$ such that

$$0 = \int_K \left(\partial_t \phi_h + \vec{V} \cdot \nabla \phi_h \right) v_h \, dx + \sum_{i=1}^{3} \int_{e_i} \min\left(\vec{V} \cdot n_{e_i}, 0 \right) \left[\phi_h \right]_{e_i} v_h^- \, ds \tag{4.4}$$

for all $v_h \in \mathcal{P}_{\mathrm{pw}}^k$ and for all $K \in \mathcal{T}_h$.

Here, n_{e_i} denotes the outward unit normal of an element K of the mesh on the edge e_i, and

$$\left[\phi_h \right]_{e_i} := \phi_h^+(x, t) - \phi_h^-(x, t)$$

denotes the jump of ϕ_h across e_i, where

$$\phi_h^{\pm}(x,t) := \lim_{\varepsilon \searrow 0} \phi_h(x \pm \varepsilon n_{e_i}, t). \tag{4.5}$$

Remark 4.2. We denote the *mass matrix* induced by the bilinear form

$$\int_K \phi_h \, v_h \, dx \quad \text{for all} \quad K \in \mathcal{T}_h$$

by $\mathcal{M}$. Similarly, the bilinear form

$$\int_K \vec{V} \cdot \nabla \phi_h \, v_h \, dx \quad \text{for all} \quad K \in \mathcal{T}_h$$

induces the *system matrix* $\mathcal{K}$.

The interpretation of (4.4) is as follows. The first term, which is obtained by multiplying (2.8a) with a test function v_h and integrating this product over an element K of the triangulation, guarantees the accuracy of the scheme. The boundary integral terms add a Roe-type stabilization on all inflow edges, i.e., on all edges on which $\vec{V} \cdot n_{e_i} < 0$. To ensure that the scheme approximates a continuous solution (the viscosity solution), $\left[\phi_h\right]_{e_i}$ is included as well. Note that this stabilization approach does not require the tuning of parameters. Moreover, the scheme literally translates to the three-dimensional setting if we replace edges of triangles by faces of tetrahedra.

Remark 4.3 (Error Estimate). In the one-dimensional case with smooth data, Cheng and Shu [29, Proposition 2.2] provide the optimal error estimate

$$\|\phi_h(t) - \phi(t)\|_{L^2} \leq C \, h^{k+1},$$

where k is the polynomial degree of the discontinuous finite element space (4.1). Unfortunately, it is not known whether this result carries over to two or more spatial dimensions.

4.2.2. Temporal Discretization

For first-order hyperbolic partial differential equations, spatial approximations of discontinuous Galerkin type have to be combined with *strong stability preserving* (SSP) Runge-Kutta methods to ensure stability of the fully discrete scheme [70]. The step from time level n to time level $n+1$ for a general *explicit* m-stage Runge-Kutta method for the autonomous system of ordinary differential equations

$$\phi_t = L(\phi) \tag{4.6}$$

with suitable initial conditions can be written in the form

$$\phi^{(0)} = \phi^n,$$

$$\phi^{(i)} = \sum_{k=0}^{i-1} \big(\alpha_{i,k}\, \phi^{(k)} + \Delta t\, \beta_{i,k}\, L(\phi^{(k)}) \big), \quad i = 1, \dots, m, \qquad (4.7)$$

$$\phi^{n+1} = \phi^{(m)},$$

where $\alpha_{i,k} \geq 0$. If $\beta_{i,k} \geq 0$ as well, then all intermediate steps of this scheme can be interpreted as convex combinations of forward Euler steps with the modified time step $\frac{\beta_{i,k}}{\alpha_{i,k}}\, \Delta t$. This is the key observation to prove the following result:

Lemma 4.4 (see [70, 150]). *If the explicit (forward) Euler method applied to* (4.6) *is strongly stable under the CFL condition*

$$\Delta t \leq \Delta t_{\mathrm{FE}} \qquad (4.8)$$

(which means that $\|\phi^n + \Delta L(\phi^n)\| \leq \|\phi^n\|$ *in a suitable norm), then the Runge-Kutta method* (4.7) *with* $\beta_{i,k} \geq 0$ *is SSP (which means that* $\|\phi^{n+1}\| \leq \|\phi^n\|$ *in the same norm) under the CFL condition*

$$\Delta t \leq c\, \Delta t_{\mathrm{FE}} \qquad (4.9)$$

with the CFL coefficient $c = \min_{i,k} \frac{\alpha_{i,k}}{\beta_{i,k}}$.

Remark 4.5.   (1) As mentioned in [70], it is not always possible to fulfill the condition $\beta_{i,k} \geq 0$ for all i, k. In this case, an associated operator $\tilde{L}$ has to be introduced to preserve the statement of Lemma 4.4.

    (2) If $c \geq 1$, the CFL condition (4.9) for the Runge-Kutta scheme is less restrictive than the CFL condition (4.8) for the explicit Euler method. This time step relaxation can be achieved at the expense of additional stages in the Runge-Kutta scheme, see [152].

    (3) Gottlieb et al. [70] prove that there are no SSP *implicit* Runge-Kutta schemes of order higher than 1. As a consequence, it suffices to consider only explicit schemes of the form (4.7) for discretizing the level set equation in time. This is in a sense good news as the level set equation, i.e., the geometric information, can be updated before making a time step in the discretization of the heat equation (3.2a)–(3.2h), see Algorithm 3.

In view of the error estimate given in Remark 4.3, a spatial discretization of order k should be combined with a Runge-Kutta method of order $k + 1$ to have an optimal order of convergence for the fully discrete scheme. In all our

TABLE 4.1. Butcher array of the optimal SSP(3,3) Runge-Kutta scheme

$$
\begin{array}{c|ccc}
0 & 0 & 0 & 0 \\
1 & 1 & 0 & 0 \\
\frac{1}{2} & \frac{1}{4} & \frac{1}{4} & 0 \\
\hline
 & \frac{1}{6} & \frac{1}{6} & \frac{2}{3}
\end{array}
$$

numerical examples, we use quadratic finite element spaces. Thus, we employ the third-order optimal SSP scheme defined by the Butcher array in Table 4.1. This scheme was designed by Spiteri and Ruuth [152] by maximizing the CFL coefficient c in (4.9). The authors show that this optimal 3-stage SSP Runge-Kutta method of order 3 fulfills the condition $\beta_{i,k} \geq 0$, and that the corresponding CFL coefficient is given by 1.

It remains to establish the CFL condition under which the time stepping scheme is stable. Such conditions are easy to formulate in the one-dimensional case and for rectangular grids in two dimensions but straightforward extensions to triangular meshes are in general not sufficient for the stability. Following Kubatko et al. [97], we impose the CFL condition

$$
\Delta t_{\mathrm{CFL}} = \frac{h_{\min}}{\sqrt{2}} \frac{1}{5 \cdot 2^{1/(k+1)}} \min\left\{ \frac{1}{\|\vec{V}\|_\infty}, \frac{1}{2} \right\}, \qquad (4.10)
$$

where $h_{\min}$ is the length of the shortest element edge of the triangulation $\mathcal{T}_h$.

4.2.3. Implementation

In this section, several issues related to the efficient implementation of the level set method are discussed. We comment on the boundary conditions used, and on the extension of a quantity that is defined on the interface to all of the computational domain. Finally, we briefly discuss the so called narrow band approach that aims at keeping the numerical effort for the level set method at a reasonable level by restricting all computations to the neighborhood of the moving boundary.

Taylor Basis. The scheme (4.4) can be implemented by using any suitable basis for the discontinuous finite element space (4.3). In particular, the standard Lagrange basis is applicable. For reasons that are explained in Section 4.5.2, we choose a so called local Taylor basis [101] to span (4.3). In this representation, the normalized degrees of freedom are proportional to the cell mean value of a function, and, in case of quadratic polynomials, the derivatives of this function up to second order, evaluated at the centroid

of the cell. The mass matrix corresponding to this Taylor basis is non-diagonal. However, setting all off-diagonal entries to zero is a conservative mass lumping strategy [101]. For the reinitialization of the level set function explained below, we switch from the Taylor basis to the standard Lagrange basis as the reinitialization relies on the nodal values of the level set function. This switching is cheap in terms of computing time. Moreover, it is not unusual for discontinuous Galerkin schemes to operate with different bases for different tasks.

Boundary Conditions. To make the Hamilton-Jacobi equation (2.8) well-posed, boundary conditions on the inflow boundaries, i.e., on those parts of the boundary of the computational domain on which $\vec{V} \cdot n < 0$, need to be specified. This is reflected by the scheme (4.4) that takes into account only the jumps across those edges on which the inflow condition is fulfilled.

Since there are no physical boundary conditions on ϕ given, we have to resort to artificial boundary conditions. Neumann-type conditions are attractive for level set computations as they do not prescribe the values of ϕ on the boundary of the computational domain. Unfortunately, such boundary conditions can not be easily implemented in the scheme (4.4). As an alternative, we impose Dirichlet boundary conditions on the time-discrete level by prescribing ϕ^n as the required Dirichlet data in the time step from ϕ^n to ϕ^{n+1}. Of course, fixing the values of ϕ on the boundary of the computational domain certainly influences the evolution of ϕ, but numerical experiments confirm that this influence is negligible if we use reasonably small time steps and a frequent reinitialization of the level set function ϕ to a signed distance function as described below.

Extension Velocity and Reinitialization. When formulating the level set equation (2.8) we tacitly made the assumption that the velocity field $\vec{V}$ is known on all of D. In contrast to, for instance, two-phase fluid flow problems in which the velocity of the fluid can be used, this is obviously not the case as the Stefan condition (2.4) defines only the normal velocity $\vec{V} \cdot n$ on the interface.

There are several (equivalent) ways to construct a vector valued velocity field with global support from this scalar quantity.

(1) The first approach is to make the natural identification (see (2.7))

$$\vec{V}_i = \frac{1}{\rho L} \left(k_S \frac{\partial y_S}{\partial x_i} - k_F \frac{\partial y_F}{\partial x_i} \right) \qquad \text{on } \Gamma_I(t), \qquad (4.11)$$

and to extend this velocity field to all of D. This approach requires two evaluations of the gradient of y.

(2) Alternatively, one can set

$$\vec{V} = (\vec{V} \cdot n)\, n \qquad \text{on } \Gamma_I(t), \qquad (4.12)$$

and use an extension of this velocity vector. This approach requires only the evaluation of $\vec{V} \cdot n$ which can be implemented using a simple jump calculation, see Section 4.3.4, and should thus be cheaper than (1). Since the velocity field defined by (4.11) has no tangential component due to (3.2h), it can be written as in (4.12) and, thus, (1) and (2) are equivalent.

(3) Finally, one can rotate the coordinate system in a way that the x_1-axis is transformed into the outer normal of $\Gamma_I(t)$. The jump of the gradient (as in (4.11)) in this new coordinate system can then be easily evaluated as it is given by $\vec{V} \cdot n$ in the direction corresponding to x_1 and zero in the direction corresponding to x_2. In the original coordinate system, we obtain the representation (4.12) and therefore, also (2) and (3) are equivalent.

As mentioned above, we consider (2) and (3) to be more efficient than (1). Thus, we discuss the evaluation of the Stefan condition (2.4) in the next section in more detail. We now turn to the question of how to compute the extension of $\vec{V}$ to all of D.

The support of a *scalar* quantity Ψ that is known on an interface only can be enlarged to all of D by means of a constant extension in normal direction. Thanks to (2.9), this is achieved by solving

$$\text{sign}(\phi)\, \nabla\Psi \cdot \nabla\phi = 0 \qquad \text{in } D, \qquad (4.13a)$$

$$\Psi = \hat{\Psi} \qquad \text{on } \Gamma_I(t). \qquad (4.13b)$$

As in [30], we add the sign term to ensure that the characteristics of this equation emanate from $\Gamma_I(t)$, see Figure 4.2(a). Consequently, the given data $\hat{\Psi}$ can be used as a boundary condition on $\Gamma_I(t)$. To construct an extension of a *vector-valued* quantity, (4.13) is solved for each component. Note that this is the case for the velocity field $\vec{V}$ that has to be extended away from the interface. This choice of extension velocity moves the interface with the correct speed. Moreover, it preserves the signed distance property of ϕ as shown by Zhao et al. [171].

We use the *fast marching method* of Kimmel and Sethian [92] to construct a signed distance function to the current position of the interface and simultaneously solve (4.13) for all components of the velocity field on the triangular mesh. This means in particular that the reinitialization of the level set function which should be performed periodically can be computed at low cost in each time step. The key idea of the fast marching scheme is to subdivide

(a) Characteristics of (4.13).   (b) Subdivision of grid points.
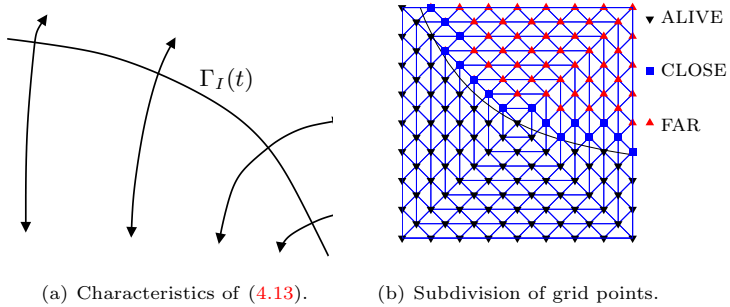
FIGURE 4.2. Construction of extension velocities by the fast marching method.

the grid points into three sets, see Figure 4.2(b). All points for which the initial condition (4.13b) is known (or can be explicitly computed) are tagged as ALIVE and remain unchanged. All points that are adjacent to ALIVE points are tagged as CLOSE and all others are tagged as FAR. The method then iteratively moves points tagged as CLOSE to the ALIVE nodes and at the same time moves nodes from the set of FAR points to the CLOSE nodes. This procedure is implemented to monotonically move the front of CLOSE nodes and update the signed distance function. During the update procedure several triangles might contribute to the value of the signed distance function at a certain node. In this case, the triangle yielding the smallest value is taken as the upwind triangle. We use the same triangle to update the components of the extension velocity. We finally remark that all fast marching computations are carried out on the finer level of the grid which is also used to determine the current interface position, see Section 4.3.4. Interpolation is used to map these values to the quadratic framework on the coarse grid.

Narrow Band Level Set Method. The major drawback of level set techniques is the considerable additional effort that is introduced by embedding the moving interface into a higher-dimensional object whose evolution is described by a partial differential equation. In cases where there is no physical quantity that can be used as the velocity field $\vec{V}$ in (2.8a), such a velocity field has to be constructed as discussed above and in Section 4.3.4. These problems are at least partly overcome by using a narrow band technique that solves the level set equation only in the vicinity of the interface [1, 31, 135], see Figure 4.3. As a consequence, the extension PDE (4.13) can also be restricted to the narrow band.
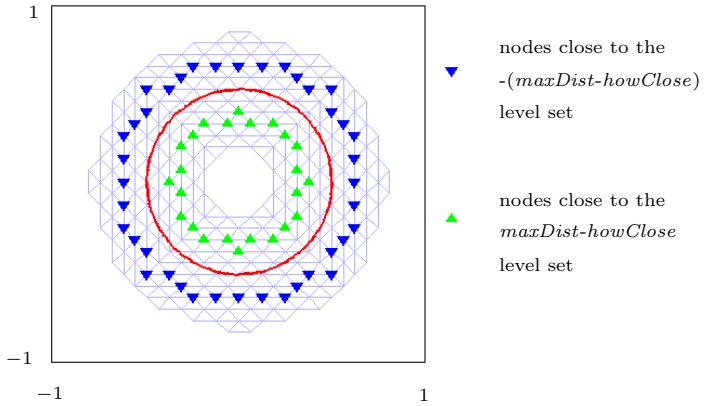
FIGURE 4.3. The interface (red line) embedded into the
narrow band (gray) that collects all nodes whose distance
from the interface is less than *maxDist*.

The localized computational domains contain only those nodes of the grid
whose distance to the current interface is less than a threshold value denoted
by *maxDist* [1]. A monitoring procedure based on the distance *howClose* of
the interface from the boundary of the current narrow band (tube) is im-
plemented to control the evolution of the tube. If this distance falls below
a predefined tolerance, the tube has to be rebuilt which requires also the
construction of a signed distance function to the current interface, e.g., by
the fast marching method. To implement the monitoring procedure, we de-
termine the $\pm$(*maxDist-howClose*) level sets of the current signed distance
function. All nodes that belong to triangles that are intersected by these
level sets and whose signed distance to the interface is larger than *maxDist-
howClose* or smaller than -(*maxDist-howClose*), respectively, are tagged. Fi-
nally, the values of the signed distance function at these nodes are checked in
each time step, and, if any of these values changes sign, the tube is rebuilt.
This idea is illustrated in Figure 4.3.

4.2.4. Numerical Examples

We verify the implemented level set solver on two benchmark examples. Vari-
ations of these test examples are frequently used to validate solvers for hy-
perbolic conservation laws and more general Hamilton-Jacobi equations, see,

e.g., [**29**, **64**, **105**]. To estimate the order of convergence, we compute the L^2 error

$$E_T^2(\phi_h) := \left(\int_{\Gamma_I(T)} \phi_h^2 \, ds \right)^{1/2} \tag{4.14}$$

as well as the L^∞ error

$$E_T^\infty(\phi_h) := \sup_{\Gamma_I(T)} |\phi_h| \tag{4.15}$$

for a decreasing sequence of grid sizes, ranging from $h = 0.4$ (which corresponds to 256 triangles in the hold-all $D = [-1, 1]^2$) to $h = 0.025$ (which corresponds to 65536 triangles). The time grid is refined with the spatial grid according to the CFL condition (4.10). In all the computations in this section, we use the given velocity field instead of the constant extension described in Section 4.2.3. Since we are only interested in the error in the interface position, it suffices to use the narrow band level set method.

Solid Body Rotation. In this example, the initial interface at time $t = 0$ is a circle with radius 0.5 centered at $(0.25, 0.25)$. We are interested in the evolution of this circle under the velocity field

$$\vec{V} = \begin{pmatrix} -x_2 \\ x_1 \end{pmatrix}$$

in the time interval $[0, T]$ with $T = 2\pi$. This velocity field causes a counterclockwise solid body rotation. The given time interval corresponds to one period of rotation, i.e., at $t = T$, the interface should have obtained its initial configuration again. The convergence behavior of the implemented level set solver on this example is documented in Table 4.2. We observe (almost) second-order convergence with respect to both (4.14) and (4.15). ◇

Swirling Flow. In this second example, a slightly rotated quatrefoil, which is the zero level set of the function [**64**]

$$\Phi(x_1, x_2) = -1 + \frac{1}{r} \sqrt{x_1^2 + x_2^2}, \quad r = 0.6 + 0.4 \sin\left(4 \arctan\left(\frac{x_2}{x_1} \right) \right),$$

undergoes a severe deformation under the velocity field

$$\vec{V} = g(t) \begin{pmatrix} \sin^2(\pi x_1) \sin(2\pi x_2) \\ -\sin^2(\pi x_2) \sin(2\pi x_1) \end{pmatrix}, \quad g(t) = \cos\left(\frac{t}{T} \pi \right),$$

in the time interval $[0, \frac{3}{2}]$, which corresponds to one period of deformation. As above, the interface should have regained its initial shape at final time. Figure 4.4 illustrates this behavior. The convergence history is reported in Table 4.3. The least squares approach suggests a linear rate with respect to both, the L^2 error measure (4.14), and the L^∞ case (4.15). Compared

TABLE 4.2. Errors and estimated orders of convergence for the solid body rotation example. The last row is based on a least-squares approach taking into account all grid sizes and all errors.

h	$E_T^2(\phi_h)$	eoc	$E_T^\infty(\phi_h)$	eoc
0.400	1.2084e−01	–	1.6952e−01	–
0.200	5.3999e−02	1.16	6.7867e−02	1.32
0.100	1.2065e−02	2.16	1.4566e−02	2.22
0.050	2.8733e−03	2.07	3.7166e−03	1.97
0.025	7.5494e−04	1.93	1.0797e−03	1.78
eoc		1.89		1.88

TABLE 4.3. Errors and estimated orders of convergence for the swirling flow example. The last row is based on a least-squares approach taking into account all grid sizes and all errors.

h	$E_T^2(\phi_h)$	eoc	$E_T^\infty(\phi_h)$	eoc
0.400000	4.6736e−02	–	6.5510e−02	–
0.200000	1.3217e−02	1.82	1.5841e−02	2.05
0.100000	6.2935e−03	1.07	8.3094e−03	0.93
0.050000	4.4397e−03	0.50	5.3264e−03	0.64
0.025000	2.8141e−03	0.66	3.5676e−03	0.58
eoc		0.97		1.00

to the solid body rotation problem, the convergence order is decreased. We attribute this to the fact that the deformation of the initial interface shape in the swirling flow example is much more severe.   ◇

Remark 4.6. In neither of the two cases, we observe cubic convergence. At a first glance, this is in contrast to Remark 4.3. However, the proposed reinitialization procedure (Section 4.2.3) is of lower order than the discontinuous Galerkin scheme (4.4) with the Runge-Kutta method given by the Butcher array 4.1. To improve on this point, one can either implement a higher-order version of the fast marching method on triangular grids [149], or use a different reinitialization PDE as in [135].

(a) $t = 0.0000$

(b) $t = 0.2143$

(c) $t = 0.4286$

(d) $t = 0.6429$

(e) $t = 0.8571$

(f) $t = 1.0714$

(g) $t = 1.2857$

(h) $t = 1.5000$
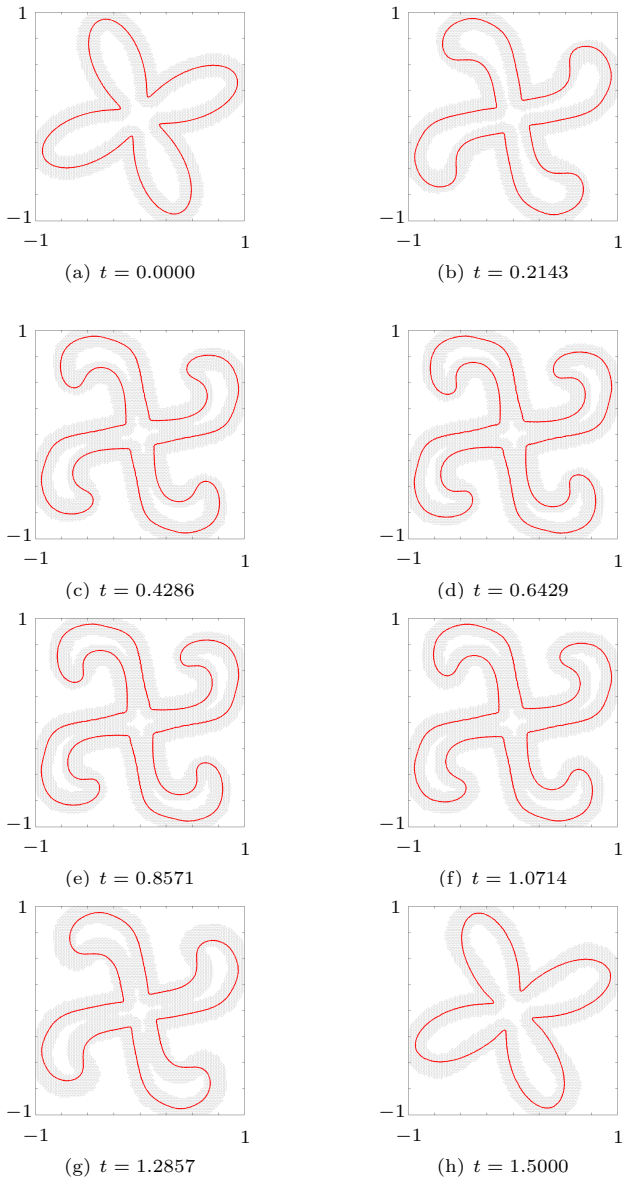
FIGURE 4.4. Evolution of the narrow band meshes and the interface in the swirling flow example on a spatial grid consisting of 16384 triangles ($h = 0.05$).

4.3   Extended Finite Element Approximation of the Temperature

Throughout this section, we focus on the description of the extended finite element method for the solution of the two-phase Stefan problem (3.2), assuming for the sake of simplicity that the heat flux g is given on all of ∂D, i.e., $\Gamma_C = \emptyset$. The extension to the situation in which the control u acts on part of the boundary is obvious as the control contributions are given in the form of Neumann boundary data.

4.3.1. Introduction

General Idea. The extended finite element method (X-FEM) was originally introduced for the solution of computational mechanics problems by Dolbow [42]. Its goal is to avoid the remeshing that is required with standard finite element approaches for problems involving, e.g., cracks or moving interfaces. Rather, the mesh is kept fixed. The counterpart of the remeshing is then a dynamic local modification of the underlying finite element spaces: In each time step, special enrichment functions that capture the characteristic features of the problem to be solved are added to the usual finite element basis. For instance, to model the discontinuities that arise in crack propagation problems, typically a Heaviside-type enrichment is constructed.

X-FEM for Solidification Problems. Solutions of solidification problems involving phase change phenomena are usually weakly discontinuous across the moving phase boundary, i.e., they are continuous but their gradient has a jump in normal direction to the moving interface. The first extended finite element approaches for such solidification problems are due to Chessa et al. [30] in the multidimensional case using a sharp level set representation of the interface and a so called abs-enrichment, and to Merle and Dolbow [110] in the one-dimensional case. Dolbow extends the latter approach to the multidimensional case and a level set representation of the moving phase boundary with other coworkers [86]. Another important contribution is the paper by Zabaras et al. [168] in which the Stefan problem is coupled with the Navier-Stokes equations in the fluid phase for the modeling of dendritic solidification in the presence of convection in the melt. Higher-order approximations are discussed in [27]. Our presentation and implementation of the X-FEM closely follows [30, 168].
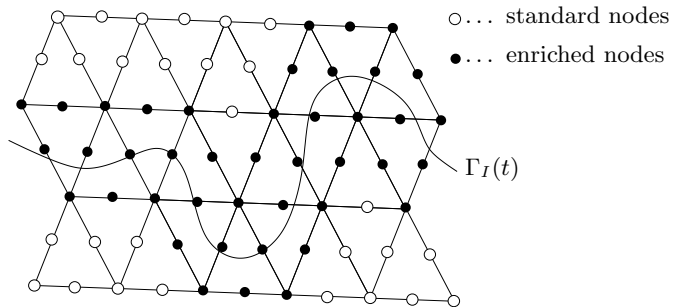
FIGURE 4.5. Illustration of local enrichment for quadratic finite elements ($k = 2$).

4.3.2. The Enriched Finite Element Approximation

We assume that we are given a triangulation $\mathcal{T}_h$ of our domain D. The extended finite element approximation of the temperature y is

$$y_h(x,t) = \sum_{i=1}^{N} v_i(x)\, y_i(t) + \sum_{j=1}^{N_e(t)} \widetilde{v}_j(x,t)\, a_j(t), \qquad (4.16)$$

where $v_i(x)$ are the usual Lagrangian finite element shape functions of order $k \geq 1$ on the triangulation $\mathcal{T}_h$ and $y_i(t)$ are the corresponding time-dependent degrees of freedom, located in the points x_i. The additional degrees of freedom $a_j(t)$ are added locally around $\Gamma_I(t)$ to the $(k+1)(k+2)/2$ nodes (in 2D) of those elements intersected by $\Gamma_I(t)$ (the so called reproducing elements), see Figure 4.5. The corresponding enrichment functions are defined as

$$\widetilde{v}_j(x,t) = v_{i(j,t)}(x)\left(\,|\phi(x,t)| - |\phi(x_{i(j,t)},t)|\,\right), \quad j = 1,\dots,N_e(t),$$

where $\phi(x_{i(j,t)},t)$ denote the nodal values of the level set function and $i(j,t)$ maps the indices of the enriched nodes at time t to the fixed degrees of freedom. The enrichment kernel $|\phi(x,t)| - |\phi(x_{i(j,t)},t)|$ (abs-enrichment) is chosen to model the phase change across $\Gamma_I(t)$, i.e., it is continuous with a discontinuous first derivative normal to the moving boundary. This kernel is multiplied with the standard shape function $v_{i(j,t)}(x)$ to preserve the sparsity of the stiffness matrix.

Remark 4.7 (The Corrected X-FEM). Sub-optimal convergence rates have been reported for the approximation (4.16). These rates are usually attributed to the fact that the proposed finite element basis functions do not form a partition-of-unity in so called blending elements, i.e., in elements in which

only some of the nodes are enriched. The corrected X-FEM of Fries [62] circumvents this problem by redefining the finite element basis functions. However, in view of the convergence rates for the curvature approximation (Sections 4.5.2–4.5.3) there is no need to improve on the approximation (4.16).

4.3.3. Discrete Energy Balance Equation

It is a particular feature of the X-FEM that in general the underlying partial differential equations must be discretized in time before the enriched finite element spaces can be defined [63]. This is because the enrichment functions $\widetilde{v}_j(x,t)$ depend on the location of the interface. We choose the implicit (backward) Euler method which is of first order to discretize (3.2a)–(3.2b) in time.

By a simple division, the heat equations (3.2a)–(3.2b) in the two-phase Stefan problem are rewritten as

$$y_t = \frac{k_S}{\rho\, c_S}\, \Delta y + \frac{1}{\rho\, c_S}\, f \qquad\qquad \text{in } \Omega_S(t),$$

$$y_t = \frac{k_F}{\rho\, c_F}\, \Delta y + \frac{1}{\rho\, c_F}\, f \qquad\qquad \text{in } \Omega_F(t).$$

Formally, we interpret this as an ordinary differential equation (ODE) of the form

$$y_t = L(t,y)$$

with an operator L,

$$L(t,y) := \frac{k(x,t)}{\rho\, c(x,t)}\, \Delta y(x,t) + \frac{1}{\rho\, c(x,t)}\, f(x,t),$$

that is linear with respect to y. Note that

$$k(x,t) := \begin{cases} k_S & \text{if } \phi(x,t) < 0 \\ k_F & \text{if } \phi(x,t) > 0 \end{cases} \quad \text{and} \quad c(x,t) := \begin{cases} c_S & \text{if } \phi(x,t) < 0 \\ c_F & \text{if } \phi(x,t) > 0 \end{cases}$$

are interpreted as functions of space and time. In the following, the superscripts $j-1$ and j refer to instances of time, e.g., $y^j(x) = y(x,t^j)$. The application of the implicit Euler method with time step $\Delta t^j = t^j - t^{j-1}$ ($j = 1,\ldots,N_T$) to this ODE yields the equation

$$y^j = y^{j-1} + \Delta t^j\, L(t^j, y^j)$$

which has to be solved for y^j in each time step. A multiplication of the discretized ODE with a test function δy and a subsequent integration over

D yields the weak form

$$\frac{1}{\Delta t^j} \int_D \delta y \, y^j \, dx = \frac{1}{\Delta t^j} \int_D \delta y \, y^{j-1} \, dx + \int_D \frac{k^j}{\rho \, c^j} \, \Delta y^j \, \delta y \, dx + \int_D \frac{f^j}{\rho \, c^j} \, \delta y \, dx.$$

As in the usual finite element framework, we integrate the Laplace operator by parts:

$$\int_D \frac{k^j}{\rho \, c^j} \, \Delta y^j \, \delta y \, dx = \int_{\partial D} \delta y \, \frac{k^j}{\rho \, c^j} \, \frac{\partial y^j}{\partial n} \, ds - \int_D \nabla y^j \, \nabla \left(\frac{k^j}{\rho \, c^j} \, \delta y \right) \, dx$$

$$= \int_{\partial D} \delta y \, \frac{g^j}{\rho \, c^j} \, ds - \int_D \frac{k^j}{\rho \, c^j} \, \nabla y^j \cdot \nabla \delta y \, dx.$$

According to the results of [**63**], the test function δy should be taken at time level j as well. Thus, the time-discrete energy balance equation in weak form is

$$\frac{1}{\Delta t^j} \int_D \delta y^j \, y^j \, dx + \int_D \frac{k^j}{\rho \, c^j} \, \nabla y^j \cdot \nabla \delta y^j \, dx$$

$$= \frac{1}{\Delta t^j} \int_D \delta y^j \, y^{j-1} \, dx + \int_{\partial D} \delta y^j \, \frac{g^j}{\rho \, c^j} \, ds + \int_D \frac{f^j}{\rho \, c^j} \, \delta y^j \, dx.$$

Replacing δy and y by their discrete counterparts, we obtain the fully discrete system

$$\left(\frac{1}{\Delta t^j} \, \mathbf{M}^j + \mathbf{K}^j \right) Y^j = \frac{1}{\Delta t^j} \, \mathbf{M}^j_{j-1} \, Y^{j-1} + \mathbf{G}^j + \mathbf{F}^j \qquad (4.17)$$

which has to be solved for the coordinate vector

$$Y^j = \left[y_1^j, \, \ldots, \, y_N^j, \, a_1^j, \, \ldots, \, a_{N_e(t^j)}^j \right]^\top$$

with respect to the finite element basis

$$B^j = \left\{ v_1(x), \, v_2(x), \, \ldots, \, v_N(x), \, \widetilde{v}_1(x, t^j), \, \ldots, \, \widetilde{v}_{N_e(t^j)}(x, t^j) \right\}. \qquad (4.18)$$

The matrices and vectors in (4.17) are defined as

$$\mathbf{M}^j = \left(\int_D \varphi_l \, \varphi_k \, dx \right)_{k,l}$$

$$\mathbf{M}^j_{j-1} = \left(\int_D \varphi_l \, \varphi_k^{j-1} \, dx \right)_{k,l}$$

$$\mathbf{K}^j = \left(\int_D \left(\nabla \varphi_l \right)^\top \frac{k}{\rho \, c} \, \nabla \varphi_k \, dx \right)_{k,l} \qquad \right\} \qquad (4.19)$$

$$\mathbf{G}^j = \left(\int_{\partial D} \varphi_l \, \frac{g}{\rho \, c} \, ds \right)_l$$

$$\mathbf{F}^j = \left(\int_D \varphi_l \, \frac{f}{\rho \, c} \, dx \right)_l$$

where $\varphi_k, \varphi_l \in B^j$, $\varphi_k^{j-1} \in B^{j-1}$, and all other quantities without a superscript are taken at time level j.

> **Remark 4.8** (Implicit Euler vs. Crank-Nicolson). It is tempting to use the Crank-Nicolson scheme instead of the implicit Euler method to obtain a higher-order time discretization at the expense of a little more work in assembling the linear system (4.17). In fact, for the Crank-Nicolson scheme one has to assemble an additional pseudo stiffness matrix $\mathbf{K}_{j-1}^j$ that is similar to $\mathbf{M}_{j-1}^j$, and two vectors $\mathbf{G}^{j-1}$ and $\mathbf{F}^{j-1}$ that represent the contributions of the Neumann boundary condition and the heat sources, respectively. Unfortunately, an application of the Crank-Nicolson scheme to problems involving free or moving boundaries might lead to oscillations in the solution, see, e.g., [**33**] and [**117**, Section 5.3]. The damping property of the implicit Euler method suppresses these oscillations, leading to better results. Our numerical experiments on the Frank sphere example (see Section 4.4) have confirmed the findings of [**33**, **117**].

4.3.4. Implementation

In this section we comment on some issues related to the implementation of the X-FEM for the two-phase Stefan problem and more general solidification problems.

Location of the Discrete Interface. For various purposes as, e.g., the numerical integration of the matrices and vectors in (4.19), the reinitialization of the level set function, and the construction of extension velocities, a discrete approximation of the interface $\Gamma_I(t)$ is needed. For linear ansatz functions, the discrete interface is determined by its (at most) two intersection points with the edges of each element. Thus, constructing a polygonal approximation to the interface is extremely simple in a linear framework, but a severe drawback of the linear representation is that it does in general not result in a good approximation of expressions that are related to second derivatives of the level set function such as, for instance, curvature. In [**58**, Chapter 4], it is even shown that the usage of linear finite elements might prevent approximations of curvature from converging. An obvious remedy is to use a higher-order ansatz space for the level set function. Unfortunately, determining the discrete interface for such higher-order approaches is not as simple as in the linear case. In the following, we focus on interface representations based on quadratic polynomials.

Fried [**58**, Section 6.2] develops a strategy, that is based on a distinction of cases that are characterized by the number of roots that the level set function has at the edges of the triangles. In each of the resulting cases, a polygonal

approximation of the discrete interface can be constructed in each triangle. As shown by Fried, this approach is very reliable. Its tedious programming is certainly a drawback. Moreover, the extension to three-dimensional problems is not obvious.

A more straightforward idea is to use a two-level grid as suggested in [**71**]. Let $\mathcal{T}_{h/2}$ be the triangulation obtained from $\mathcal{T}_h$ by one regular refinement. We define $\mathcal{I}(\phi_h)$ as the continuous piecewise linear function on $\mathcal{T}_{h/2}$ that interpolates ϕ_h at the vertices of all four triangles that form a subdivision of an element of $\mathcal{T}_h$. Then the location of the discrete interface is determined as

$$\Gamma_2(t) := \left\{ \, x \in D \mid \mathcal{I}\big(\phi_h(\cdot, t)\big)(x) = 0 \, \right\},$$

see Figure 4.6. As in the method proposed by Fried, the resulting discrete interface is polygonal in all of the elements of the triangulation. Note that the approaches in [**58**, **71**] exhibit sub-optimal convergence rates. This behavior is similar to polygonal approximations of curved domain boundaries in the usual finite element context.

Motivated by this observation, Cheng and Fries [**27**] propose yet another way to determine the discrete interface in a higher-order framework. The idea is to use a non-polygonal interface approximation which in turn means that the integration in the X-FEM has to be based on isoparametric methods. The optimal order of this method (as demonstrated in [**27**]) thus comes at the cost of more complicated integration techniques.

Taking all the advantages and disadvantages of the three methods just discussed into account, we choose the approach by Groß et al. [**71**] as it is most convenient to program and it literally translates to three dimensions if needed. We mention that, apart from sub-optimal convergence rates, we did not encounter any problems with this approach in our numerical experiments. If the discrete interface found in this way consists of several non-connected parts, we ignore those parts whose diameters are less than the length of the longest edge in the triangulation. This approach stabilizes the evolution of the interface, for instance, if changes of topology occur.

Numerical Integration.   Because the kernels of the enrichment functions $\widetilde{v}_j(x, t)$ are not differentiable across $\Gamma_I(t)$, standard numerical integration routines might not produce reasonable approximations to the integrals in (4.19). This is remedied as follows.

- To compute the entries of $\mathbf{M}^j, \mathbf{K}^j, \mathbf{G}^j$ and $\mathbf{F}^j$, we first subdivide all intersected elements according to the position of the discrete interface as indicated by Figure 4.7(a). We then apply standard numerical integration routines of appropriate order on each of these
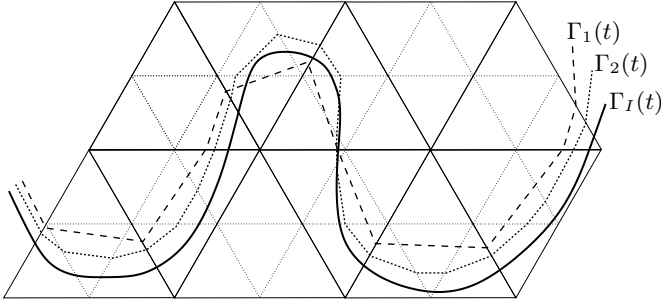
FIGURE 4.6. Determining the position of the discrete interface using linear ($\Gamma_1(t)$) and quadratic ($\Gamma_2(t)$) finite element spaces.

sub-triangles. This approach is proposed in [115] in the context of computational mechanics and is also used successfully by Chessa et al. [30] for the treatment of phase change problems.

- In case of $\mathbf{M}^j_{j-1}$, such an exact subdivision is not applicable (or at least very difficult to implement) as an element might be intersected by two interfaces that in turn might intersect. Therefore, we regularly refine all intersected elements and apply numerical integration schemes on the resulting triangulation to compute the entries of $\mathbf{M}^j_{j-1}$. This approach can be attributed to Dolbow [42] and is adapted by Zabaras et al. [168]. This situation is illustrated by Figure 4.7(b).

Evaluating the Stefan Condition. The Stefan condition

$$\rho\,L\,\vec{V}\cdot n = k_S\,\frac{\partial y_S}{\partial n} - k_F\,\frac{\partial y_F}{\partial n} = \left[k\,\nabla y\right]_F^S\cdot n \qquad\text{on } \Gamma_I(t) \qquad (2.4)$$

requires the evaluation of ∇y on $\Gamma_I(t)$. Due to the discontinuity of ∇y across $\Gamma_I(t)$ a straightforward evaluation is not possible. Since we are seeking only the normal component of the velocity, the domain integral method of Ji and Dolbow [87] could be applied. A more efficient approach to evaluating the normal velocity is the jump calculation used by Zabaras et al. [168], which we adapt here.

In addition to the point x_d on $\Gamma_I(t)$, the temperature is evaluated at three points, denoted by $x_S^{\delta/4}$, $x_S^{3\,\delta/4}$, x_S^{δ} and $x_F^{\delta/4}$, $x_F^{3\,\delta/4}$, x_F^{δ}, respectively, that are located on normals through x_d to $\Gamma_I(t)$ on each side of the interface. The distances of these points to $\Gamma_I(t)$ are $\frac{1}{4}\,\delta$, $\frac{3}{4}\,\delta$ and δ, where δ is chosen as the

(a) Exact subdivision.   (b) Regular refinement.
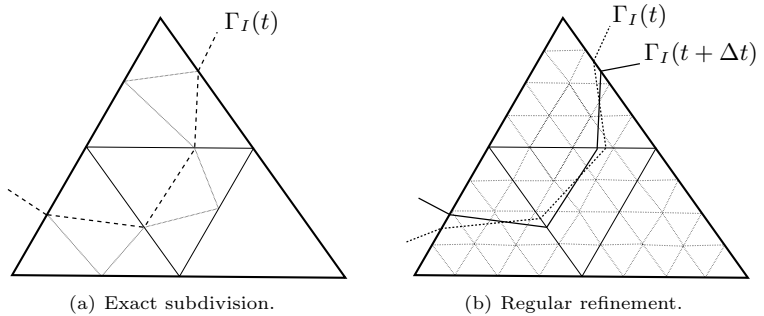
FIGURE 4.7. Numerical integration on intersected elements.

average element size. The slopes of the least squares lines through the pairs

$$\left\{ \left(0, y(x_d)\right), \left(\frac{\delta}{4}, y\big(x_{S/F}^{\delta/4}\big)\right), \left(\frac{\delta}{2}, y\big(x_{S/F}^{\delta/2}\big)\right), \left(\frac{3}{4}\,\delta, y\big(x_{S/F}^{3\,\delta/4}\big)\right), \left(\delta, y\big(x_{S/F}^{\delta}\big)\right) \right\}$$

are then taken as approximations to the temperature gradients in normal direction. Thus, the normal velocity of the interface is evaluated according to

$$\vec{V}\cdot n = \frac{1}{\rho\, L}\left[k_S\,\frac{2}{5}\frac{2\,y(x_d) + y\big(x_S^{\delta/4}\big) - y\big(x_S^{3\,\delta/4}\big) - 2\,y\big(x_S^{\delta}\big)}{\delta}\right.$$
$$\left. - k_F\,\frac{2}{5}\frac{2\,y\big(x_F^{\delta}\big) + y\big(x_F^{3\,\delta/4}\big) - y\big(x_F^{\delta/4}\big) - 2\,y(x_d)}{\delta}\right]$$

at the point x_d on $\Gamma_I(t)$. This construction is of course more involved and also slightly more costly than the simple jump calculation proposed in [**168**], but all numerical experiments have confirmed that this choice of the normal velocity is robust, reliable and, most important, reasonably accurate.

Enforcing the Interface Condition (3.2h)**.** The linear system (4.17) does not take into account the interface condition (3.2h). In [**30, 168**], this condition is enforced by deriving explicit constraint equations that are then added to (4.17) as penalty terms. An alternative to this explicit method is adapted from [**87**]. At each time level t^j, $j = 1, \ldots, N_T$, we require only the weak form

$$\int_{\Gamma_I(t^j)} \big(y_h - y_M\big)\, v\, ds = 0 \quad \text{ for all } v \in B^j$$

of (3.2h), where all continuous quantities are replaced by their discrete coun-
terparts using the finite element basis (4.18). This weak form can be ex-
pressed as the equivalent linear system

$$\mathbf{Q}^j\, Y^j = Y_I^j$$

that is added as a penalty term to (4.17). Thus, in each time step, we have
to solve

$$
\left(\frac{1}{\Delta t^j}\, \mathbf{M}^j + \mathbf{K}^j + \mu\, (\mathbf{Q}^j)^\top \mathbf{Q}^j \right) Y^j
$$

$$
= \frac{1}{\Delta t^j}\, \mathbf{M}^j_{j-1}\, Y^{j-1} + \mathbf{G}^j + \mathbf{F}^j + \mu\, (\mathbf{Q}^j)^\top Y_I^j
\tag{4.20}
$$

for Y^j for some value of the penalty parameter $\mu > 0$.

Remark 4.9 (Lagrange Multipliers for the Interface Condition). As explained
in [**87**], the isothermal interface condition can also be enforced by introducing
a Lagrange multiplier. This leads to a problem with saddle point structure
for which the inf-sup-stability of the discretization has to be proved.

Remark 4.10 (Including the Control). For the application of the discussed
extended finite element approximation of the temperature in the numerical
solution of optimal control problems, only one minor change is necessary.
As the control contributions are given in the form of Neumann boundary
data, they are assembled in the same way as a normal Neumann boundary
condition and added to $\mathbf{G}^j$.

4.4   An Algorithm for Solving the Forward Problem

Since the extended finite element approximation of y relies on the geometric
information provided by the level set function ϕ, it is natural to first advance
the level set equation one time step and then solve (4.20) to update the
temperature. Such a procedure can be realized thanks to the explicit time
discretization of the level set equation, see Section 4.2.2. This observation
already sets up the basic structure of an algorithm for the solution of the two-
phase Stefan problem. However, the energy balance equations (3.2a)–(3.2h)
are discretized in time using the implicit Euler method with the time steps
Δt^j, $j = 1, \ldots, N_T$, while a Runge-Kutta scheme with time steps $\Delta t^j_{\mathrm{CFL}}$, $j =
1, \ldots, N_T$, that must conform to the CFL condition (4.10) is used for the level
set equation (2.8). These time steps must be synchronized.
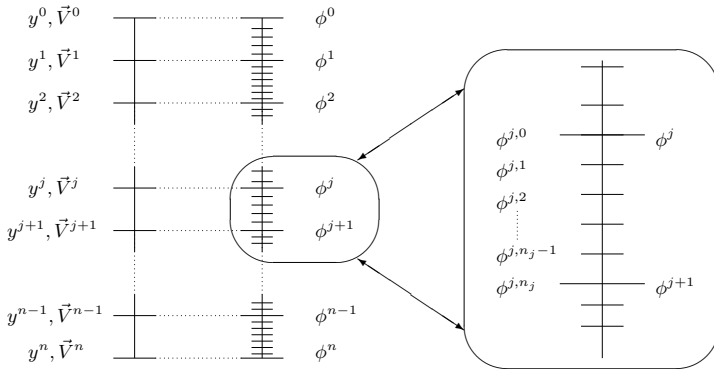
FIGURE 4.8. Interplay of the time stepping schemes.

In practice, this synchronization is realized by fixing the time steps Δt^j for the heat equation, while $\Delta t^j_{\mathrm{CFL}}$ is determined by the CFL condition (4.10). If $\Delta t^j_{\mathrm{CFL}}$ is smaller than the desired step size for the heat equation, several time steps for the level set equation are executed to arrive at the next point of the time grid for the heat equation. This procedure is illustrated by Figure 4.8. A benefit of such a fixed time grid is that the number of optimization variables is known a priori and does not change during an iterative optimization procedure. In addition, interpolation between different time steps can be avoided. For these reasons, we use a fixed equidistant time grid in all our computations.

Our solution strategy is summarized in Algorithm 3. Its formulation is tailored to the application to optimal control problems. In particular, all system matrices are stored for the efficient solution of the adjoint system. This approach is explained in more detail in Sections 4.5.2 and 4.6. In Algorithm 3, we use the notation $y^j = y(t^j)$, $\Gamma^j_I = \Gamma_I(t^j)$, and so on. NB^j denotes the narrow band in which all level set related computations are carried out at time step t^j.

The Frank Sphere. The growing Frank Sphere [56] is a perfect benchmark example (used, e.g., in [5, 25, 26, 67]) to verify the implementation of Algorithm 3 and to determine the order of convergence as an exact solution for both, the temperature and the interface position, is known. The setup of the Frank sphere is such that a solid nucleus which is initially a circle of radius

---

Algorithm 3 Solver for the Two-Phase Stefan Problem

Input: $\quad D, \Gamma_I(0), y_0, \phi^0, y_M, \rho, c_S, c_F, k_S, k_F, L, f, g, u, \{t^j\}_{j=0}^{N_T}, \mu$
Output: $y^j, \phi^j, \Gamma_I^j, \vec{V}^j, \text{NB}^j, \Delta t_{\text{CFL}}^j, \mathbf{M}^j, \mathbf{K}^j, \mathbf{Q}^j \quad$ for $j = 0, \ldots, N_T$
$\quad \mathcal{M}^j, \mathcal{K}^j \quad$ for $j = 0, \ldots, N_T - 1$, $\quad$ and $\quad \mathbf{M}_{j-1}^j \quad$ for $j = 1, \ldots, N_T$

1: Initialize NB^0, $\vec{V}^0$ and Δt_{CFL}^0, and assemble $\mathbf{M}^0$, $\mathbf{K}^0$ and $\mathbf{Q}^0$, $j \to 1$.
2: **while** $j \leq N_T$ **do**
3: $\quad$ $t_\phi \to 0$, $m \to 1$.
4: $\quad$ Assemble $\mathcal{M}^{j-1}$ and $\mathcal{K}^{j-1}$ for the scheme (4.4).
5: $\quad$ **while** $t_\phi < t^j - t^{j-1}$ **do**
6: $\quad\quad$ Compute $\phi^{j-1,m}$ using $\Delta t = \min\left\{\Delta t_{\text{CFL}}^{j-1}, t^j - t^{j-1} - t_\phi\right\}$.
7: $\quad\quad$ Update the narrow band NB^j if necessary.
8: $\quad\quad$ Reinitialize ϕ if necessary.
9: $\quad\quad$ $m \to m+1$, $t_\phi \to t_\phi + \Delta t$.
10: $\quad$ **end while**
11: $\quad$ Determine Γ_I^j and the enriched nodes.
12: $\quad$ Assemble $\mathbf{M}^j$, $\mathbf{K}^j$, $\mathbf{M}_{j-1}^j$, $\mathbf{Q}^j$, $\mathbf{G}^j$, $\mathbf{F}^j$ and Y_I^j.
13: $\quad$ Solve the linear system (4.20) for y^j.
14: $\quad$ Evaluate $\vec{V}^j$ and reinitialize ϕ^j by the fast marching method.
15: $\quad$ Compute Δt_{CFL}^j.
16: $\quad$ $j \to j+1$.
17: **end while**

---

s_0 at the equilibrium temperature $y_M = 0$ grows into an undercooled liquid in the infinite domain $\mathbb{R}^2$. The initial radius of the nucleus, s_0, is related to the temperature at infinity, y_∞, by the equation

$$y_\infty = \frac{s_0}{2} \frac{F(s_0)}{F'(s_0)}.$$

The value $s_0 = 0.25$ corresponds to $y_\infty = -0.05709187113307$ [**25**]. At time t, the exact temperature distribution is

$$y(x,t) = \tilde{y}(s) = \begin{cases} y_\infty\left(1 - \frac{F(s)}{F(s_0)}\right) & s > s_0, \\ 0 & s \leq s_0, \end{cases} \qquad (4.21)$$

where the similarity variable $s = \frac{r}{\sqrt{t}}$ depends on the radius $r = \sqrt{x_1^2 + x_2^2}$, and

$$F(s) = \int_{s^2/4}^{\infty} \frac{e^{-t}}{t} \, dt.$$

Thus, at any instance of time, the interface is the boundary of

$$\Omega_S(t) = \{(x_1, x_2) \in \mathbb{R}^2 \mid \sqrt{x_1^2 + x_2^2} \le s_0 \sqrt{t}\},$$

i.e., it is a circle with radius $s_0 \sqrt{t}$.

To solve this problem numerically in the time interval $[1, 2]$, we use the hold-all $D = [-1, 1]^2$ and the parameters

$$\rho = L = c_S = c_F = k_S = k_F = 1, \ y_M = 0.$$

The coarsest discretization ($h = 0.4$) corresponds to 144 triangles and 50 time steps, while the finest grid ($h = 0.025$) consists of 36864 triangles and 800 time steps are taken in this case. Exact Dirichlet boundary conditions are imposed on ∂D using (4.21). The error indicators for the temperature at $t = T$,

$$E_T^2(y_h) := \left(\int_D |y_h(x, T) - y(x, T)|^2 \, dx \right)^{1/2}$$

and

$$E_T^\infty(y_h) := \sup_D |y_h(x, T) - y(x, T)|,$$

are of L^2 and L^∞ type, respectively. Here, y_h denotes the numerical solution, and y is the exact solution as given in (4.21). For measuring the error in the interface position, we use (4.14) and (4.15). As documented in Table 4.4 and Table 4.5, the convergence rate in all four cases is slightly less than linear. Potential reasons for this sub-optimal behavior are indicated in Remark 4.6. In addition, the Frank sphere example has been found to be ill-posed [66], making its accurate numerical solution a challenging task. However, compared with the results in [25], where the same parameters are used, we can state that our solver exhibits reasonable accuracy. ⋄

Solidification in a Corner. In addition to the Frank sphere example, we validate Algorithm 3 by considering the benchmark problem of a material solidifying in an infinite corner that has been treated, for instance, in [8, 30, 103, 168]. We simulate this problem by solving the two-phase Stefan problem in the domain $D = [0, 14] \times [0, 14]$. The parameters are chosen as

$$\rho = 1, \ L = 0.25, \ c_S = c_F = k_S = k_F = 1$$

resulting in equal thermal diffusivities in both phases. The equilibrium temperature is $y_M = 0$, the initial temperature is $y_0(x) = 0.3$. As in the Frank sphere example, no heat sources are present. The boundary conditions are given by the Dirichlet condition $y = -1$ on the lower and the left part of ∂D and the insulation condition $\frac{\partial y}{\partial n} = 0$ on the upper and the right part of ∂D.

TABLE 4.4. Errors and estimated orders of convergence for
the temperature in the Frank sphere example at $t = T$.

h	$E_T^2(y_h)$	eoc	$E_T^\infty(y_h)$	eoc
0.400	8.0462e-03	–	1.1409e-02	–
0.200	5.2930e-03	0.60	7.8064e-03	0.55
0.100	2.6942e-03	0.97	4.3767e-03	0.83
0.050	1.3958e-03	0.95	2.4855e-03	0.82
0.025	7.4430e-04	0.91	1.4822e-03	0.75
eoc		0.88		0.75

TABLE 4.5. Errors and estimated orders of convergence for
the interface position in the Frank sphere example at $t = T$.

h	$E_T^2(\phi_h)$	eoc	$E_T^\infty(\phi_h)$	eoc
0.400	1.9575e-01	–	1.6698e-01	–
0.200	1.3178e-01	0.57	1.1265e-01	0.57
0.100	6.6174e-02	0.99	5.7688e-02	0.97
0.050	3.4302e-02	0.95	3.2080e-02	0.85
0.025	1.8719e-02	0.87	1.8272e-02	0.81
eoc		0.87		0.82

As cited in [8], the interface position in dimensionless coordinates

$$x_i^* = \frac{x_i}{\sqrt{4\,a\,t}}$$

is constant in time and given by

$$x_2^* = \left(\lambda^\omega + \frac{\zeta}{(x_1^*)^\omega - \lambda^\omega}\right)^{1/\omega} \tag{4.22}$$

for an infinite region. The constants $\lambda \approx 0.70766$, $\omega \approx 5.02$ and $\zeta \approx 0.159$ are determined numerically, and a is the thermal diffusivity that has to be equal in both phases:

$$a = \frac{k_S}{\rho\,c_S} = \frac{k_F}{\rho\,c_F} = 1.$$

Figure 4.9 shows this dimensionless interface in comparison with interface positions obtained by Algorithm 3 at four different time steps in the interval $[0, 4]$. The prediction of the interface is reasonably close to the analytic solution at all four time steps. In addition, Figure 4.10 shows the temperature
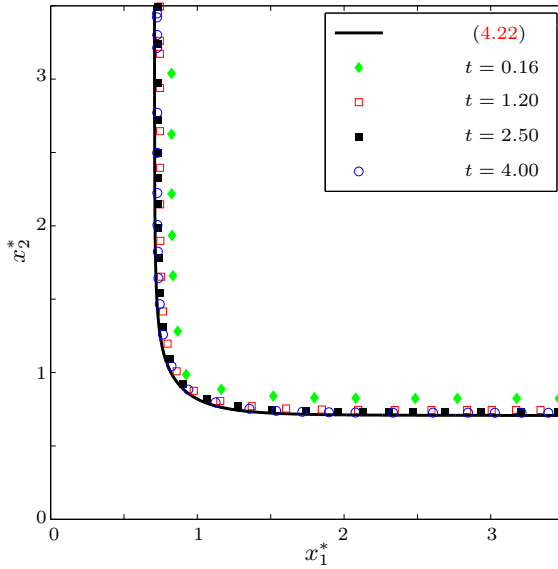
FIGURE 4.9. Analytic and numerical solution for the corner solidification problem at four time steps in dimensionless coordinates.

distribution for the solidification process corresponding to the four time steps in Figure 4.9. These results were obtained with a discretization involving 16384 triangles and 1000 time steps.   ◇

4.5   Discretization of the Adjoint Level Set Equation

One way of discretizing the adjoint Stefan condition (3.10k)–(3.10l) is to go back one step in the derivation of the optimality conditions and to rewrite (3.8) as the first-order PDE

$$\rho \, L \, |\nabla\phi| \left(\dot{\Psi} + \Psi \, \mathrm{div}_{\Gamma_I(t)} \vec{W} \right) = -\frac{\gamma_2}{2} \left(\frac{\partial}{\partial n} \left(|\phi_d|^2 \right) + \kappa \, |\phi_d|^2 \right) + \frac{\partial y}{\partial n} \, p_I$$

$$\rho \, L \, |\nabla\phi| \, \Psi(0) = -\frac{\gamma_4}{2} \left(\frac{\partial}{\partial n} \left(|\phi_T|^2 \right) + \kappa \, |\phi_T|^2 \right)$$

(3.9)

on the moving surface $\Gamma_I(t)$.

(a) $t = 0.16$

(b) $t = 1.20$

(c) $t = 2.50$

(d) $t = 4.00$
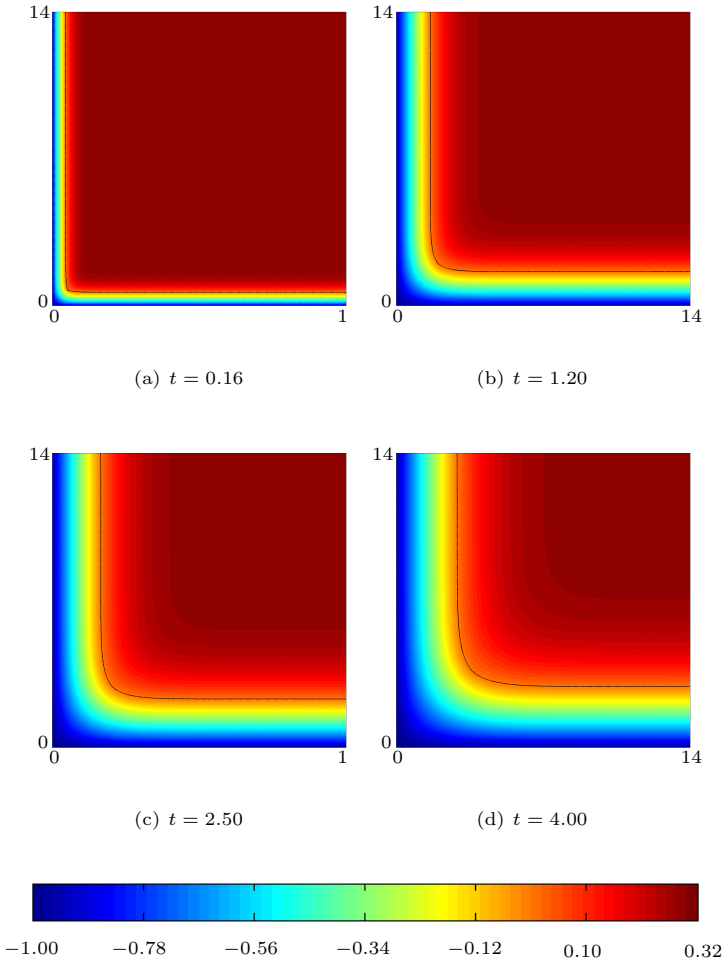
FIGURE 4.10. Temperature distribution for the corner solidification problem at four time steps.

Numerical methods for partial differential equations on moving or evolving surfaces are a rather recent research topic in numerical and applied mathematics. Nonetheless, there is already a broad spectrum of numerical schemes

for conservation equations to choose from. Dziuk and Elliott [49] consider a conservation equation with a diffusive term. They assume an evolving polygonal approximation of the surface which allows for the natural definition of finite element spaces on the surface. The resulting finite element basis functions enjoy a transport property that implies a significant simplification of the scheme. In the follow-up paper [50], the same authors exploit a level set framework. By an application of the coarea formula, the conservation equation on the moving surface is extended to an equation on a certain fixed domain, on which standard finite element spaces can be defined. This approach may be combined with the h-narrow band method of Deckelnick et al. [39] to make the computations more efficient. Lenz et al. [104] translate the finite element method of [49] to a finite volume framework. As in the previously mentioned works, the underlying PDE is a conservation equation with a diffusive term. Adalsteinsson and Sethian [2] and Xu and Zhao [165] pursue a somewhat different idea. In both cases, the quantities involved in the conservation equation on the moving interface are extended to a narrow band by standard level set techniques, i.e., by a constant extension in normal direction. This allows for the extension of the given PDE to neighboring level sets of the interface, and, consequently, for the use of standard finite difference schemes for second-order PDEs on fixed domains.

Unfortunately the PDE (3.9) lacks diffusive terms and, thus, the available discretization strategies described above all exhibit stability problems. This could be circumvented by adapting the finite volume methods of Du and coworkers [43, 44] or Lenz et al. [104] to first-order equations. As an alternative, we note that all derivatives in the first-order conservation law (3.10k) on $\Gamma_I(t)$ are globally defined. Thus, this equation can be directly extended to all of D, or at least to a narrow band around $\Gamma_I(t)$, by using a constant extension of the terminal condition (3.10l) and the forcing term on the right hand side of (3.10k) as in [2, 165]. In the next subsection, we present a suitable discretization of the resulting partial differential equation.

4.5.1. Spatial and Temporal Discretization

It turns out that after applying the constant extension procedure described above, the first-order conservation equation (3.8) on the moving interface $\Gamma_I(t)$ transforms into a first-order conservation law in D which can be written in the standard form

$$-\psi_t - \operatorname{div}(\psi\,\vec{V}) = r \qquad \text{in } D, \qquad (4.23a)$$

$$\psi(T) = r_T \qquad \text{in } D, \qquad (4.23b)$$

where r and r_T denote constant extensions in normal direction to $\Gamma_I(t)$ of the right hand side of (3.8a) (or, equivalently, (3.10k)) and of the terminal condition (3.8b) (or, equivalently, (3.10l)), both normalized by $\frac{1}{\rho\,L\,|\nabla\phi|}$.

Spatial Discretization. The conservation law (4.23) can be solved by finite difference, finite volume, or stabilized finite element methods. However, as we have already chosen to use a discontinuous Galerkin scheme for the spatial discretization of the level set equation, it is natural to use a similar strategy for its adjoint as well. Discontinuous Galerkin schemes for first-order conservation laws have received a lot of attention during the last two decades, see, e.g., [34] and the references therein. They exhibit several properties that make them attractive, for instance, local conservation and the ease of implementation of higher-order methods, to mention only two.

The approach of Kuzmin [101] is particularly appealing because it does not involve any parameters that have to be tuned, and it avoids the detection of troubled cells. As in Section 4.2.1, we assume that we are given the triangulation $\mathcal{T}_h$ of D on which we define the space $\mathcal{P}^k_{\mathrm{pw}}$, see (4.3). To obtain the scheme, we multiply (4.23a) with a suitable test function w and integrate over an arbitrary element K of $\mathcal{T}_h$. By integration-by-parts, the divergence acting on ψ is transformed into a gradient acting on the test function w. After replacing all continuous quantities by their discrete counterparts from $\mathcal{P}^k_{\mathrm{pw}}$, the scheme reads:

Find $\psi_h(x,t) \in \mathcal{P}^k_{\mathrm{pw}}$ such that

$$\int_K -\left(\partial_t \psi_h\right) w_h + \psi_h\, \vec{V}\cdot\nabla w_h\,dx - \int_{\partial K} w_h\,\hat{\psi}_h\,\vec{V}\cdot n\,ds = \int_K r\,w_h\,dx$$

$$(4.24)$$

for all $w_h \in \mathcal{P}^k_{\mathrm{pw}}$ and for all $K \in \mathcal{T}_h$.

The numerical flux $\hat{\psi}_h$ in the boundary integral is defined as

$$\hat{\psi}_h(x,t) = \begin{cases} \psi_h^+(x,t) & -\vec{V}\cdot n < 0,\ x \in \bar{D}\setminus\partial D, \\ \bar{\psi}(x,t) & -\vec{V}\cdot n < 0,\ x \in \partial D, \\ \psi_h^-(x,t) & -\vec{V}\cdot n \geq 0,\ x \in \bar{D}, \end{cases}$$

where $\bar{\psi}$ are Dirichlet boundary data, and $\psi_h^+(x,t), \psi_h^-(x,t)$ are to be understood in the sense of (4.5). The minus sign in front of the normal velocity $\vec{V}\cdot n$ is necessary as the direction of the velocity is reversed compared to the level set equation. A vertex-based slope limiter has to be used when implementing (4.24), we refer to [101] for the details.

Temporal Discretization. The discussion of the temporal discretization of the level set equation (2.8) in Section 4.2.2 also covers the temporal discretization

of the corresponding adjoint equation (3.8). As motivated below, the finite element spaces for the adjoint equations are the same as for the forward equations, and, thus, the strong stability preserving Runge-Kutta method specified by the Butcher array in Table 4.1 is applicable. The time steps are restricted by the CFL condition (4.10).

4.5.2. Implementation

This section highlights some aspects of the implementation of the discontinuous Galerkin scheme (4.24).

Boundary Conditions. To derive the adjoint system (3.10), we included only a restriction of the level set equation to the interface, the Stefan condition, in the forward system (3.2). As a consequence, no boundary conditions for the level set equation have to be specified on the continuous level—it suffices to implement suitable boundary conditions on the fully discrete level, see Section 4.2.3. Another implication of this approach is of course that the derivation of the adjoint system does not yield suitable boundary conditions for the adjoint level set equation. Thus, the Dirichlet boundary data $\bar{\psi}$ in the definition of the numerical flux $\hat{\psi}_h$ are not given naturally. Rather, artificial boundary conditions are implemented in the same way as for the level set equation, i.e., in the time step from ψ^{j+1} to ψ^j, the boundary data $\bar{\psi} = \psi^{j+1}$ are taken. To minimize the influence of these conditions, we use a reinitialization procedure that is similar to the reinitialization of the level set function ϕ, see Section 4.2.3. The adjoint state ψ is evaluated at the interface and then extended constantly in normal direction to all of the current narrow band by solving (4.13) by the fast marching method.

Curvature. For the discretization of the curvature κ that arises in the right hand sides of (3.10k) and (3.10l), we make use of the finite element scheme proposed by Fried [58, Chapter 4]. We extend the relation (2.10) from $\Gamma_I(t)$ to all of D, multiply by a proper test function w and integrate over the given hold-all:

$$\int_D \kappa\, w\, dx = \int_D w\, \operatorname{div} \frac{\nabla \phi}{|\nabla \phi|}\, dx.$$

Integration by parts on the right hand side yields

$$\int_D \kappa\, w\, dx = \int_{\partial D} w\, \frac{\nabla \phi}{|\nabla \phi|} \cdot n\, ds - \int_D \nabla w \cdot \frac{\nabla \phi}{|\nabla \phi|}\, dx,$$

which is the basis for defining a weak curvature of the interface $\Gamma_I(t)$. Choosing Dirichlet boundary conditions on ∂D implies that $w = 0$ at the boundary. Thus, this weak form simplifies to

$$\int_D \kappa\, w\, dx = - \int_D \nabla w \cdot \frac{\nabla \phi}{|\nabla \phi|}\, dx \quad \forall w \in V_0^\kappa, \qquad (4.25)$$

where

$$V^\kappa := \{w \in C(\bar{D}) \mid w|_K \in P^2(K) \ \text{ for all } \ K \in \mathcal{T}\},$$
$$V_0^\kappa := V^\kappa \cap H_0^1(D).$$

As the gradient of ϕ possibly vanishes in certain non-smooth configurations, Fried proposes to regularize the denominator $|\nabla\phi|$ in (4.25) by replacing it by the quantity $\sqrt{|\nabla\phi|^2 + \epsilon_\kappa^2}$ for small $\epsilon_\kappa > 0$. We follow his advice, and we introduce additional regularization into (4.25) by adding a diffusive term of the form $-\epsilon_\kappa \Delta\kappa$. Thus, to obtain the discrete curvature, we solve the problem:

Find $\kappa \in V^\kappa$ such that

$$\int_D \kappa\, w\, dx + \epsilon_\kappa \int_D \nabla w \cdot \nabla\kappa = -\int_D \nabla w \cdot \frac{\nabla\phi}{\sqrt{|\nabla\phi|^2 + \epsilon_\kappa^2}}\, dx \qquad (4.26)$$

for all $w \in V_0^\kappa$ with the boundary condition $\kappa = \kappa_0$ on ∂D.

Remark 4.11. (1) Fried [**58**, Chapter 4] shows that using linear finite elements to solve (4.26) might prohibit convergence of the method. This is the reason for choosing quadratic finite element spaces, in particular in the solution of (4.26), but consequently also for the X-FEM for approximating the temperature and its adjoint, see Section 4.3.

(2) Because ϕ is computed in a narrow band around the current position of $\Gamma_I(t)$ only, we have to restrict the computation of κ to the same narrow band. This affects the definition of the spaces V^κ and V_0^κ and the evaluation of the integrals in (4.26).

Efficient Implementation and Taylor Basis. As for the level set equation (2.8) in the solution of the system (3.2), it suffices to solve (4.24) in a narrow band around the current position of $\Gamma_I(t)$. Note that the interface positions and the corresponding narrow bands at any instance of time are already known from the solution of the forward problem (3.2). A strategy for the solution of the adjoint level set equation in this situation is thus given as follows, assuming that the forcing terms r and r_T in (4.23) are independent of the adjoint temperature p:

- Initialize $\psi(x, T)$ by (4.23b) and evaluate the source term in (4.23a).
- While $t > 0$
  - Evolve (4.24) for one time step.
  - Extend $\psi(x, t)$ off the interface constantly in normal direction.
  - Evaluate the source term in (4.23a).

A more detailed description is given in Algorithm 4. Of course, a coupling of the schemes (4.4) and (4.24) to solve the level set equation and its adjoint simultaneously is also possible.

The vertex-based slope limiter designed in [**101**] aims at limiting variations in the spatial derivatives of the solution. If the mass matrix of the scheme (4.24) is non-diagonal, the application of an additional limiting procedure for temporal derivatives of the solution is necessary. This is the motivation for using a local Taylor basis in which a conservative mass lumping is achieved by setting all off-diagonal entries of the mass matrix equal to zero. To make the implementation consistent, and for the sake of efficiency, we use the same Taylor basis also in the discontinuous Galerkin scheme (4.4) for the level set equation (2.8) in the solution of (3.2), see Section 4.2.3. As a consequence, the mass matrix that is induced by the bilinear form

$$\int_K \psi \, w \, dx \quad \text{for all} \quad K \in \mathcal{T}_h$$

is the mass matrix corresponding to (4.4), provided that we use the same polynomial degree in the spaces of trial functions, see (4.3). In addition, the system matrix that is induced by the bilinear form

$$\int_K \psi \, \vec{V} \cdot \nabla w \, dx \quad \text{for all} \quad K \in \mathcal{T}_h$$

is the transpose of the matrix that is induced by the corresponding bilinear form in (4.4), provided again that we use the same polynomial degree in the spaces of trial functions. Thus, the matrices from solving (2.8) in the forward problem are stored and then invoked again during the solution of the adjoint problem.

4.5.3. Numerical Examples

Convergence of the Weak Curvature. We test the convergence of solutions of equation (4.26) in two different situations. The first test example involves a smooth interface whose curvature is defined everywhere. The interface in the second test case is a square whose curvature is not defined at the four corners. In both cases, we use the norm

$$E_\infty^{\epsilon_\kappa}(\kappa_h) := \|\kappa^* - \kappa_h\|_{\infty,\Gamma} = \sup_\Gamma |\kappa^* - \kappa_h|$$

to estimate the errors. Here, κ^* denotes the exact curvature of the interface Γ, and κ_h is the solution of (4.26) corresponding to the regularization parameter ϵ_κ. In all our numerical experiments, the default value for the regularization parameter ϵ_κ is defined as $\epsilon_\kappa^h := 10^{-4}\sqrt{h}$, where h is the longest of all triangle edges in the mesh. The underlying computational domain is the

TABLE 4.6. Convergence test for (4.26) on a circle with radius 0.15 and different values of ϵ_κ.

h	$\epsilon_\kappa = 10^{-1}$	eoc	$\epsilon_\kappa = 10^{-3}$	eoc	$\epsilon_\kappa = 10^{-5}$	eoc	$\epsilon_\kappa = \epsilon_\kappa^h$	eoc
0.4000	5.88e+00	–	2.03e+00	–	3.27e+00	–	3.10e+00	–
0.2000	5.63e+00	0.06	4.50e−01	2.02	8.73e−01	1.90	6.24e−01	2.31
0.1000	2.81e+00	1.00	4.06e−01	0.30	2.68e−01	1.70	1.99e−01	1.65
0.0500	2.75e+00	0.03	3.14e+00	-2.95	8.23e−02	1.70	5.61e−02	1.83
0.0250	1.29e+01	-2.23	1.50e+00	1.06	3.32e−02	1.31	4.23e−02	0.41
0.0125	3.28e+01	-1.35	2.30e+01	-3.94	3.19e−01	-3.26	2.55e−01	-2.59

TABLE 4.7. Convergence test for (4.26) on a circle with radius 0.3 and different values of ϵ_κ.

h	$\epsilon_\kappa = 10^{-1}$	eoc	$\epsilon_\kappa = 10^{-3}$	eoc	$\epsilon_\kappa = 10^{-5}$	eoc	$\epsilon_\kappa = \epsilon_\kappa^h$	eoc
0.4000	2.88e+00	–	2.36e−01	–	5.37e−01	–	4.43e−01	–
0.2000	3.21e+00	-0.16	2.50e−02	3.24	1.64e−01	1.71	1.38e−01	1.68
0.1000	7.37e−01	2.13	3.28e−01	-3.71	7.64e−02	1.10	5.32e−02	1.38
0.0500	6.07e+00	-3.04	1.24e+00	-1.92	2.04e−02	1.91	1.51e−02	1.82
0.0250	1.62e+01	-1.42	4.62e+00	-1.90	1.21e−02	0.76	1.79e−02	-0.25
0.0125	3.61e+01	-1.16	2.63e+01	-2.51	1.50e−01	-3.64	1.22e−01	-2.77

TABLE 4.8. Convergence test for (4.26) on a circle with radius 0.45 and different values of ϵ_κ.

h	$\epsilon_\kappa = 10^{-1}$	eoc	$\epsilon_\kappa = 10^{-3}$	eoc	$\epsilon_\kappa = 10^{-5}$	eoc	$\epsilon_\kappa = \epsilon_\kappa^h$	eoc
0.4000	2.09e+00	–	5.20e−01	–	5.36e−01	–	4.97e−01	–
0.2000	2.19e+00	-0.06	3.74e−01	0.47	2.65e−01	1.01	2.45e−01	1.02
0.1000	1.45e+00	0.59	5.97e−01	-0.67	4.30e−02	2.62	2.55e−02	3.26
0.0500	6.42e+00	-2.14	1.17e+00	-0.97	8.17e−03	2.39	6.57e−03	1.96
0.0250	1.75e+01	-1.45	5.91e+00	-2.34	7.98e−03	0.03	1.19e−02	-0.86
0.0125	3.76e+01	-1.10	2.78e+01	-2.24	9.45e−02	-3.57	7.84e−02	-2.72

square $D = [-0.5, 0.5]^2$. As in Section 4.2.4, we decrease the grid size from $h = 0.4$ (which corresponds to 64 triangles) to $h = 0.0125$ (which corresponds to 65536 triangles).

(1) *A smooth example:* The considered interface is a circle, centered at the origin, whose exact curvature is given by the reciprocal of its radius. We solve (4.26) for different radii and vary the grid size and the regularization parameter ϵ_κ for each of these radii. The results

TABLE 4.9. Convergence test for (4.25) on a circle with radius 0.15 and different values of ϵ_κ.

h	$\epsilon_\kappa = 10^{-1}$	eoc	$\epsilon_\kappa = 10^{-3}$	eoc	$\epsilon_\kappa = 10^{-5}$	eoc	$\epsilon_\kappa = \epsilon_\kappa^h$	eoc
0.4000	7.15e+00	–	3.29e+00	–	3.31e+00	–	3.31e+00	–
0.2000	6.28e+00	0.19	1.11e+00	1.56	1.06e+00	1.64	1.06e+00	1.64
0.1000	6.55e+00	-0.06	1.08e+00	0.04	3.65e−01	1.54	3.65e−01	1.54
0.0500	6.63e+00	-0.02	3.76e+00	-1.80	2.20e−01	0.73	2.17e−01	0.75
0.0250	6.66e+00	-0.01	5.88e+00	-0.64	1.27e−01	0.79	1.40e−01	0.64
0.0125	6.67e+00	-0.00	6.47e+00	-0.14	3.51e−01	-1.46	2.83e−01	-1.02

TABLE 4.10. Convergence test for (4.25) on a circle with radius 0.3 and different values of ϵ_κ.

h	$\epsilon_\kappa = 10^{-1}$	eoc	$\epsilon_\kappa = 10^{-3}$	eoc	$\epsilon_\kappa = 10^{-5}$	eoc	$\epsilon_\kappa = \epsilon_\kappa^h$	eoc
0.4000	2.59e+00	–	5.66e−01	–	5.64e−01	–	5.64e−01	–
0.2000	3.09e+00	-0.25	2.08e−01	1.44	1.82e−01	1.63	1.82e−01	1.63
0.1000	3.27e+00	-0.08	3.90e−01	-0.90	1.11e−01	0.72	1.10e−01	0.72
0.0500	3.32e+00	-0.02	1.90e+00	-2.28	5.33e−02	1.05	5.48e−02	1.01
0.0250	3.33e+00	-0.00	2.93e+00	-0.63	2.14e−02	1.32	2.76e−02	0.99
0.0125	3.34e+00	-0.00	3.24e+00	-0.14	1.82e−01	-3.09	1.48e−01	-2.42

TABLE 4.11. Convergence test for (4.25) on a circle with radius 0.45 and different values of ϵ_κ.

h	$\epsilon_\kappa = 10^{-1}$	eoc	$\epsilon_\kappa = 10^{-3}$	eoc	$\epsilon_\kappa = 10^{-5}$	eoc	$\epsilon_\kappa = \epsilon_\kappa^h$	eoc
0.4000	1.63e+00	–	5.44e−01	–	5.46e−01	–	5.46e−01	–
0.2000	2.07e+00	-0.35	2.90e−01	0.91	2.74e−01	0.99	2.74e−01	0.99
0.1000	2.18e+00	-0.07	2.91e−01	-0.00	7.89e−02	1.80	7.87e−02	1.80
0.0500	2.21e+00	-0.02	1.26e+00	-2.11	2.10e−02	1.91	2.20e−02	1.84
0.0250	2.22e+00	-0.01	1.96e+00	-0.64	1.74e−02	0.27	2.15e−02	0.03
0.0125	2.23e+00	-0.00	2.16e+00	-0.14	1.19e−01	-2.78	9.65e−02	-2.16

are reported in Tables 4.6–4.8. We repeat these experiments with the same setup, but we remove the diffusive regularization part, i.e., we solve (4.25) instead of (4.26). The results are reported in Tables 4.9–4.11.

(2) *A non-smooth example:* The considered interface is a square, centered at the origin. In this case, the curvature is zero away from the four corners, in which it is not defined. We take this into

account when computing the errors by neglecting the four corner
points of the square. Similar to the first test case, we solve (4.26)
for different side lengths of the square and again vary the grid size
and the regularization parameter ϵ_κ. The results are reported in
Tables 4.12–4.14.

In summary, we interpret these results as follows. For large values of the
regularization parameter ϵ_κ, the errors in all three test cases are rather large
and we do not observe convergence. In fact, the error increases in almost
all cases. As ϵ_κ is decreased, the errors go down in general and we observe
convergence, albeit at rather irregular rates. This is not true when passing to
the finest grid on which the error increases again. We attribute this behavior
to the fact that the boundary of the computational domain, the narrow band,
is too close to the interface, see Figure 4.11. As a consequence, the artificial
boundary conditions κ_0 that we pose in (4.26) significantly influence the
values of the weak curvature. This may be remedied by enlarging the narrow
band in case of fine grid computations. At moderate grid sizes, this effect
can be ignored. A comparison of Tables 4.6–4.8 and 4.9–4.11 explains the
additional regularization that we introduced by adding a diffusive term to
the scheme (4.25). The solutions we obtain on basis of the fully regularized
problem (4.26) are in general more well-behaved than the solutions to (4.25).
To be more precise, the error is smaller when using the additional diffusive
regularization and we observe better convergence rates.   ◇

A Test Example for the Adjoint Level Set Equation. We now verify the
proposed solver for conservation laws on moving surfaces that is used to
solve the adjoint level set equation in Algorithm 4 on a test example for
which the exact solution is obvious. Once again, the square $D = [-1, 1]^2$
serves as the hold-all. At initial time $t = 0$, the interface is a circle with
radius 0.25, centered at $(0.5, 0.5)^\top$. The initial distribution

$$\psi(0) = \cos\left(2\arctan\frac{x_2 - 0.5}{x_1 - 0.5}\right)$$

of the adjoint level set function is periodic. In the time interval $[0, 1]$, the con-
stant velocity field $\vec{V} = (-1, -1)^\top$ moves the interface to the circle with cen-
ter point $(-0.5, -0.5)^\top$, the radius remains unchanged. We set all constants
equal to unity and neglect source terms. As the chosen velocity field $\vec{V}$ is in
particular divergence-free, we solve the pure transport equation (see (3.9))
$\dot{\psi} = 0$ along the moving circle. At any instance of time, the exact solution
obviously has the same distribution as the initial data. We calculate the
solution numerically for the same decreasing sequence of grid sizes as in Sec-
tion 4.2.4. At the same time, the time steps are refined in accordance with

TABLE 4.12. Convergence test for (4.26) on a square with side length 0.4 and different values of ϵ_κ.

h	$\epsilon_\kappa = 10^{-1}$	eoc	$\epsilon_\kappa = 10^{-3}$	eoc	$\epsilon_\kappa = 10^{-5}$	eoc	$\epsilon_\kappa = \epsilon_\kappa^h$	eoc
0.4000	6.39e−01	–	1.64e+01	–	2.70e+01	–	2.60e+01	–
0.2000	9.04e−02	2.82	1.77e+01	-0.11	4.09e+01	-0.60	3.83e+01	-0.56
0.1000	3.66e+00	-5.34	1.61e+01	0.13	5.20e+01	-0.35	4.74e+01	-0.31
0.0500	9.56e+00	-1.38	6.82e+00	1.24	2.37e+01	1.13	2.87e+01	0.72
0.0250	1.95e+01	-1.03	7.60e+00	-0.16	1.13e+00	4.39	6.05e+00	2.24
0.0125	3.94e+01	-1.01	2.95e+01	-1.96	1.29e+01	-3.51	1.16e+01	-0.93

TABLE 4.13. Convergence test for (4.26) on a square with side length 0.6 and different values of ϵ_κ.

h	$\epsilon_\kappa = 10^{-1}$	eoc	$\epsilon_\kappa = 10^{-3}$	eoc	$\epsilon_\kappa = 10^{-5}$	eoc	$\epsilon_\kappa = \epsilon_\kappa^h$	eoc
0.4000	4.48e−01	–	1.55e+01	–	2.69e+01	–	2.57e+01	–
0.2000	1.17e−01	1.94	1.54e+01	0.01	3.21e+01	-0.26	3.03e+01	-0.24
0.1000	4.01e+00	-5.10	1.42e+01	0.12	2.88e+01	0.16	2.82e+01	0.10
0.0500	9.39e+00	-1.23	5.93e+00	1.26	1.46e+01	0.98	5.50e+00	2.36
0.0250	1.95e+01	-1.05	7.61e+00	-0.36	5.92e+00	1.30	6.59e+00	-0.26
0.0125	3.99e+01	-1.04	2.95e+01	-1.96	3.31e+00	0.84	2.76e+00	1.26

TABLE 4.14. Convergence test for (4.26) on a square with side length 0.8 and different values of ϵ_κ.

h	$\epsilon_\kappa = 10^{-1}$	eoc	$\epsilon_\kappa = 10^{-3}$	eoc	$\epsilon_\kappa = 10^{-5}$	eoc	$\epsilon_\kappa = \epsilon_\kappa^h$	eoc
0.4000	2.40e−01	–	1.39e+01	–	2.12e+01	–	2.06e+01	–
0.2000	6.54e−02	1.88	1.42e+01	-0.04	2.80e+01	-0.40	2.64e+01	-0.36
0.1000	1.18e+00	-4.17	1.20e+01	0.24	1.43e+01	0.97	1.12e+01	1.24
0.0500	9.37e+00	-2.99	5.00e+00	1.27	2.04e+01	-0.51	1.20e+01	-0.11
0.0250	1.95e+01	-1.06	7.66e+00	-0.62	8.48e−01	4.59	1.33e+00	3.18
0.0125	3.93e+01	-1.01	2.94e+01	-1.94	8.05e−01	0.07	6.23e−01	1.09

the CFL condition (4.10). The known exact interface position is provided in each time step to eliminate additional errors that are introduced by solving the level set equation for the evolution of the interface. We measure the error at $t = T$ in an L^2 as well as in an L^∞ sense (see Sections 4.2.4 and 4.4)

$$E_T^2(\psi_h) := \left(\int_{\Gamma_I(T)} |\psi_h - \psi|^2 \, ds \right)^{1/2}, \quad E_T^\infty(\psi_h) := \sup_{\Gamma_I(T)} |\psi_h - \psi|.$$

(a) $h = 0.1000$ (b) $h = 0.0500$

(c) $h = 0.0250$ (d) $h = 0.0125$
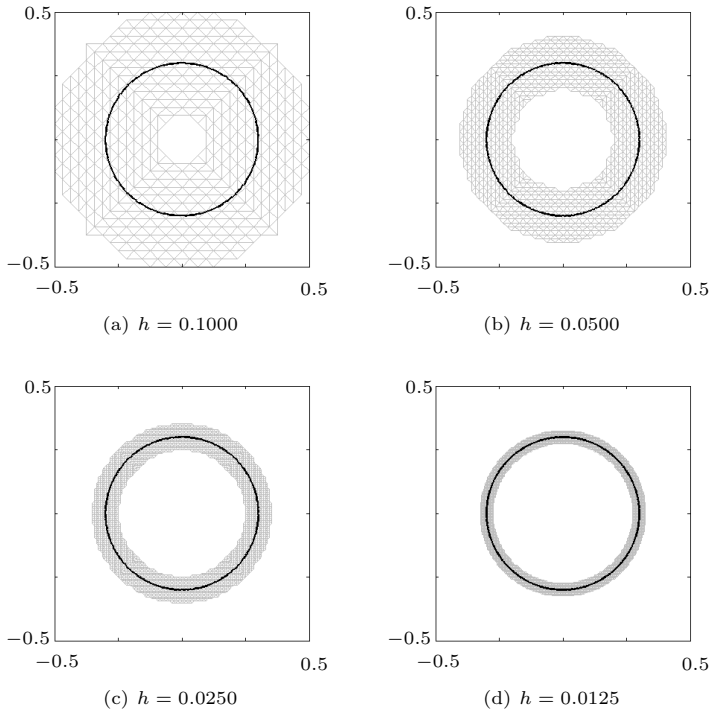
FIGURE 4.11. Narrow band meshes for different grid sizes h as used in the computation of the curvature of a circle with radius 0.3.

The results are reported in Table 4.15. We observe that the method converges in this test case. The convergence rates with respect to both error indicators are rather low. As for the level set equation, this can be at least partially attributed to the fact that the reinitialization we use is of lower order, see Remark 4.6. Figure 4.12 shows the evolution of the interface along with the surrounding narrow band, and the distribution of the adjoint level set function ψ_h for a discretization of the given hold-all with 16384 triangles (which corresponds to the grid size $h = 0.05$) and 807 time steps.   ⋄

TABLE 4.15. Errors and estimated orders of convergence for the transport equation on the moving interface. The last row is based on a least-squares approach taking into account all grid sizes and all errors.

h	$E_T^2(\psi_h)$	eoc	$E_T^\infty(\psi_h)$	eoc
0.400	6.1393e−01	–	7.7532e−01	–
0.200	1.4660e−01	2.07	2.4822e−01	1.64
0.100	9.8521e−02	0.57	1.8420e−01	0.43
0.050	3.6755e−02	1.42	8.3621e−02	1.14
0.025	1.9948e−02	0.88	7.4096e−02	0.17
eoc		1.19		0.83

4.6   An Algorithm for Solving the Adjoint Problem

X-FEM Approximation of the Adjoint Temperature. We have already seen in Section 3.3.3 that the equations (3.10a)–(3.10j) governing the adjoint temperature p in the system (3.10) have the same basic structure as the corresponding equations (3.2a)–(3.2h) for the temperature y in the two-phase Stefan problem (3.2). Consequently, the extended finite element approximation that we discussed in Section 4.3 is applicable to the discretization of the adjoint temperature as well:

$$p_h(x,t) = \sum_{i=1}^{N} v_i(x)\, p_i(t) + \sum_{j=1}^{N_e(t)} \widetilde{v}_j(x,t)\, b_j(t).$$

Note that the geometric information that is needed to define the enrichment functions $\widetilde{v}_j(x,t)$ is already known from the solution of the forward problem. In fact, the (pseudo) mass and the stiffness matrices that are assembled during the solution of the forward system (3.2) (or its discretized version (4.20), respectively) can be stored and reused to solve the adjoint heat equation. This is similar to the solution strategy for the adjoint level set equation.

The only major difference between the heat equations in (3.2) and (3.10) is in the interface conditions that prescribe the equilibrium temperature at $\Gamma_I(t)$. As in Section 4.3.4, we require only a weak form of the interface condition (3.10j):

$$\int_{\Gamma_I(t)} \left(p - \psi\, |\nabla\phi|\right) v\, ds = 0 \quad \forall v.$$

(a) $t = 0.00$

(b) $t = 0.33$

(c) $t = 0.66$

(d) $t = 1.00$
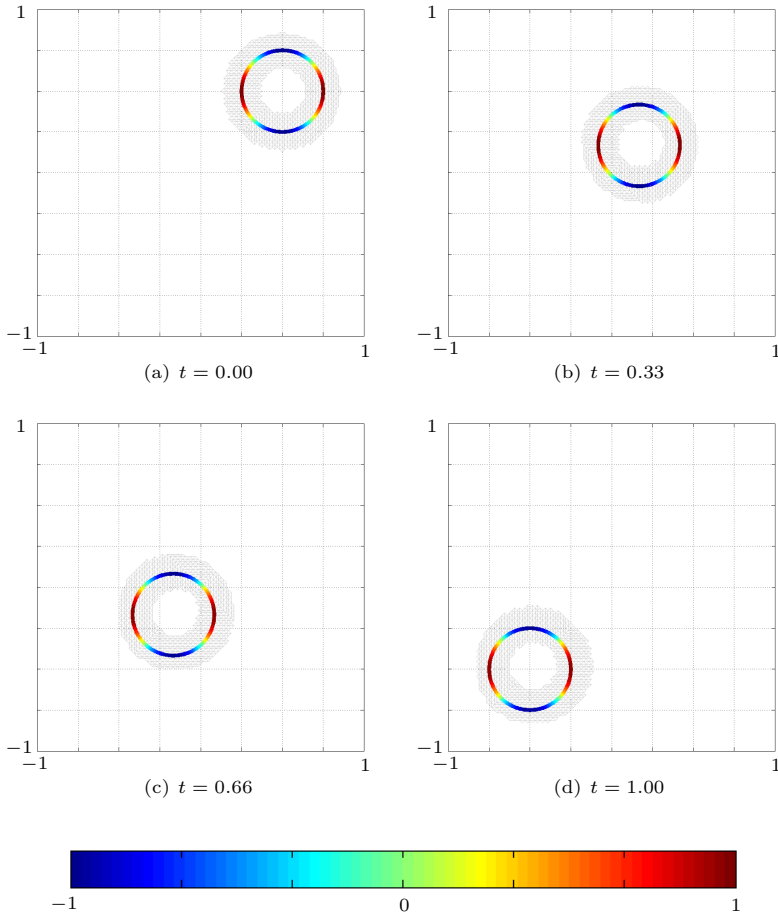
FIGURE 4.12. Solutions of the pure transport equation $\dot{\psi} = 0$ along a moving circle at different time steps.

Replacing the continuous quantities by their discrete counterparts using the finite element basis (4.18) gives rise to the linear system

$$\mathbf{Q}^j \, P^j = P_I^j$$

that we add as a penalty term to the linear system that emerges from applying the X-FEM to the adjoint heat equation along the lines of Section 4.3.3. Note that the matrix in this penalty term is the same as in the system (4.20). Thus, we end up with the system of linear equations

$$
\left(\frac{1}{\Delta t^{j+1}} \, \mathbf{M}^j + \mathbf{K}^j + \mu \left(\mathbf{Q}^j \right)^\top \mathbf{Q}^j \right) P^j
$$
$$
= \frac{1}{\Delta t^{j+1}} \, \left(\mathbf{M}_j^{j+1} \right)^\top \, P^{j+1} + \mu \left(\mathbf{Q}^j \right)^\top P_I^j
\tag{4.27}
$$

that has to be solved for the coordinate vector

$$
P^j = \left[p_1^j, \, \ldots, \, p_N^j, \, b_1^j, \, \ldots, \, b_{N_e(t^j)}^j \right]^\top
$$

with respect to the finite element basis (4.18) for some penalty parameter $\mu > 0$ and for $j = N_T - 1, \ldots, 0$. As mentioned above, the matrices and vectors in this equation are defined as in (4.19).

Remark 4.12. (1) The adjoint heat equation is backwards in time. Thus the roles of ansatz and test function are interchanged with respect to the discretization of the forward system. This is reflected by using the transpose of the non-symmetric matrix $\mathbf{M}_j^{j+1}$ on the right hand side of (4.27).

(2) We do not discuss the discretization of the forcing terms in (3.10a)–(3.10d) in detail as they can be included in (4.27) in the same way as the source term in the discretization of the forward system.

Solution Strategy. The coupling condition (3.10j) between the two adjoint states p and ψ and the implicit time discretization of the adjoint heat equation lead the way to an algorithm for the solution of the adjoint system (3.10). In each time step, we first update the adjoint level set function ψ by the DG scheme (4.24) and the explicit Runge-Kutta method that we discussed in Section 4.2.2. The new value of ψ is then used to update the adjoint temperature p by solving the linear system (4.27). This approach is similar to the solution strategy for the forward problem (3.2) in which we first update the geometric information by evolving the level set equation one time step and then update the temperature by solving (4.20). These ideas are summarized in Algorithm 4. As in Algorithm 3, we use the notation $y^j = y(t^j)$, and so on, and NB^j denotes the narrow band at time t^j. Note that ϕ^j and $\vec{V}^j$ are given only locally in NB^j and not globally in all of D. This explains the necessity of steps 6 and 11. Mapping a quantity from NB^{j-1} to NB^j (or in the reverse direction) is implemented by copying

the values of the quantity at nodes close to the interface in NB^{j-1} to the corresponding nodes in NB^j and applying the constant extension procedure described in Section 4.2.3. The initialization of the adjoint level set function ψ and the evaluation of the source terms in steps 2 and 16 are implemented in analogy to the evaluation of the Stefan condition in the solution of the forward problem, see Section 4.3.4.

Algorithm 4 Solver for the Adjoint Two-Phase Stefan Problem

Input: D, ρ, c_S, c_F, k_S, k_F, L, γ_1, γ_2, γ_3, γ_4, μ, y_T, ϕ_T,
 for $j = 0, \ldots, N_T$: t^j, y^j, ϕ^j, Γ_I^j, NB^j, y_d^j, ϕ_d^j, $\mathbf{M}^j$, $\mathbf{K}^j$, $\mathbf{Q}^j$,
 for $j = 0, \ldots, N_T - 1$: $\mathcal{M}^j$, $\mathcal{K}^j$,
 for $j = 1, \ldots, N_T$: $\mathbf{M}_{j-1}^j$
Output: p^j, ψ^j for $j = 0, \ldots, N_T$

1: $j \to N_T$.
2: Initialize p^j and ψ^j in NB^j, see (3.10c)–(3.10d) and (3.10l).
3: Evaluate the source term in (3.10k) in NB^j.
4: **while** $j \geq 1$ **do**
5:    **if** $\text{NB}^j \neq \text{NB}^{j-1}$ **then**
6:      Map ϕ^{j-1} and $\vec{V}^{j-1}$ from NB^{j-1} to NB^j.
7:    **end if**
8:    Compute ψ^{j-1} in NB^j.
9:    Apply the slope limiter to ψ^{j-1} in NB^j.
10:    **if** $\text{NB}^j \neq \text{NB}^{j-1}$ **then**
11:      Map ψ^{j-1} from NB^j to NB^{j-1}.
12:    **end if**
13:    Reinitialize ψ^{j-1} in NB^{j-1}.
14:    Implement the interface condition (3.10j) by a penalty approach.
15:    Solve the adjoint heat equation (4.27) to obtain p^{j-1}.
16:    Update the source terms in (3.10k).
17:    $j \to j - 1$.
18: **end while**

---

5 Numerical Examples

Contents

This chapter contains five numerical examples to validate the proposed optimal control approach to motion planning for the two-phase Stefan problem in level set formulation. The first test case is included to demonstrate that controling the interface motion can counteract nature, in the sense that the initial interface position is kept almost constant in the controled case, while the natural motion of the interface in the case of perfect insulation is to shrink. The second example uses a similar geometric setup as the first one, but the controled interface moves in the same direction as the uncontroled interface. The resulting temperature distribution is non-physical, and this motivates the inclusion of control constraints in Section 5.3. In all of these test cases, the interface is a closed curve. As an additional challenge, we introduce a change of topology in the desired interface motion which is to be tracked in the fourth example. We close this chapter with the case of so called unidirectional solidification in which the control goal is to have a flat interface move monotonically in one direction. This last example serves as the motivation for introducing state constraints, see Chapter 6.

General Setup. Unless otherwise stated, we use the following settings throughout this chapter. The constants in the two-phase Stefan problem are taken as

$$k_S = 1, \quad k_F = \tfrac{1}{2}, \quad c_S = 1, \quad c_F = 1, \quad L = 1, \quad \rho = 1, \quad y_M = 0,$$

and the initial temperature distribution is

$$y_0 = \begin{cases} \phi_0 & \text{in } \Omega_S(0), \\ \tfrac{1}{2}\,\phi_0 & \text{in } \Omega_F(0). \end{cases}$$
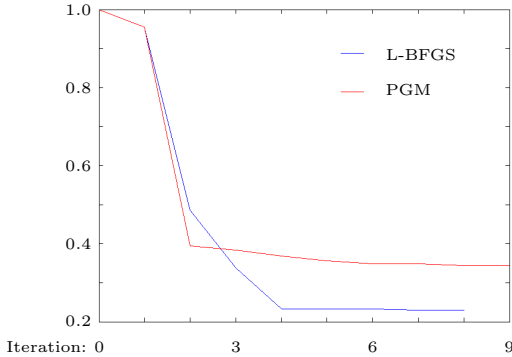
FIGURE 5.1. The relative cost functionals $\widehat{J}(u^j)/\widehat{J}(u^0)$ for the control problem of Section 5.1.

Moreover, we omit temperature tracking terms completely, i.e., $\gamma_1 = \gamma_3 = 0$ in all of the examples to follow. The tolerances in the convergence criteria of Algorithm 1 and Algorithm 2 are

$$\tau_a^u = 10^{-8}, \tau_r^u = 10^{-8}, \quad \tau_a^{\nabla} = 10^{-4}, \tau_r^{\nabla} = 10^{-4},$$
$$\text{MAXITER} = 100, \quad \tau^{\sigma} = 10^{-7}.$$

In all test cases, $u^0 \equiv 0$ serves as the initial guess for the control. We store $m = 5$ pairs (s^j, g^j) for the update of the inverse Hessian approximation in the limited memory BFGS method.

Computing Environment. The finite element discretization introduced in Chapter 4 was implemented in MATLAB. Some of the more time consuming program parts, e.g., the fast marching method, were translated to C++ using the corresponding MATLAB interface. Except for the PDE toolbox supplied by MATLAB which was used to generate the meshes, and the code for estimating the order of convergence by a least-squares approach which was implemented by Frank Schmidt, no external code was used. All computations were carried out on an Intel®Xeon®Dual Core processor with 3.0 GHz and 64 MB RAM.

5.1 Keeping a Constant Position

Setup. We choose the annulus $D = \{x \in \mathbb{R}^2 \mid 0.2^2 \le x_1^2 + x_2^2 \le 0.7^2\}$ as the hold-all. The initial configuration is such that the solid phase is adjacent
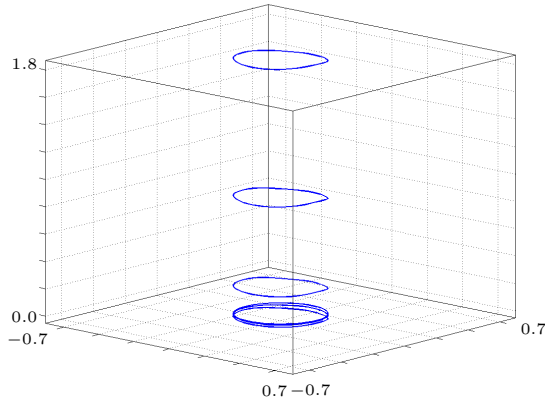
FIGURE 5.2. The optimal control for the problem of Section 5.1 computed by the L-BFGS method at time steps $t \in \{0.0, 0.06, 0.12, 0.18, 0.24, 0.3\}$ (top to bottom).

to the outer part of ∂D, the circle with radius 0.7 (denoted by $\Gamma_N^{0.7}$), and the fluid phase is adjacent to the inner part of ∂D, the circle with radius 0.2 (denoted by $\Gamma_C^{0.2}$). The two phases are separated by a circle with radius 0.45, and the control goal is to keep this interface position constant until the terminal time $T = 0.3$. This setup and the control goal correspond to the choice

$$\phi_d(x_1, x_2, t) = \phi_T(x_1, x_2) = -\sqrt{x_1^2 + x_2^2} + 0.45.$$

The control u acts only on $\Gamma_C^{0.2}$, and we impose the insulation condition

$$k_S \frac{\partial y}{\partial n} = 0 \qquad\qquad \text{on } \Gamma_N^{0.7}.$$

We discretize the hold-all using 3384 triangles and the time interval $[0, 0.3]$ is subdivided into 200 equal slices ($\Delta t^j = 0.0015$). This discretization corresponds to 9648 unknowns. We run Algorithm 1 and Algorithm 2 with the parameters

$$\gamma_2 = 100, \quad \gamma_4 = 1, \quad \gamma_5 = 10^{-2}.$$

Interpretation of the Results. After 8 iterations, the limited memory BFGS method stops because of condition (T4). The computed optimal control, the resulting interface evolution, and the corresponding temperature distribution

are shown in Figures 5.2–5.4. The gradient method (abbreviated by PGM) stops after 9 iterations. Figure 5.1 compares the two relative cost functionals. In this example, the numbers of iterations needed by the two methods are comparable. However, L-BFGS stops with a smaller value of the cost functional than PGM, indicating that PGM stopped too early. By extrapolating the behavior of PGM, we see that it would need much more iterations than L-BFGS to obtain the same value of the cost functional.

Figure 5.3 demonstrates that the controled interface remains close to the desired constant interface position. Since the control is only active on the inner part of the boundary, $\Gamma_C^{0.2}$, this behavior can only be achieved by a positive heat flux into the fluid phase $\Omega_F(t)$, see Figure 5.2. After $t \approx 0.18$, there is barely any control activity, the corresponding lines in Figure 5.2 are almost indistinguishable. As demonstrated by Figure 5.4(e)–(f), the resulting temperature distribution at $t = T$ is identical to the equilibrium temperature, a state in which solid and fluid phases can exist in equilibrium, keeping the interface position constant [72, Section 2.1.4].

(a) $t = 0.00$

(b) $t = 0.06$

(c) $t = 0.12$

(d) $t = 0.18$

(e) $t = 0.24$

(f) $t = 0.30$
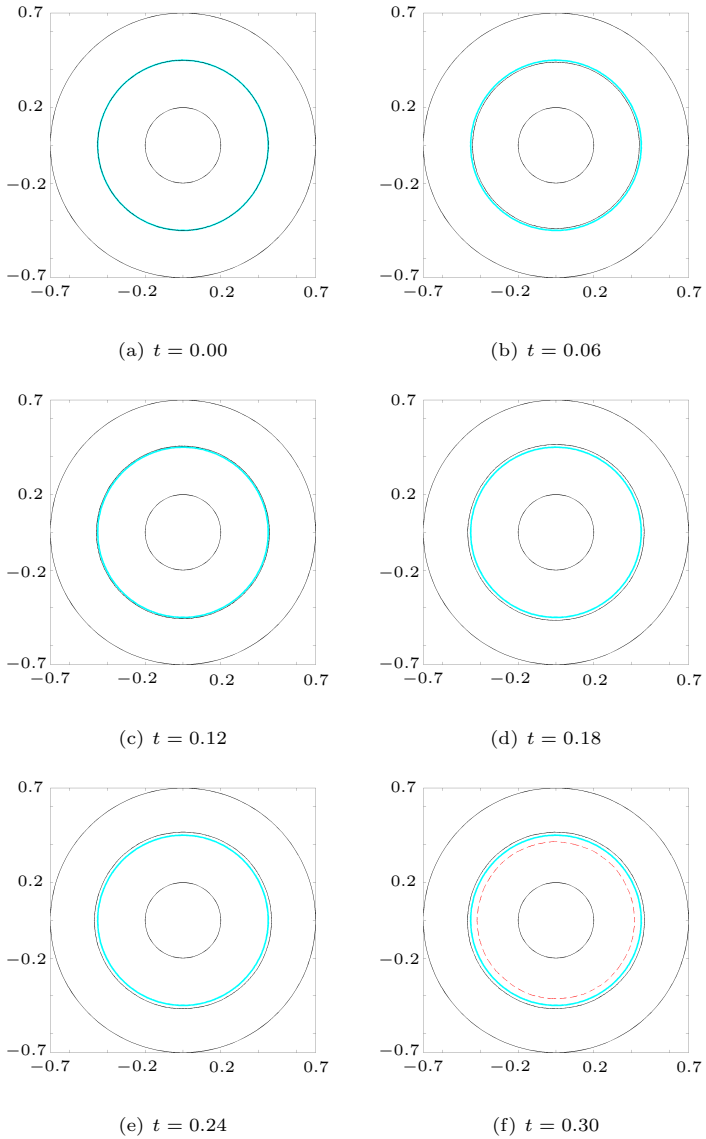
FIGURE 5.3. The interface position corresponding to the computed control (black, thin line) and the desired motion (cyan, thick line) for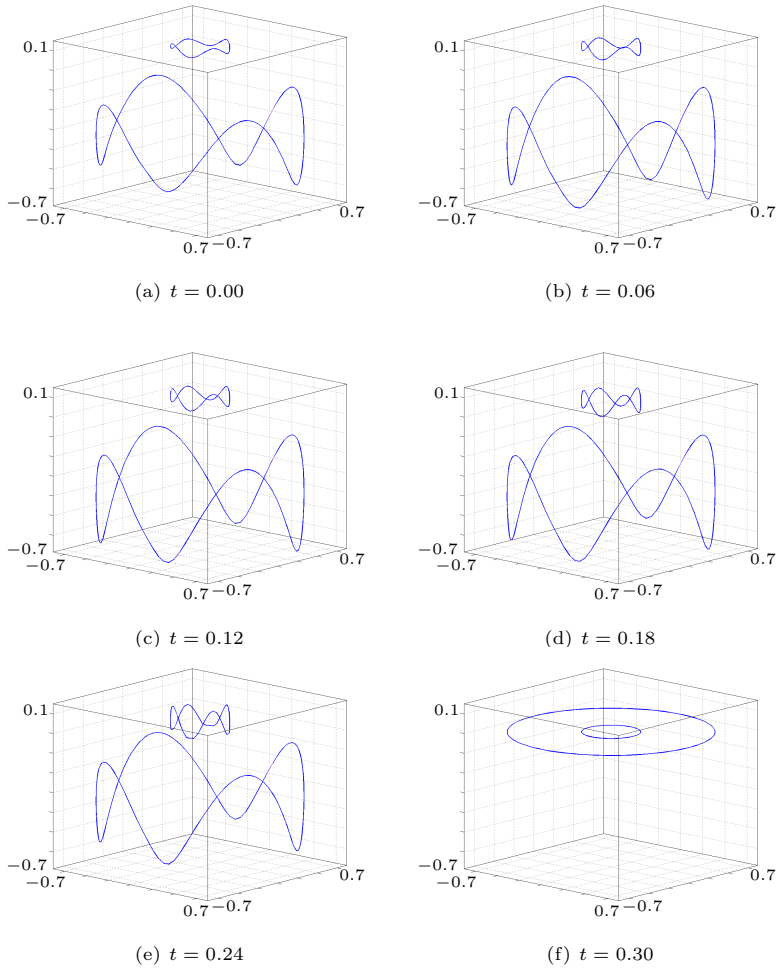 the control problem of Section 5.1 at different time steps. The final interface position in the uncontroled case is shown in red (dashed line).

(a) $t = 0.00$

(b) $t = 0.06$

(c) $t = 0.12$

(d) $t = 0.18$

(e) $t = 0.24$

(f) $t = 0.30$

(g) Temperature scale.
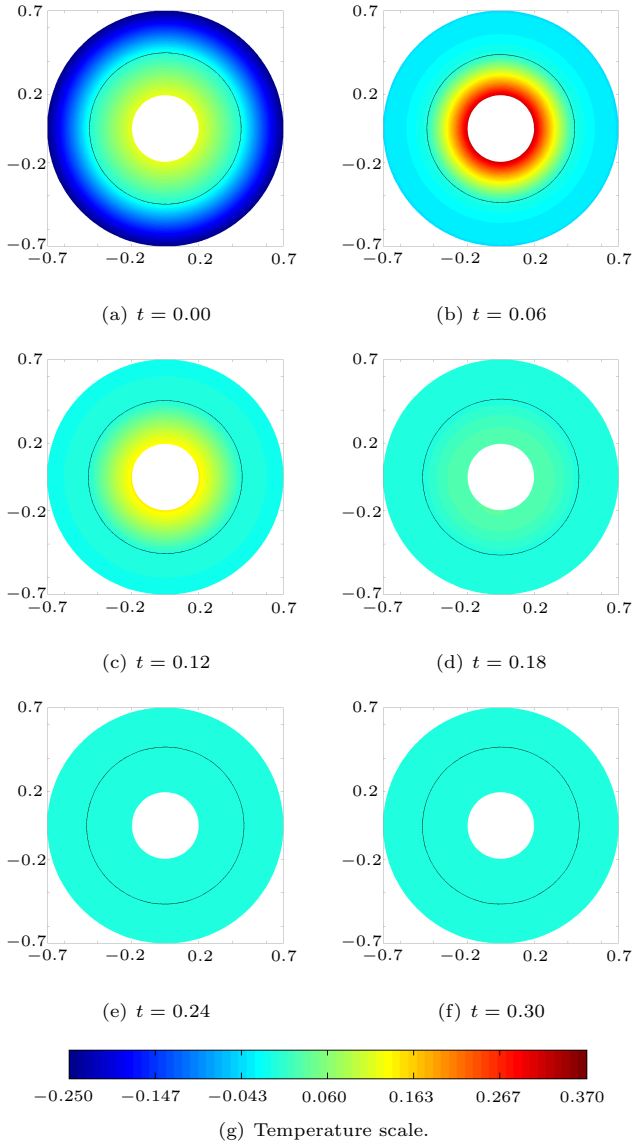
FIGURE 5.4. The temperature distribution and the inter-
face evolution corresponding to the computed control for
the control problem of Section 5.1 at different time steps.
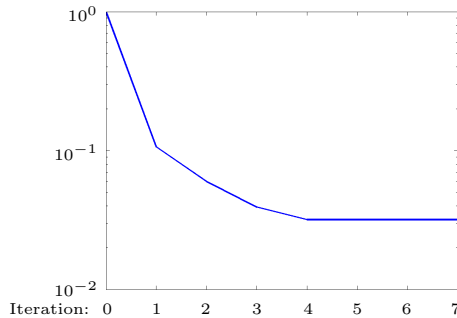
FIGURE 5.5. The relative cost functional $\widehat{J}(u^j)/\widehat{J}(u^0)$ for the unconstrained control problem of Section 5.2 in semi-logarithmic scale.

5.2   Shrinking to a Circle

Setup. The hold-all is the same as in Section 5.1, i.e., $D = \{x \in \mathbb{R}^2 \mid 0.2^2 \leq x_1^2 + x_2^2 \leq 0.7^2\}$, but now, we let the control be active on the whole boundary of this domain. We use the notation $\Gamma_C^{0.2}$ and $\Gamma_C^{0.7}$ to distinguish the two parts of the boundary. The positions of the two phases at initial time $t = 0$ are unchanged with respect to Section 5.1, but now the interface is a closed curve that distantly resembles a flower. The control goal is to have this interface shrink uniformly to a circle with radius 0.35 in the time interval $[0, 0.3]$. The functions ϕ_d and ϕ_T representing this desired interface motion in the cost functional are constructed numerically by the fast marching scheme as the signed distance functions to the zero level sets of the function

$$z(r, \varphi, t) = r - \frac{1-t}{2} + \frac{0.3 - t}{3} \sin(4\,\varphi),$$

where (r, φ) are the polar coordinates of $(x_1, x_2) \in D$. We choose the same spatial and temporal discretizations as before. Since the control boundary is now larger, this results in 33768 optimization variables. Algorithm 2 is run with the parameters

$$\gamma_2 = 1, \quad \gamma_4 = 1, \quad \gamma_5 = 10^{-2}.$$

Interpretation of the Results. The L-BFGS method stops after 7 iterations because of condition (T4). The results are reported in Figures 5.5–5.8. Figure 5.6 indicates that the tracking of the desired interface works well, although there is a deviation from the prescribed interface motion towards the

end of the process. This can be attributed to the fact that $u(\cdot, T) = 0$ since we have omitted temperature tracking terms from the cost functional, see Remark 3.8. While the control remains almost the same on $\Gamma_C^{0.7}$ for a remarkably long time interval, it changes rather rapidly on $\Gamma_C^{0.2}$. In particular, the control attains negative values on $\Gamma_C^{0.2}$, causing the temperature to fall beneath the equilibrium temperature y_M in regions close to $\Gamma_C^{0.2}$, see Figure 5.8(d)–(e). As the two-phase Stefan problem without Gibbs-Thomson correction can not account for undercooling effects (see (2.6)), new interfaces between the fluid and the solid phases are expected to emerge in these regions. However, this is not the case, as we observe from Figure 5.8. This shows a limitation of the level set formulation of the two-phase Stefan problem, or, to be more precise, of the discretization presented in Chapter 4: Without an additional interpolation routine that compares the current interface to the y_M-level set of the temperature and updates the interface if necessary, we might end up in situations in which there is a gap between the mathematical model and the numerical results. As we shall see in the next section, this can be remedied by imposing control constraints, at least in this particular example.

5.3   Shrinking to a Circle with Control Constraints

Setup. The geometric setup, the control goal and the choice of the weights in the cost functional are the same as in Section 5.2. To prevent the optimization process from running into non-physical situations as in the last Section, we impose the control constraints

$$u \geq 0 \quad \text{on } \Gamma_C^{0.2} \quad \text{and} \quad u \leq 0 \quad \text{on } \Gamma_C^{0.7}.$$

These constraints ensure that no fluid-solid interfaces emerge in regions close to the boundary of the domain due to control activity.

Interpretation of the Results. We solve this control-constrained problem using the projected gradient method, Algorithm 1. With the choice

$$\tau_a^u = 10^{-12}, \quad \tau_r^u = 10^{-12}, \quad \tau^\sigma = 10^{-10},$$

Algorithm 1 stops after 12 iterations. Figures 5.9–5.11 show that the tracking of the desired interface motion is qualitatively as good as in the absence of control constraints. In fact, the optimal value of the cost functional changes negligibly from 0.001503 to 0.001773. Figure 5.12(e) and Figure 5.10 demonstrate that the control constraint is indeed active on $\Gamma_C^{0.2}$ while the behavior of the control is almost unchanged on $\Gamma_C^{0.7}$. Except for $t = T$, the control is always negative on this outer part of the boundary, and the constraint is never active there. Finally, Figure 5.13 depicts the resulting temperature

(a) $t = 0.00$

(b) $t = 0.06$

(c) $t = 0.12$
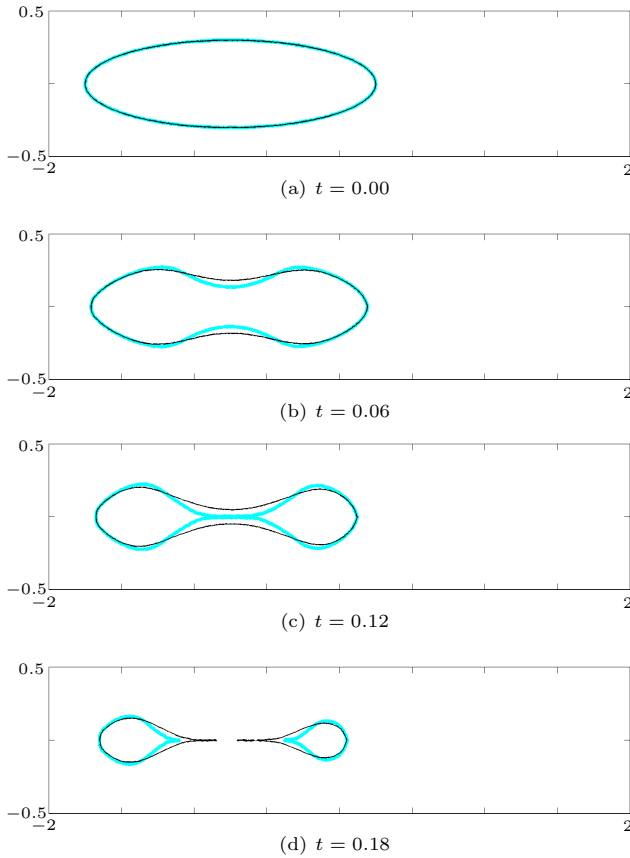
(d) $t = 0.18$

(e) $t = 0.24$

(f) $t = 0.30$
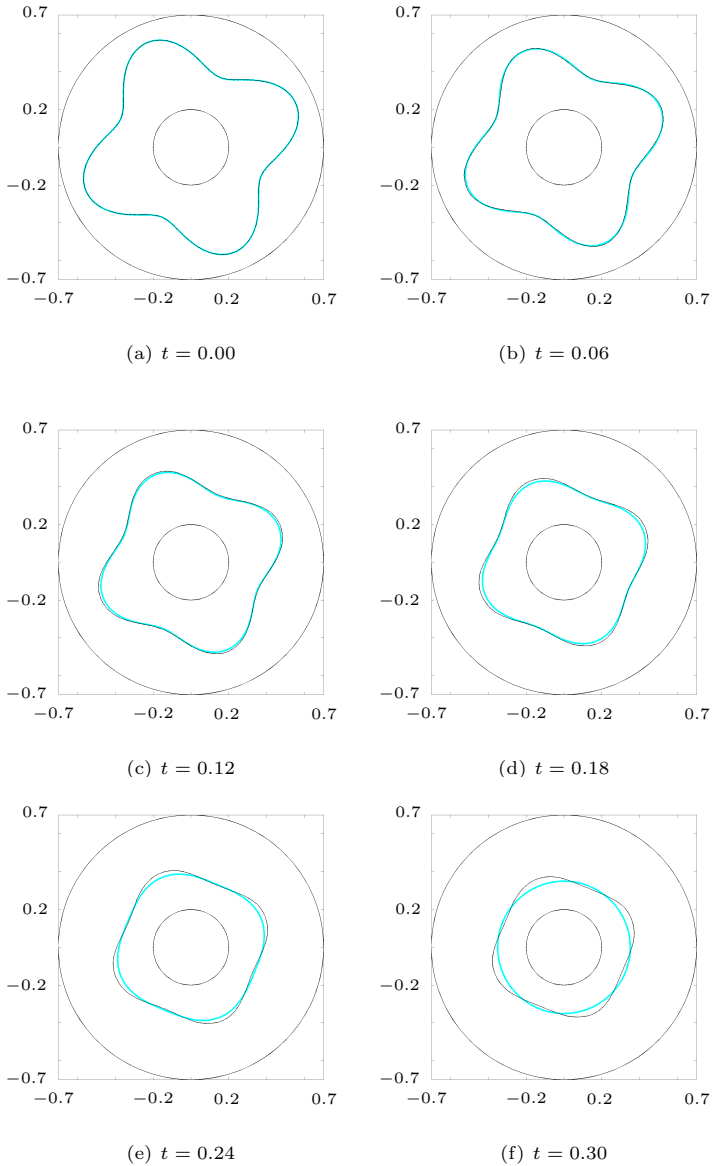
FIGURE 5.6. The interface position corresponding to the computed control (black, thin line) and the desired motion (cyan, thick line) for the unconstrained control problem of Section 5.2 at different time steps.

(a) $t = 0.00$

(b) $t = 0.06$

(c) $t = 0.12$

(d) $t = 0.18$

(e) $t = 0.24$

(f) $t = 0.30$
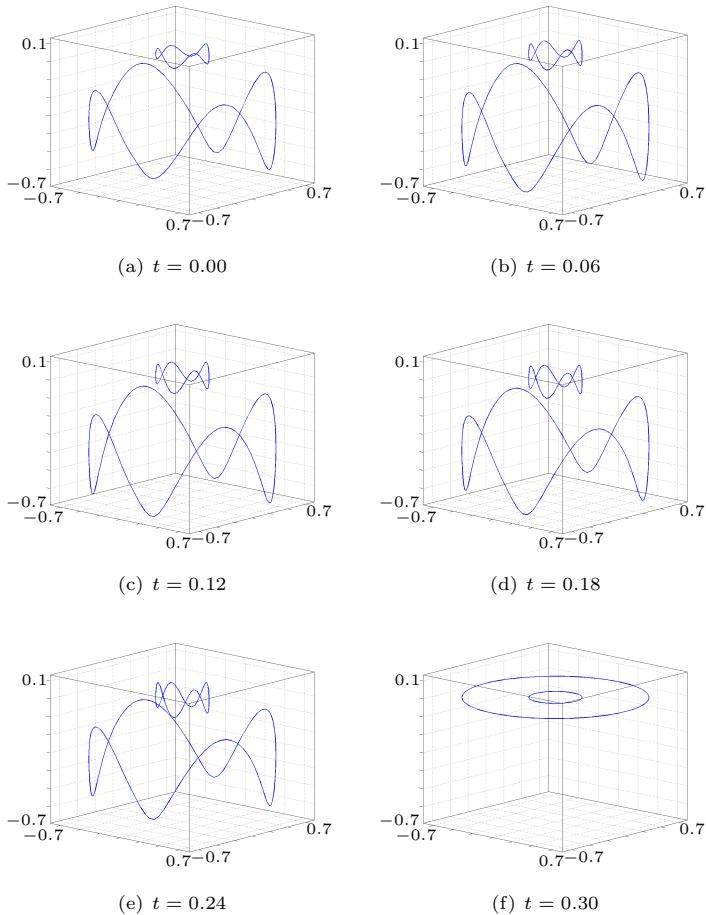
FIGURE 5.7. The computed control for the unconstrained control problem of Section 5.2 at different time steps.

distribution, and we observe that the gap between the mathematical model and the numerical results that we faced in the absence of control constraints is gone, i.e., the requirements (2.6) are fulfilled at all times.

(a) $t = 0.00$

(b) $t = 0.06$

(c) $t = 0.12$

(d) $t = 0.18$

(g) Temperature scale.
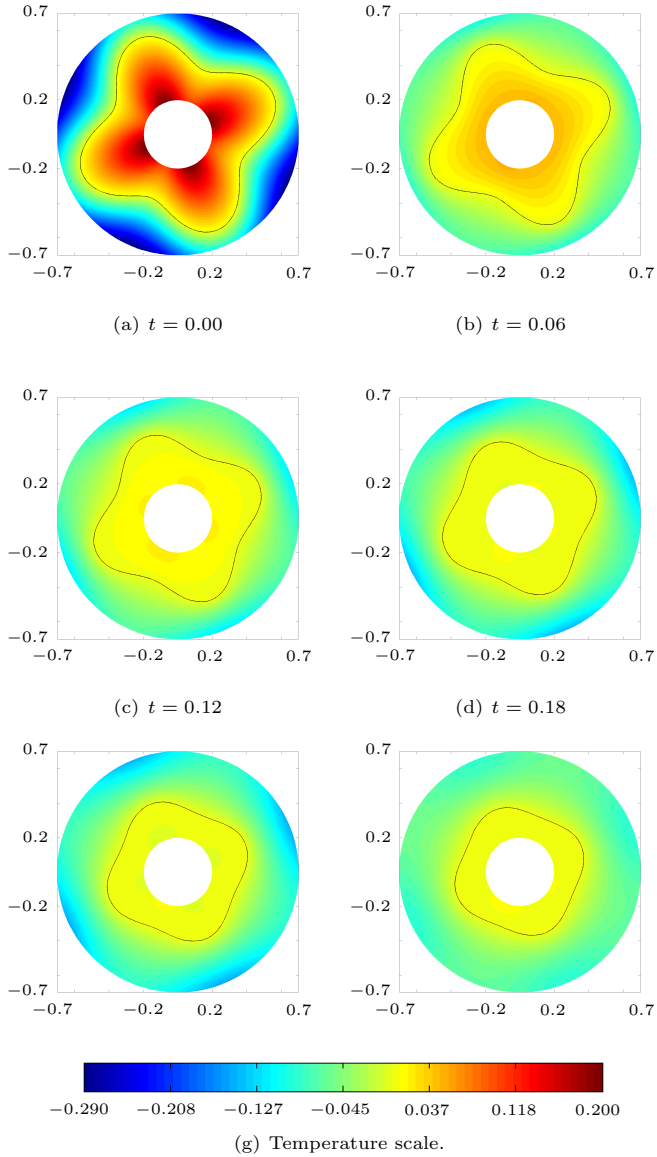
FIGURE 5.8. The temperature distribution and the interface evolution corresponding to the computed control for the unconstrained control problem of Section 5.2 at different time steps.
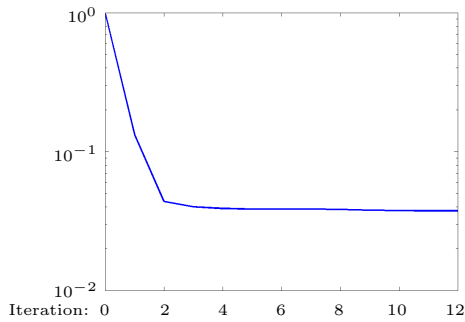
FIGURE 5.9. The relative cost functional $\widehat{J}(u^j)/\widehat{J}(u^0)$ for the constrained control problem of Section 5.3 in semi-logarithmic scale.

(a) $t = 0.255$ (b) $t = 0.285$
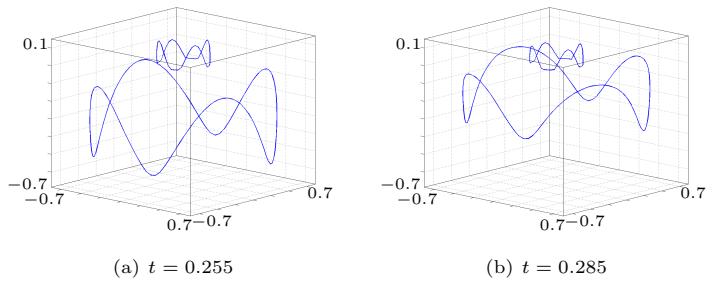
FIGURE 5.10. Activity of the control constraint in the problem of Section 5.3 at two different time steps.

(a) $t = 0.00$

(b) $t = 0.06$

(c) $t = 0.12$

(d) $t = 0.18$

(e) $t = 0.24$

(f) $t = 0.30$
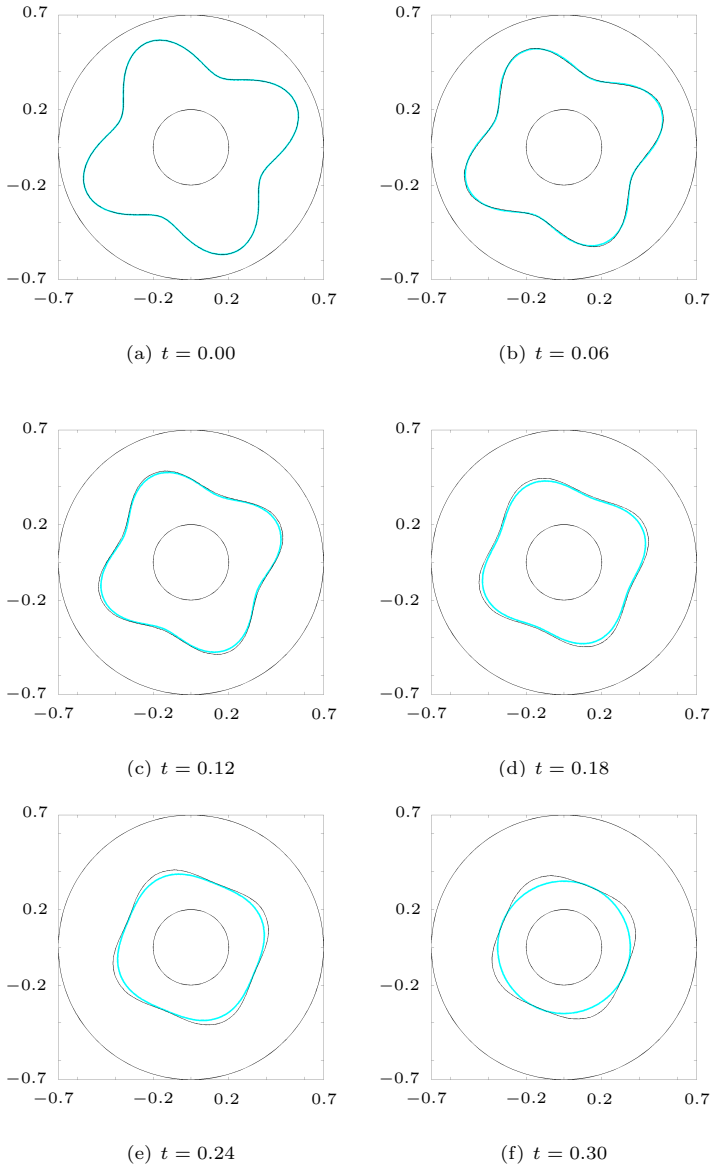
FIGURE 5.11. The interface position corresponding to the computed control (black, thin line) and the desired motion (cyan, thick line) for the constrained control problem of Section 5.3 at different time steps.

(a) $t = 0.00$

(b) $t = 0.06$

(c) $t = 0.12$

(d) $t = 0.18$

(e) $t = 0.24$

(f) $t = 0.30$

FIGURE 5.12. The computed control for the constrained control problem of Section 5.3 at different time steps.

(a) $t = 0.00$

(b) $t = 0.06$

(c) $t = 0.12$

(d) $t = 0.18$

(e) $t = 0.24$

(f) $t = 0.30$

$$-0.290 \quad -0.208 \quad -0.127 \quad -0.045 \quad 0.037 \quad 0.118 \quad 0.200$$

(g) Temperature scale.
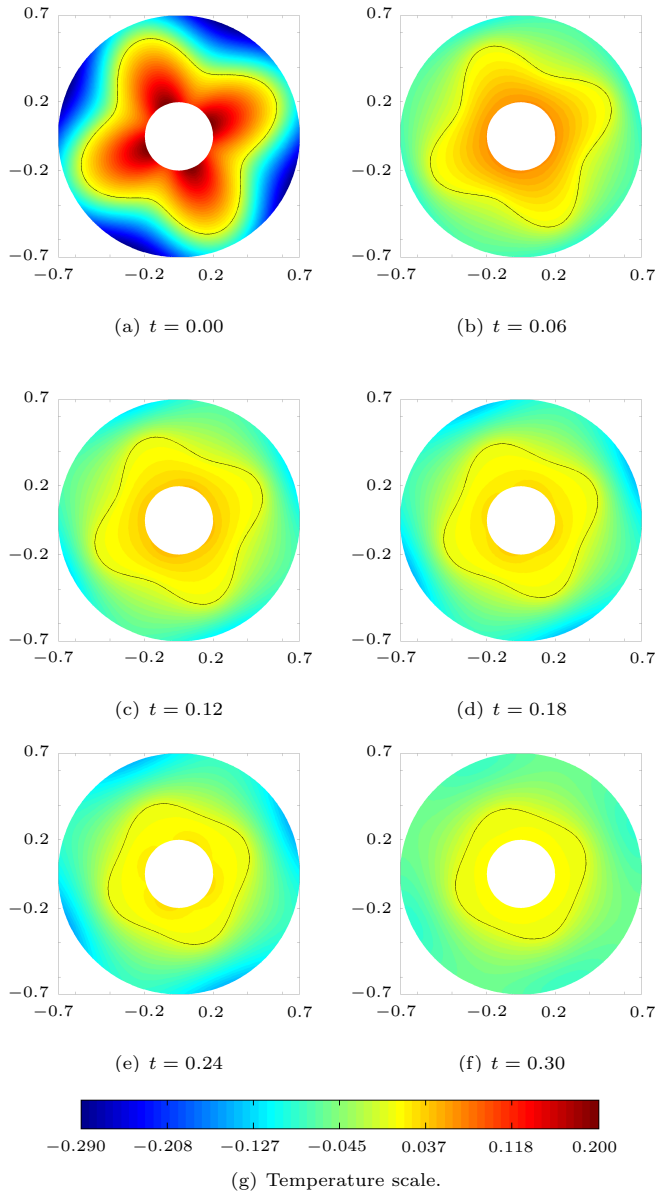
FIGURE 5.13. The temperature distribution and interface evolution corresponding to the computed control for the constrained control problem of Section 5.3 at different time steps.
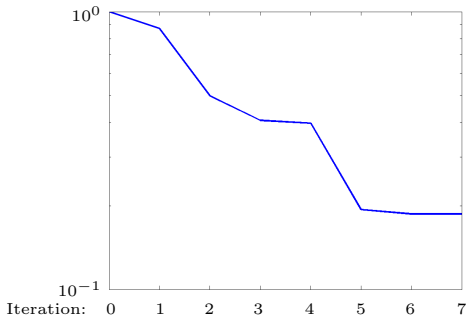
FIGURE 5.14. The relative cost functional $\widehat{J}(u^j)/\widehat{J}(u^0)$ for the control problem of Section 5.4 in the absence of control constraints in semi-logarithmic scale.
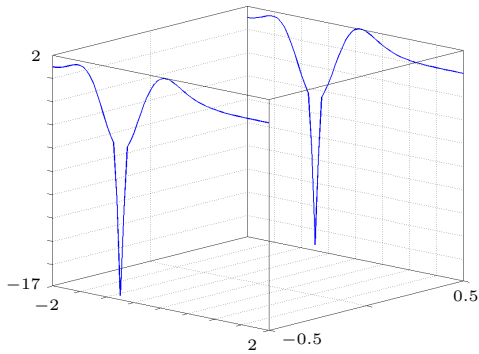
FIGURE 5.15. Snapshot of the computed optimal control for the problem of Section 5.4 at $t = 0$ if no control constraint is present.

5.4 Tracking a Change of Topology

One of the distinguishing features of the level set method is its capability to handle changes of topology. The example we discuss in this section demonstrates that our optimal control approach inherits this property.

(a) $t = 0.08$

(b) $t = 0.18$
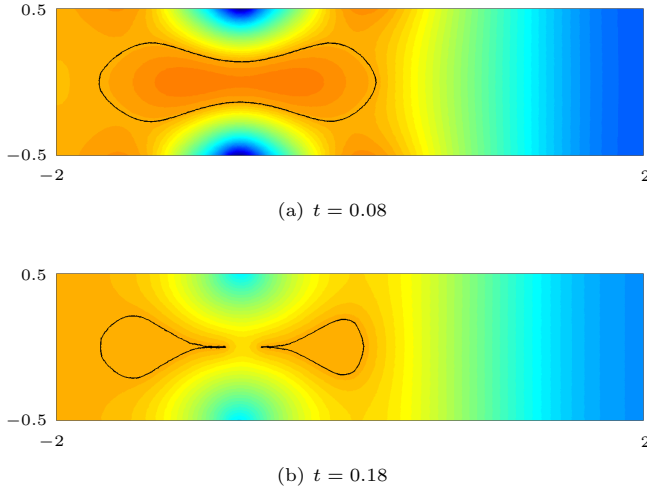
FIGURE 5.16. The temperature distribution in the control problem of Section 5.4 if no control constraint is present at two different instances of time.

Setup. We consider the rectangular hold-all $D = [-2, 2] \times [-0.5, 0.5]$. The initial configuration is such that the solid phase, which is adjacent to ∂D, completely encloses the fluid phase. As in Section 5.3, the desired interface motion corresponds to an inwards solidification, starting from an ellipse-like shape at $t = 0$. A pinch-off should occur at $t \approx 0.124$. The level set functions ϕ_d and ϕ_T which encode the desired interface evolution are taken as the signed distance functions to the evolving interface obtained during a simulation run with given Neumann temperature boundary data. Fast marching reinitialization as described in Section 4.2.3 is used. The boundary is decomposed into two parts $\partial D = \Gamma_N \cup \Gamma_C$ that are defined by

$$\Gamma_N = \big([-0.5, 0.5] \times \{-2\}\big) \cup \big([-0.5, 0.5] \times \{2\}\big),$$
$$\Gamma_C = \big([-2, 2] \times \{-0.5\}\big) \cup \big([2, 2] \times \{0.5\}\big).$$

This time we do not impose any constraints on the control u. The Neumann data on Γ_N are homogeneous, and the initial temperature is assumed to be

$$y_0 = \begin{cases} \phi_0 & \text{in } \Omega_S(0), \\ 3\,\phi_0 & \text{in } \Omega_F(0). \end{cases}$$

(a) $t = 0.00$

(b) $t = 0.06$

(c) $t = 0.12$

(d) $t = 0.18$
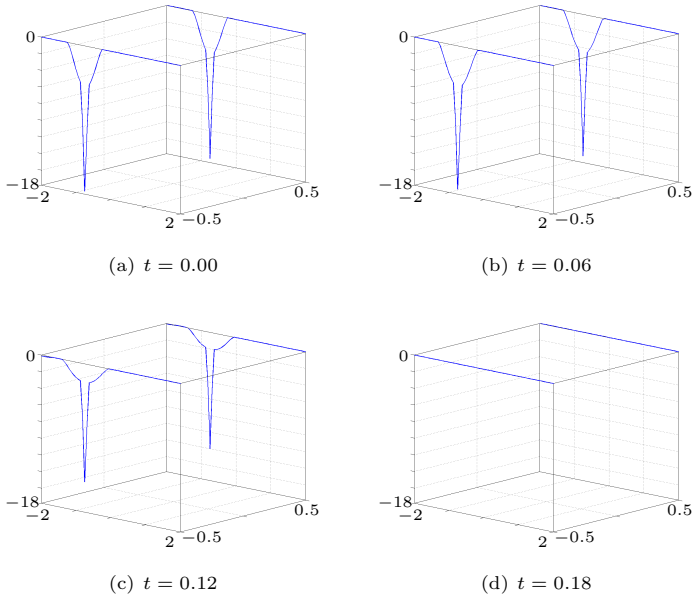
FIGURE 5.17. The computed control for the control problem of Section 5.4 at different time steps. The constraint (5.1) is clearly active.

The domain is discretized using 4096 triangles and we take 90 time steps in the interval $[0, 0.18]$. This discretization results in a total of 11830 optimization variables. We use the parameters $\gamma_1 = 8$, $\gamma_2 = 1$, $\gamma_3 = 10^{-4}$ in the cost functional and apply Algorithm 2 with a scaled down version of the Neumann data used to generate the desired interface evolution as the initial guess u^0.

Interpretation of the Results. The BFGS method stops after 7 iterations because of (T4). Figure 5.14 shows the decrease of the relative cost functional. Due to the good initial guess we used for the control, the reduction of the cost functional is not too impressive. After four iterations, the BFGS method recognizes the change of topology. This corresponds to the kink in the relative cost functional. A snapshot of the computed optimal control is shown in Figure 5.15 and the resulting temperature distribution is shown in

Figure 5.16. We observe that the change of topology is indeed recognized and appropriately tracked by the proposed optimal control approach. However, the temperature distribution violates the assumption (2.6), as can be seen in Figure 5.16(a). This non-physical configuration is caused by the fact that the control is positive on certain parts of Γ_C as indicated in Figure 5.15. This situation is similar to what we have seen in Section 5.2. Again, we impose the control constraint

$$u \leq 0 \qquad\qquad \text{on } \Gamma_C \qquad\qquad (5.1)$$

to ensure that the temperature distribution does not violate (2.6).

After projecting it to the set of admissible controls, we use the solution of the unconstrained case as the initial guess for the control and run the projected gradient method with the same parameters as above. It turns out that this initial guess is already close to a solution of the constrained problem. The projected gradient method stops after only 5 iterations because of (T4) without having made significant progress. The results are reported in Figures 5.17–5.19. We observe in Figure 5.18 that the change of topology is still resolved. The temperature distribution is now well-behaved in the sense that it does not violate the assumption (2.6) anymore, see Figure 5.19. This means in particular, that the solution we have found is physically meaningful. The computed optimal control is depicted in Figure 5.17, where we clearly observe that the constraint (5.1) is active.

(a) $t = 0.00$

(b) $t = 0.06$

(c) $t = 0.12$

(d) $t = 0.18$

FIGURE 5.18. The interface position corresponding to the computed control (black, thin line) and the desired motion (cyan, thick line) for the control-constrained problem of Section 5.4 at different time steps.

(a) $t = 0.00$

(b) $t = 0.06$

(c) $t = 0.12$

(d) $t = 0.18$

(e) Temperature scale.
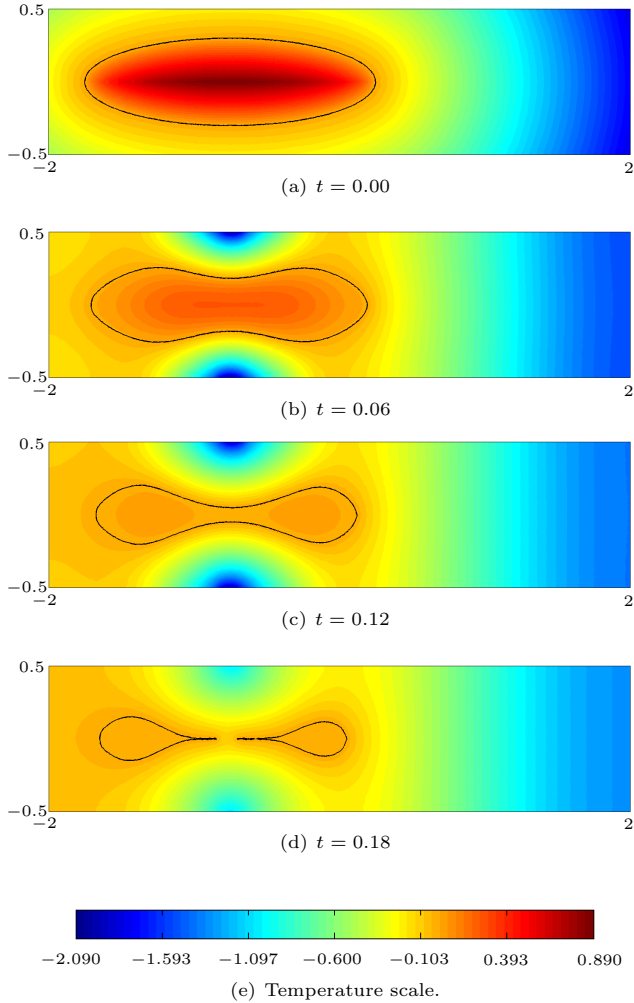
FIGURE 5.19. The temperature distribution and the interface evolution corresponding to the computed optimal control for the problem of Section 5.4 with the constraint (5.1) at different time steps.

5.5   Unidirectional Solidification

Setup. In this last section of Chapter 5, we consider a unidirectional so-
lidification problem in the hold-all $D = [-1, 1] \times [-0.5, 0.5]$. The initial
interface position is a straight line connecting the points $(-0.6, -0.5)^\top$ and
$(-0.6, 0.5)^\top$, and the control goal is to move this straight line to the right in
the time interval $[0, 1]$ such that the final position at $x_1 = 0.6$ is reached. In
this setup, the functions ϕ_d and ϕ_T encoding the desired interface evolution
can again be computed explicitly:

$$\phi_d(x_1, x_2, t) = x_1 - 1.2\,t + 0.6, \quad \phi_T(x_1, x_2) = x_1 - 0.6.$$

We assume that the control u is active only on the left part of the boundary,
i.e., $\Gamma_C = \{-1\} \times [-0.5, 0.5]$. The remaining parts of the boundary are in
principle insulated, but during the time interval $[0.3, 0.7]$ a shock appears
close to the control boundary Γ_C that pushes the interface in the right
direction but at the same time destroys the flat shape of the interface, see
Figure 5.20(a). Thus, the task of the control is to move the interface to the
right and to counteract the prescribed heat flux to preserve the flat interface
shape.

The discretization of the rectangular hold-all consisting of 4800 triangles
and a subdivision of the given time interval into 200 equal slices ($\Delta t^j =$
0.005) result in a total of 5829 unknowns. Note that the geometric setup and
the control goal are comparable to previous work, see, for instance, [**167**]
and [**79**].

We run Algorithm 2 with the parameters

$$\gamma_2 = 12, \quad \gamma_4 = 1, \quad \gamma_5 = 10^{-6}.$$

Interpretation of the Results. The resulting interface motion computed with
the BFGS method is compared with the desired interface motion in Fig-
ure 5.20(b). Figure 5.21 depicts the relative cost functional. In addition,
the optimal control computed by the BFGS method is shown in Figure 5.22
for all $t \in [0, 1]$. The corresponding temperature distribution at different
instances of time can be found in Figure 5.23. The careful reader will notice
that the computed control and, consequently, the corresponding temperature
distribution are not symmetric, although the chosen setup is symmetric. This
is due to the unsymmetric grid that is used in this computation. It is not a
shortcoming of the proposed optimal control approach.

After a short start-up phase, the tracking of the desired interface motion is
almost perfect. Since the control acts only on the left part of the boundary
and is thus rather far away from the interface position, this behavior might
not be expected. As in the previous examples, there is again a deviation from

(a) Uncontroled interface at $t \in \{0, 0.25, 0.5, 1, 0.75\}$ (left to right).

(b) Controled interface at $t \in \{0.0, 0.1, 0.2, \ldots, 1.0\}$ (left to right).
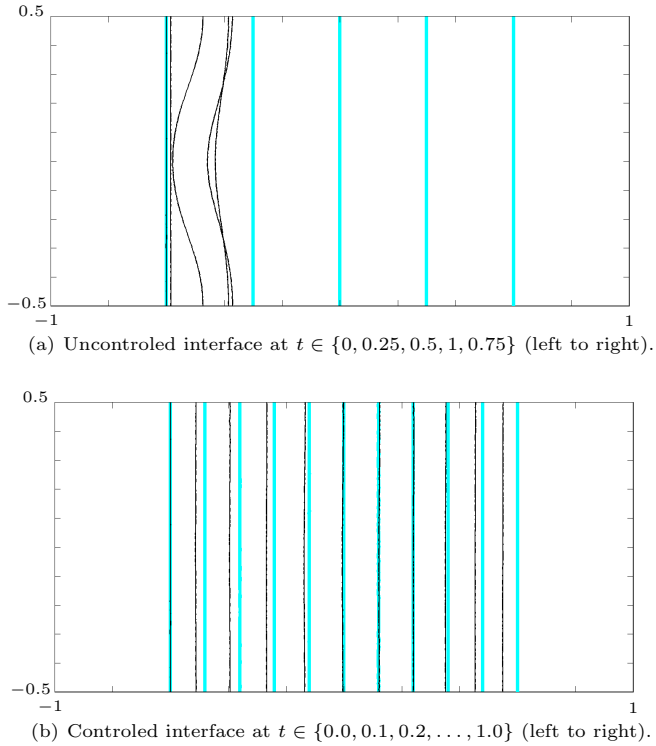
FIGURE 5.20. The interface positions in the uncontroled and the controled case of the unidirectional solidification problem of Section 5.5. The actual motion is depicted as the thin line (black), the desired interface positions are represented as thick lines (cyan).

the desired interface motion towards the end of the time interval. The reason is of course the same as before: We have omitted temperature tracking terms completely.
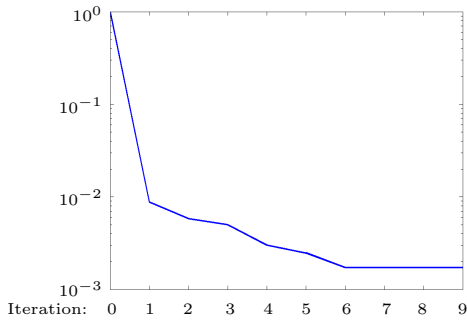
FIGURE 5.21. The relative cost functional $\widehat{J}(u^j)/\widehat{J}(u^0)$ for the control problem of Section 5.5 in semi-logarithmic scale.
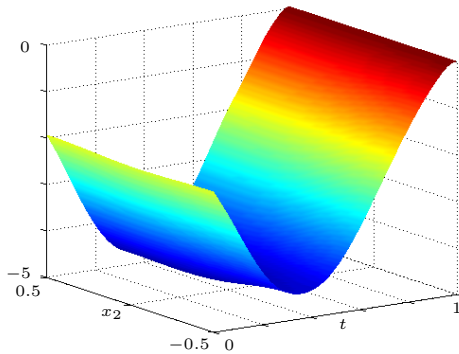
FIGURE 5.22. The optimal control for the unidirectional solidification problem of Section 5.5 computed by the BFGS method.

(a) $t = 0.00$

(b) $t = 0.25$

(c) $t = 0.50$

(d) $t = 0.75$

(e) $t = 1.00$

$-3.780 \quad -3.017 \quad -2.253 \quad -1.490 \quad -0.727 \quad 0.037 \quad 0.800$

(f) Temperature scale.
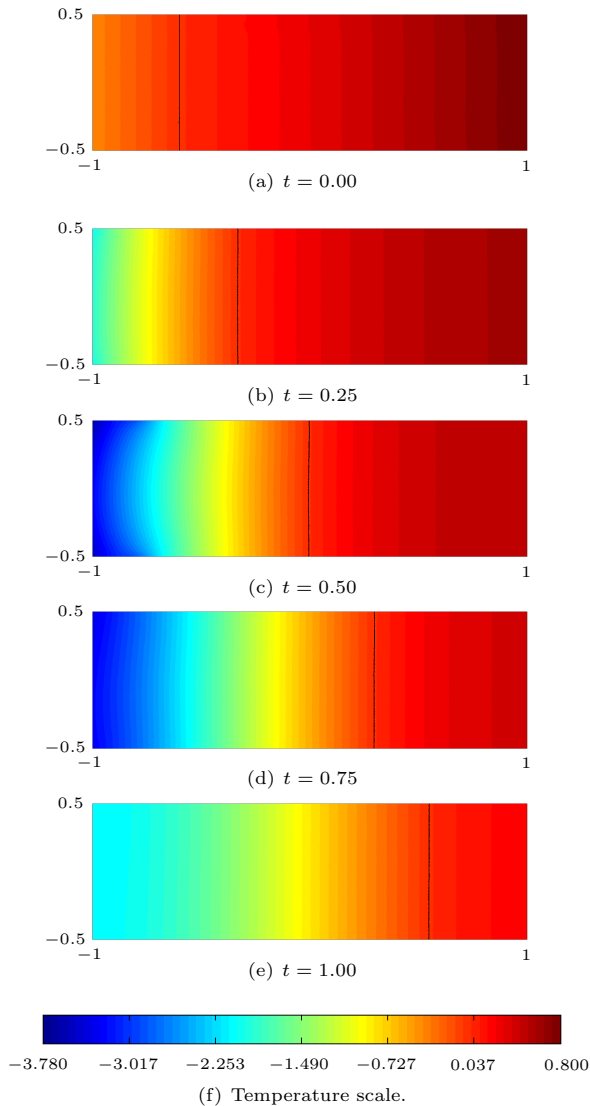
FIGURE 5.23. The temperature distribution and the interface evolution corresponding to the optimal control for the unidirectional solidification problem of Section 5.5 computed by the BFGS method at time steps $t \in \{0, 0.25, 0.5, 0.75, 1\}$.

6 Motion Planning Subject to a State Constraint

In this chapter, we discuss a motion planning problem subject to a constraint on the position of the moving interface. We briefly review regularization techniques for state-constrained optimal control problems. The Moreau-Yosida regularization is then applied to the motion planning problem under consideration. First-order necessary optimality conditions are derived by extending the optimality conditions obtained for the unconstrained motion planning problem in Chapter 3. We comment on some issues concerning the implementation of the adjoint-based (projected) gradient method (Algorithm 1) and the limited memory BFGS method (Algorithm 2) for the solution of the regularized problem, and close this chapter with numerical results.

6.1 Principles of State-Constrained Optimal Control

In analogy to the control-constrained optimal control problem (OCPCC), we formulate the abstract state-constrained problem

$$\min_{y \in \mathcal{Y}, u \in \mathcal{U}} J(y, u)$$

s. t.

$$e(y, u) = 0,$$
$$g(y) \leq 0 \quad \text{in } \Omega_0,$$

(OCPSC)

where the pointwise *state constraint* $g(y) \leq 0$ is posed in the subset Ω_0 of the domain Ω on which the state y is defined.

The difficulty with state-constrained optimal control problems is that Lagrange multipliers associated to state constraints exhibit only low regularity. In general, they belong to a space of measures on Ω_0, see [24] for an elliptic example. This lack of regularity affects the theoretical analysis of state-constrained optimal control problems as well as their discretization and their numerical solution. Without aiming for completeness, we comment on some of the strategies to circumvent these difficulties.

- The *Lavrentiev regularization* of Meyer et al. [112], see also [111], relaxes the pure state constraint into a mixed control-state constraint. This transformation is motivated by the observation that Lagrange multipliers to such mixed constraints enjoy more regularity. Typically, they are measurable functions, see, for instance, [7, 15]. The drawback of the Lavrentiev regularization is that it can only be applied if the domain on which the control is defined and the domain on which the state constraint is posed match. In the case of a boundary control and a state constraint in the interior of the domain that we have in mind, this approach is thus not applicable.

- Krumbiegel and Rösch [96] extend the Lavrentiev regularization by introducing a *virtual control* that is defined on the domain on which the state constraint is posed. The pure state constraint is then relaxed into a mixed constraint as discussed above. Introducing an auxiliary variable, the virtual control, obviously implies that the dimension of the discretized problems in the virtual control concept is increased compared to other regularization techniques.

- *Interior point* or *barrier methods* [144, 145] replace the state constraint by a suitable smooth functional that tends to infinity as the solution approaches the bound. However, an application of these techniques is beyond the scope of this work.

We treat the state constraint by the *Moreau-Yosida regularization* which is due to Ito and Kunisch [85]. The cost functional is penalized with a term that measures the violation of the state constraint. The resulting optimal control problem has the form

$$\min_{y\in\mathcal{Y},u\in\mathcal{U}} J_\gamma(y,u)$$

s. t. $\qquad\qquad\qquad\qquad\qquad\qquad\qquad$ (OCPSC$_\gamma$)

$$e(y,u)=0$$

with the penalized cost functional

$$J_\gamma(y, u) = J(y, u) + \frac{\gamma}{2} \int_{\Omega_0} \max\{0, g(y)\}^2 \, dx. \tag{6.1}$$

(OCPSC$_\gamma$) is a standard optimal control problem in which only the state equation appears as a constraint. As the non-smooth function $\max\{0, \cdot\}$ is squared, the reformulated cost functional J_γ is differentiable. To enforce the state constraint, the penalty parameter γ must theoretically be driven to infinity. In practice, (OCPSC$_\gamma$) is often solved for some increasing sequence of values for γ. This process can be automated by path-following techniques [76].

6.2   The State-Constrained Optimal Control Problem

In Section 5.5, we discussed a unidirectional solidification problem in which the task was to follow a prescribed flat interface motion. Since the cost functional did not contain any temperature tracking terms, the control in this example had to vanish at $t = T$, see Remark 3.8. As a consequence, there was a considerable deviation of the controled interface from the desired interface at final time. In certain situations, for instance if it is important that a minimal amount of material has solidified up to a certain instance of time, such a deviation is not tolerable. A potential workaround is to increase the weight γ_4 in the cost functional to enforce that the controled interface is closer to the desired interface position at the end of the process. However, this modification can not guarantee that the deviation is small enough.

A suitable state constraint on the position of the controled interface ensures that the observed deviation between the controled and the desired interfaces at $t = T$ is below a given tolerance. For instance, we can demand that the distance between the two interfaces must be less than one percent of the size of the hold-all in x_1-direction. This constraint can be expressed by requiring that the modulus of the signed distance function ϕ_d modeling the desired interface motion must not be larger than 0.02 on the current interface position:

$$|\phi_d(\cdot, t)| \le 0.02 \quad \text{on } \Gamma_I(t) \quad \text{for all} \quad t \in [0, T].$$

Equivalently, we can rewrite this single constraint as two differentiable constraints

$$\left.\begin{array}{ll} \phi_d(\cdot, t) \le 0.02 & \text{on } \Gamma_I(t) \\ -\phi_d(\cdot, t) \le 0.02 & \text{on } \Gamma_I(t) \end{array}\right\} \quad \text{for all} \quad t \in [0, T]. \tag{6.2}$$

Thus, we are concerned with the state-constrained motion planning problem

$$\min_{y,\phi,u} J(y,\phi,u) \quad \text{subject to} \quad (3.2) \quad \text{and} \quad (6.2), \qquad \text{(MPPSC)}$$

in which temperature tracking terms are omitted, i.e., $\gamma_1 = \gamma_3 = 0$ in the cost functional (3.3). A consequence of this particular choice is pointed out in Remark 3.8.

6.3   First-Order Necessary Optimality Conditions

We apply the Moreau-Yosida regularization introduced in Section 6.1 to remove the state constraint (6.2) from the optimal control problem (MPPSC). As in Sections 3.3.1–3.3.4, we omit the dx, ds and dt for the sake of brevity. According to (6.1), the penalized cost functional is

$$J_\gamma(y,\phi,u) = \frac{\gamma_2}{2} \int_0^T \int_{\Gamma_I(t)} |\phi_d|^2 + \frac{\gamma_4}{2} \int_{\Gamma_I(T)} |\phi_T|^2 + \frac{\gamma_5}{2} \int_0^T \int_{\Gamma_C} |u|^2$$
$$+ \frac{\gamma}{2} \int_0^T \int_{\Gamma_I(t)} \left(\max\{0, \phi_d - 0.02\}^2 + \max\{0, -\phi_d - 0.02\}^2 \right).$$

Now, we have to derive first-order necessary optimality conditions for the problem

$$\min_{y,\phi,u} J_\gamma(y,\phi,u) \quad \text{subject to} \quad (3.2). \qquad \text{(MPPSC}_\gamma\text{)}$$

Structurally, problem (MPPSC$_\gamma$) is of the form (OCPCC). Consequently, the Lagrange formalism can again be used to derive an adjoint system and a gradient equation. The Lagrange functional is defined as in (3.4) with $J(y,\phi,u)$ replaced by $J_\gamma(y,\phi,u)$:

$$\mathcal{L}(y,\,\phi,\,u,\,p,\,p_I,\,\psi) = J_\gamma(y,\phi,u) - \int_0^T \int_D (-f)\,p$$
$$- \int_0^T \int_{\Omega_S(t)} \left(\rho\,c_S\,y_t - k_S\,\Delta y \right) p - \int_0^T \int_{\Omega_F(t)} \left(\rho\,c_F\,y_t - k_F\,\Delta y \right) p$$
$$- \int_0^T \int_{\Gamma_N^S(t)} \left(k_S\,\tfrac{\partial y}{\partial n} - g \right) p - \int_0^T \int_{\Gamma_C^S} \left(k_S\,\tfrac{\partial y}{\partial n} - u \right) p$$
$$- \int_0^T \int_{\Gamma_N^F(t)} \left(k_F\,\tfrac{\partial y}{\partial n} - g \right) p - \int_0^T \int_{\Gamma_C^F} \left(k_F\,\tfrac{\partial y}{\partial n} - u \right) p$$
$$- \int_0^T \int_{\Gamma_I(t)} (y - y_M)\,p_I - \int_0^T \int_{\Gamma_I(t)} \left(\rho\,L\,\phi_t + \left[k\,\nabla y \right]_F^S \cdot \nabla\phi \right) \psi.$$

As we shall see in the following, the Moreau-Yosida regularization of the state constraint (6.2) requires only minor modifications in the first-order optimality conditions derived in Section 3.3 for the unconstrained problem (MPP).

The Adjoint Temperature. Since the penalty term that we added to the cost functional is independent of the temperature y, the argumentation of Section 3.3.1 is still valid and does not have to be changed, with the exception that the multipliers for the Neumann boundary conditions are replaced by the adjoint temperature p in the above definition of the Lagrange functional. Thus, the equations governing the adjoint temperature for (MPPSC$_\gamma$) are (3.10a)–(3.10j).

The Adjoint Level Set Function. Concerning its structure, the penalty term in the Moreau-Yosida regularization is similar to the interface tracking terms in the cost functional. Therefore, its derivative with respect to variations in the level set function ϕ can be calculated using the shape calculus tools from Appendix A. An application of (A.13) yields

$$
D \left[\!\!\left[\frac{\gamma}{2} \int_0^T \int_{\Gamma_I(t)} \max\{0, \phi_d - 0.02\}^2 + \max\{0, -\phi_d - 0.02\}^2; \delta\phi \right]\!\!\right]
$$

$$
= -\frac{\gamma}{2} \int_0^T \int_{\Gamma_I(t)} \frac{\delta\phi}{|\nabla\phi|} \left(\frac{\partial}{\partial n}\left(\max\{0, \phi_d - 0.02\}^2\right) + \kappa \, \max\{0, \phi_d - 0.02\}^2 \right)
$$

$$
- \frac{\gamma}{2} \int_0^T \int_{\Gamma_I(t)} \frac{\delta\phi}{|\nabla\phi|} \left(\frac{\partial}{\partial n}\left(\max\{0, -\phi_d - 0.02\}^2\right) + \kappa \, \max\{0, -\phi_d - 0.02\}^2 \right).
$$

As mentioned above, $\max\{0, \cdot\}^2$ is differentiable, and, thus, this relation for the variation of the Moreau-Yosida penalty term is (at least formally) well-defined. We do not simplify it any further because for the numerical implementation the current representation is already well-suited.

The Gradient Equation. The penalty term in the Moreau-Yosida regularization is independent of the control u. Thus, no changes need to be made in the gradient equation (3.11).

Summary of the Optimality Conditions. The complete adjoint system for (MPPSC$_\gamma$) is:

$$
-\rho\, c_S\, p_t - k_S\, \Delta p = 0 \qquad\qquad\qquad\qquad \text{in } \Omega_S(t) \quad (6.3\text{a})
$$

$$
-\rho\, c_F\, p_t - k_F\, \Delta p = 0 \qquad\qquad\qquad\qquad \text{in } \Omega_F(t) \quad (6.3\text{b})
$$

$$
p(T) = 0 \qquad\qquad\qquad\qquad\qquad\qquad \text{in } D \quad (6.3\text{c})
$$

$$
k_S\, \frac{\partial p}{\partial n} = 0 \qquad\qquad\qquad\qquad\qquad \text{on } \Gamma_C^S \quad (6.3\text{d})
$$

$$
k_F\, \frac{\partial p}{\partial n} = 0 \qquad\qquad\qquad\qquad\qquad \text{on } \Gamma_C^F \quad (6.3\text{e})
$$

$$k_S \, \frac{\partial p}{\partial n} = 0 \qquad\qquad\qquad\text{on } \Gamma_N^S(t) \quad (6.3\text{f})$$

$$k_F \, \frac{\partial p}{\partial n} = 0 \qquad\qquad\qquad\text{on } \Gamma_N^F(t) \quad (6.3\text{g})$$

$$p_I = \rho \left[c \right]_F^S p \, \vec{V} \cdot n - \left[k \, \nabla p \right]_F^S \cdot n \qquad\text{on } \Gamma_I(t) \quad (6.3\text{h})$$

$$p = \psi \left| \nabla \phi \right| \qquad\qquad\qquad\text{on } \Gamma_I(t) \quad (6.3\text{i})$$

$$-\hat{L} \left(\psi_t + \operatorname{div}(\psi \, \vec{V}) \right) = \frac{\partial y}{\partial n} \, p_I - \frac{\gamma_2}{2} \left(\frac{\partial}{\partial n} |\phi_d|^2 + \kappa |\phi_d|^2 \right)$$
$$- \frac{\gamma}{2} \left[\frac{\partial}{\partial n} \left(\max\{0, \phi_d - 0.02\}^2 \right) \right.$$
$$\left. + \kappa \, \max\{0, \phi_d - 0.02\}^2 \right]$$
$$- \frac{\gamma}{2} \left[\frac{\partial}{\partial n} \left(\max\{0, -\phi_d - 0.02\}^2 \right) \right.$$
$$\left. + \kappa \, \max\{0, -\phi_d - 0.02\}^2 \right] \qquad\text{on } \Gamma_I(t) \quad (6.3\text{j})$$

$$\hat{L} \, \psi(T) = -\frac{\gamma_4}{2} \left(\frac{\partial}{\partial n} |\phi_T|^2 + \kappa |\phi_T|^2 \right) \qquad\text{on } \Gamma_I(T) \quad (6.3\text{k})$$

$$\hat{L} := \rho \, L \left| \nabla \phi \right|. \qquad\qquad\qquad (6.3\text{l})$$

Compared to (3.10a)–(3.10d), the forcing terms on the right hand sides of (6.3a)–(6.3c) have disappeared due to the choice $\gamma_1 = \gamma_3 = 0$. The only other change with respect to the adjoint system (3.10) concerns the right hand side of the adjoint level set equation (6.3j) to which the Moreau-Yosida regularization of the state constraint (6.2) contributes an additional forcing term.

In summary, the optimality system of the optimal control problem (MPPSC$_\gamma$) in the absence of control constraints is given by

- the forward system (3.2),
- the adjoint system (6.3) and
- the gradient equation (3.11).

Remark 6.1 (Including Control Constraints). If control constraints are added to (MPPSC), the gradient equation (3.11) has to be replaced by the corresponding variational inequality as discussed in Section 3.1.

6.4 Optimization Methods

It is straightforward to adapt Algorithm 1 and Algorithm 2 to the solution of (MPPSC$_\gamma$). To illustrate that only minor changes are necessary, the resulting

---

Algorithm 5 Adjoint-Based Gradient Method for State Constraints

Input: u^0
Output: $\widehat{u}, \widehat{y}, \widehat{\phi}, \widehat{p}, \widehat{\psi}$

1: $j = 0$.
2: **while** the convergence condition is not fulfilled **do**
3:     Solve the forward problem (3.2) for y^j and ϕ^j.
4:     Solve the adjoint problem (6.3) for p^j and ψ^j.
5:     Construct the descent direction from (3.11)

$$v^j = -(\gamma_5\, u^j + p^j).$$

6:     Determine σ^j from

$$\sigma^j := \arg\min \widehat{J}\big(u^j + \sigma\, v^j\big).$$

7:     Set $u^{j+1} = u^j + \sigma^j\, v^j$, $j \to \overline{j} + 1$.
8: **end while**

---

solution strategy in the case of the projected gradient method is stated in Algorithm 5, assuming that there are no additional control constraints present. Note that control constraints of box type can be incorporated by inserting a projection in steps 6 and 7. We omit the translated version of the limited memory BFGS method for the sake of brevity. The remarks in Section 3.4.1 concerning Algorithm 1 and Algorithm 2 also apply to Algorithm 5 and an appropriate adaption of the BFGS method, respectively.

The implementation of Algorithm 5 relies on the discretization approach for the forward and the adjoint systems that we have used for the implementation of Algorithm 1. Only minor changes are necessary in the evaluation of the cost functional which is needed for performing the line search based on the Armijo rule. In addition, the evaluation of the forcing terms in the adjoint level set equation (6.3j) has to be extended to include the forcing terms resulting from the Moreau-Yosida regularization of the state constraint (6.2). These changes are obviously also necessary when applying the BFGS method.

6.5   Numerical Results

Setup. As indicated in Section 6.2, the setup in this example is the same as in Section 5.5, i.e., $D = [-1, 1] \times [-0.5, 0.5]$ is the hold-all, and we choose the control horizon $[0, 1]$. We also use the same spatial and temporal discretizations as in Section 5.5. The constraint violation is measured in terms of the

(a) Interface motion as computed in Section 5.5.

(b) Interface motion with the state constraint (6.2), $\gamma = 1000$.
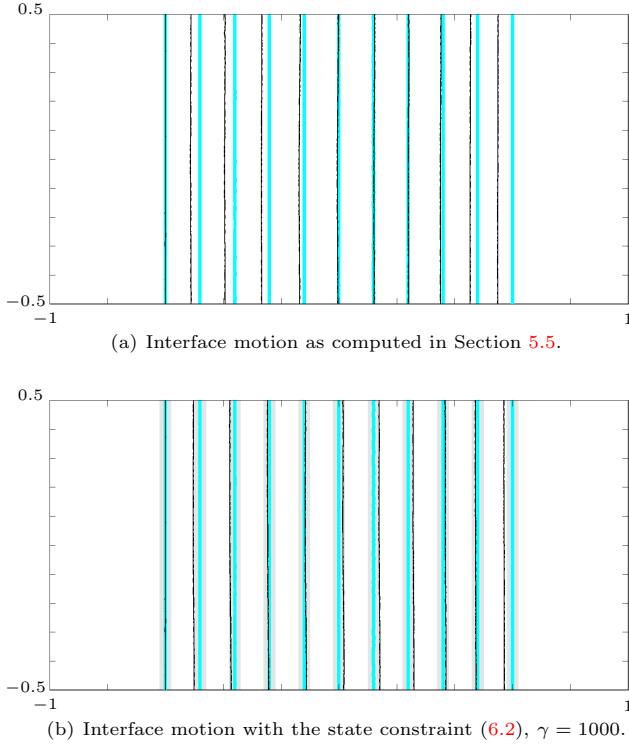
FIGURE 6.1. The interface positions corresponding to the computed control (black, thin line) and the desired motion (cyan, thick line) for the unconstrained problem of Section 5.5 and the state-constrained problem of Section 6.5 at time steps $t \in \{0, 0.1, 0.2, \ldots, 1\}$ (left to right).

Moreau-Yosida penalty term:

$$\mathcal{V}(\gamma) := \int_0^T \int_{\Gamma_I(t)} \max\{0, \phi_d - 0.02\}^2 + \max\{0, -\phi_d - 0.02\}^2 \, ds \, dt. \quad (6.4)$$

Interpretation of the Results. We solve the state-constrained optimal control problem (MPPSC$_\gamma$) for $\gamma \in \{0, 10, 100, 1000\}$ using the limited memory BFGS method, Algorithm 2. Note that $\gamma = 0$ means that we actually have

TABLE 6.1. Constraint violation in the unidirectional so-
lidification example in dependence on the Moreau-Yosida
penalty parameter.

γ	$\mathcal{V}(\gamma)$
0	0.0000770718
10	0.0000543645
100	0.0000064746
1000	0.0000016678

to solve the unconstrained problem of Section 5.5. The results are reported
in Table 6.1 and, for $\gamma = 1000$, in Figures 6.1–6.4.

The data in Table 6.1 tell us that, as γ is increased, the violation of the
state constraint, $\mathcal{V}(\gamma)$, goes down, as expected. For $\gamma = 1000$, the limited
memory BFGS method stops after 13 iterations because of (T1). The de-
crease of the corresponding relative cost functional is shown in Figure 6.2.
The computed optimal control can be found in Figure 6.3, and the result-
ing interface evolution and the corresponding temperature distributions are
shown in Figure 6.1(b) and Figure 6.4, respectively. For convenience of the
reader, and to make the comparison easier, the evolution of the interface
in the unconstrained case (cf. Section 5.5) is reproduced in Figure 6.1(a).
We observe that, except for the terminal time where there is still a slight
deviation, the interface always stays within the desired region around the
prescribed interface evolution which is printed as a gray rectangle in Fig-
ure 6.1(b). This is achieved by speeding up the solidification such that, in
contrast to the unconstrained case in which the controled interface almost
always stays left of the desired interface (Figure 6.1(a)), the controled inter-
face is running ahead of the desired interface for a certain time interval as
demonstrated by Figure 6.1(b). A comparison of the controls corresponding
to the unconstrained (Figure 5.22) and to the constrained case (Figure 6.3)
shows how this speed-up is administered: At the beginning of the process,
the control in the constrained case is more active than the control in the
unconstrained case.
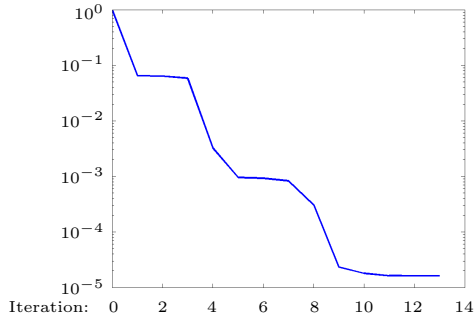
FIGURE 6.2. The relative cost functional $\widehat{J}_\gamma(u^j)/\widehat{J}_\gamma(u^0)$ for the state-constrained control problem of Section 6.5 for $\gamma = 1000$ in semi-logarithmic scale.
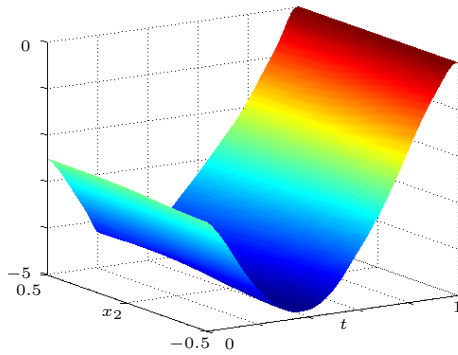
FIGURE 6.3. The computed control for the state-constrained control problem of Section 6.5 for $t \in [0,1]$ and for $\gamma = 1000$.

(a) $t = 0.00$

(b) $t = 0.25$

(c) $t = 0.50$

(d) $t = 0.75$

(e) $t = 1.00$

(f) Temperature scale.
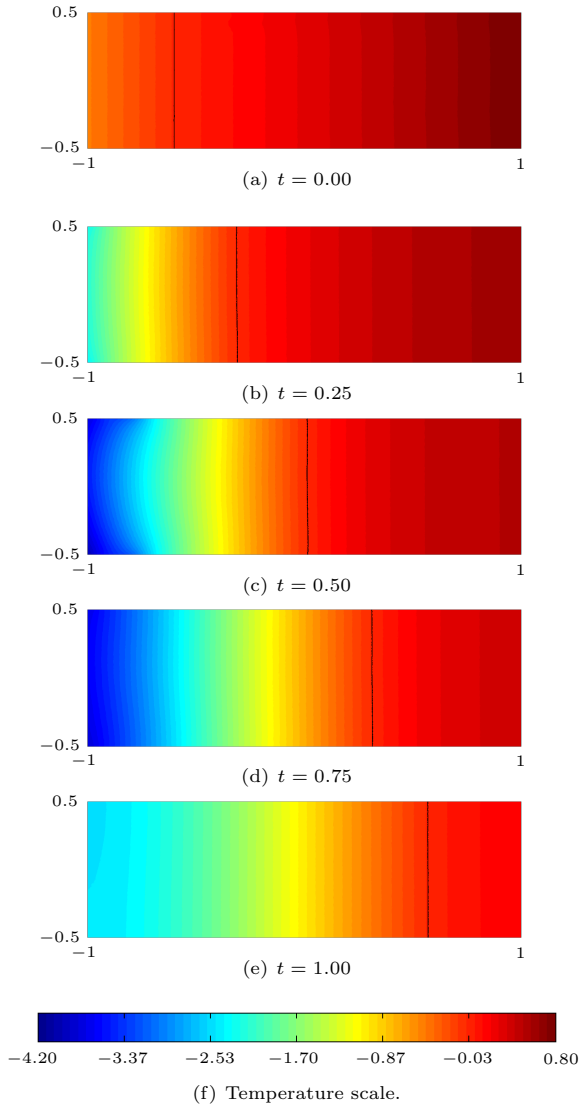
FIGURE 6.4. The temperature distribution and the inter-
face evolution corresponding to the optimal control for the
state-constrained problem of Section 6.5 computed with
the BFGS method for $\gamma = 1000$ at time steps $t \in \{0, 0.25, 0.5, 0.75, 1\}$.

7 Conclusions and Perspectives

7.1 Discussion and Conclusions

This thesis discusses motion planning for the classical two-phase Stefan problem in level set formulation. The proposed approach advances research on the optimal control of free and moving boundary problems in several directions.

Level Set Formulation. In contrast to previous approaches, the moving interface which separates the fluid phases from the solid phases is represented by the *level set method*, thus allowing for more geometric flexibility. In addition to unidirectional solidification problems, *closed interfaces* and *changes of topology* are handled naturally within this framework as demonstrated by the numerical examples. The considerable additional effort that is introduced by the level set method is kept at a reasonable level by using the narrow band method that goes along nicely with the proposed optimal control approach.

First-Order Necessary Optimality Conditions. The tracking-type cost functional incorporates observations of the temperature distribution in the hold-all and, in particular, of the interface position. The *formal derivation of first-order necessary optimality conditions* for the resulting optimal control problems subject to *control constraints* of box type in Chapter 3 is a major contribution of this thesis. This derivation is based on the Lagrange formalism and relies on shape calculus tools to take into account the geometric variations introduced by perturbations of the level set function. As neither the existence nor the uniqueness of solutions of the two-phase Stefan problem in the general level set formulation are known, it is not clear in which function spaces one should work. Thus the proposed optimal control approach is purely formal.

Discretization. The second major contribution of this thesis concerns the *discretization of the arising forward and adjoint systems*. Representing the

interface as the zero level set of a function requires solving the *level set equation* which in the proposed framework is a linear first-order Hamilton-Jacobi equation. To obtain the viscosity solution, a *discontinuous Galerkin* scheme is adapted. A suitable *explicit Runge-Kutta* method serves as the time stepping scheme. In addition, the level set method requires a *reinitialization* routine for the level set function and an *extension procedure* to construct a velocity field that advects the level set function. Both goals are met by using the *fast marching method*. All of these methods were available in the literature and necessitated only minor modifications, mostly because a triangular grid is used in this thesis, while a rectangular grid is far more popular in the literature. The *discretization of the curvature* which arises naturally in the optimality conditions requires a higher-order approximation of the level set function. Thus, quadratic finite element spaces are used throughout this thesis. For capturing the phase change characteristics of the *temperature*, the *extended finite element method* is applied. To conform with the level set solver, a quadratic finite element space is used. A *polygonal approximation of the discrete interface* allows for simple, yet efficient, numerical integration routines for assembling mass and stiffness matrices over elements that are intersected by the interface. This discretization strategy is one of the first attempts at applying the extended finite element method for optimal control purposes. Another finding of this thesis is that the adjoint system which is used for the efficient computation of the gradient has a structure that can be exploited advantageously in the numerical solution. The adjoint equation to the level set equation is *a first-order conservation law on the moving interface* (which is a moving curve in 2D and a moving surface in 3D). Numerical schemes for equations of this type have not been developed before as one of the usual assumptions in the modeling of conservation laws on moving surfaces is the existence of a flux that introduces diffusive terms. Thus, an important contribution of this thesis is the design of a numerical scheme for first-order conservation laws on moving surfaces in a level set context. A *discontinuous Galerkin* method is in this case used for the spatial discretization, while the same *explicit Runge-Kutta* method as for the level set equation is used for the time-stepping. The mass and the system matrices needed to evaluate this scheme can be re-used from the solution of the level set equation. Numerical experiments confirm the convergence of this approach. In addition, they demonstrate that our strategy benefits from the geometric flexibility of the level set method, i.e., closed interfaces and changes of topology can be handled when solving first-order conservation laws on moving surfaces. However, a theoretical foundation of this approach has not been established so far.

State Constraints. So far, most of the optimal control approaches for the two-phase Stefan problem that considered state constraints made use of a weak formulation of the forward problem avoiding an explicit interface representation. Typically, only state constraints on the enthalpy—which is nothing but a transformed version of the temperature—can then be posed. The level set approach used in this thesis provides a flexible framework for posing constraints on, e.g., the position of the interface. A reason for doing so might be to prevent rapid solidification, thus improving material quality.

7.2 Perspectives

The optimal control approach developed in this thesis can serve as a starting point for various directions of future research. Before commenting on some more specific issues, we mention three general aspects that might initiate future work. The motivation to consider motion planning problems for the two-phase Stefan problem was intrinsic. From a mathematician's point of view, the results are satisfactory. However, it would be interesting to assess the performance of the proposed optimal control approach in *real world applications*. Such a study might require an extension of the first-order optimality conditions and the numerical methods to the *three-dimensional* setting. The analysis of Chapters 3 and 6 carries over to this case literally if the curvature of the interface is replaced by the mean curvature. All numerical methods are basically suited for three dimensions although the implementation is significantly more complicated than in the current setting. In particular, the numerical integration on intersected elements is rather involved. Finally, it might be interesting to see in how far the proposed techniques extend to *shape optimization problems* for the two-phase Stefan problem as the motion of the interface can also be influenced by the design of the boundary of the hold-all. We now turn to some more specific comments on potential extensions.

The Mathematical Model. Among the many potential extensions of the two-phase Stefan problem in the proposed level set formulation, we mention the *Gibbs-Thomson correction* and the *Navier-Stokes equations*. It is expected that the proposed shape calculus based techniques for computing the first-order optimality system are applicable in these two cases with minor modifications. For instance, in case of the Gibbs-Thomson correction, one needs to take into account the variation of the curvature with respect to variations in the level set function, see Remark 3.4. The discretization of the curvature has already been addressed. Coupling the Navier-Stokes system to the heat equation in an extended finite element framework is also possible, see [168]. In addition, a generalization to m-phase Stefan problems should be realizable. However, if more than two phases are present, one

level set function is not sufficient to describe the geometric configuration. This complicates the derivation of the optimality conditions as well as the implementation and the numerical solution.

Numerical Methods. A challenging problem concerning the *numerical solution* of the forward and the adjoint systems is the implementation of a "true" *higher-order method*. The current implementation is based on quadratic polynomials. However, the motivation to depart from linear finite elements was to have a convergent discretization of the curvature, and not primarily to have an improved convergence rate. All the numerical experiments indicate that the implemented solver converges linearly. To improve on this point, several changes are necessary. As indicated in Remark 4.6, the reinitialization of the level set function and the construction of extension velocities must be replaced, either by a higher-order fast marching method or by using a different reinitialization PDE. The discrete interface should be non-polygonal which requires isoparametric integration routines for assembling the extended finite element systems. Finally, the time discretization of the heat equation with the implicit Euler method has to be improved. As pointed out, the Crank-Nicolson scheme tends to preserve oscillations. Lobatto or Radau time stepping methods might provide an alternative. A modification that potentially renders the current implementation more efficient is to use the *discontinuous Galerkin* scheme proposed by Yan and Osher [166] which is applicable to the non-linear version of the level set equation, and, thus, requires the construction of a scalar velocity only. A potential drawback of this scheme is that it might not be compatible with the adjoint level set equation in the sense that the matrices that are assembled during the solution of the level set equation can not be reused for the solution of the corresponding adjoint equation.

Optimization. Throughout this text, we focused on a quadratic *cost functional* of tracking type. Other cost functionals, e.g., of L^1 or L^∞ type, might be relevant for applications. Such non-standard cost functionals introduce additional mathematical challenges. Since certain shapes of the interface, for instance, flat or convex interfaces, are preferable over others, adding a term that *penalizes* the (sign of the) *curvature* to the cost functional is for sure worth looking at. It was pointed out that taking the derivative of the curvature with respect to perturbations in the level set function is an issue that arises in such configurations. To *solve the optimization problems*, the projected gradient method and the limited memory BFGS method were implemented. An extension to CG-type algorithms is for sure within reach. However, methods that rely on second-order information, e.g., SQP, require additional work to provide Hessians. Higher-order shape calculus tools might be applicable for computing second derivatives. The implementation of alternative approaches for treating control and state constraints as, for instance,

the active set method or semi-smooth Newton methods, and, in particular, of other *regularization methods for state constraints* is another potential starting point for future research. An extension of the techniques proposed in this thesis to *more complicated state constraints* is for sure possible. A natural candidate are constraints on the temperature or even on its gradient. Another issue concerning the computation of derivatives is the usage of *automatic differentiation* (AD) to provide gradient information. Due to the geometric non-linearities contained in the two-phase Stefan problem, the application of AD tools is expected to be non-trivial.

A Shape Calculus Primer

<div align="center">Contents</div>

This chapter contains some basic definitions, formulæ and results from shape calculus and tangential calculus, along with two transport theorems. As explained in Section 2.4, the existence and the uniqueness of solutions of the two-phase Stefan problem in level set formulation are not known. Consequently, the regularity of the temperature and the interface is also an open problem. Therefore, all the calculations in Section 3.3 are only formally correct. In particular, we assume that all quantities involved are smooth enough so that the shape calculus tools are applicable. As a consequence, and for the sake of brevity, we state the results in this chapter mostly without their precise assumptions. Unless otherwise stated, we use the textbooks [40, 151] as our primary sources. We mention that the same formulæ for derivatives of domain and boundary integrals can be obtained by using perturbations of the given boundary in normal direction as shown, e.g., by Pironneau [136].

A.1 Ingredients of Shape Calculus

A *shape functional* $J : \mathbb{O} \to \mathbb{R}$ is a map from a given set $\mathbb{O}$ of admissible domains, for instance, C^k domains contained in a hold-all D, to the real numbers. A sensitivity analysis for shape functionals is based on perturbations $\{\Omega_\lambda\}$ of a given domain $\Omega = \Omega_0$. If Ω and Ω_λ enjoy the same topological properties and the same smoothness for $0 < \lambda < \epsilon$, a family of *transformations* T_λ with certain smoothness properties (see (A.1)–(A.2) for the case that all domains are constrained to lie in a fixed hold-all D) can be constructed that transforms Ω into Ω_λ. If Ω and the family $\{T_\lambda\}$ are given,

then $\Omega_\lambda = T_\lambda(\Omega)$ defines the transformed domains uniquely. The converse is not true in general.

In two spatial dimensions, an example of such a transformation is the parameter-dependent level set representation of curves. Assume that a family of functions Φ_λ, that depend on the parameter λ and are defined on a fixed set $\bar{D}$, is given. This family induces the transformation $T_\lambda = \Phi_\lambda^{-1}(0)$, and the corresponding perturbed domains are defined by

$$\Omega_\lambda = \{x \in D \,|\, \Phi_\lambda(x) < 0\}\,.$$

Instead of 0, any other level set could be used.

The Speed Method. The *speed method* [**151**, Section 2.9] provides a framework to construct the needed transformations via so called speed vector fields (velocity fields). In the following, we consider a bounded domain $D \subset \mathbb{R}^d$ with smooth or at least piecewise C^k boundary ∂D. Let $T_\lambda : \bar{D} \to \bar{D}$ be a one-to-one mapping that satisfies the smoothness properties

$$T_\lambda \in C^k(\bar{D}, \mathbb{R}^d) \quad \text{and} \quad T_\lambda^{-1} \in C^k(\bar{D}, \mathbb{R}^d), \tag{A.1}$$

and

$$\lambda \mapsto T_\lambda(x), \quad \lambda \mapsto T_\lambda^{-1}(x) \quad \in C\big([0, \epsilon)\big) \quad \forall x \in \bar{D}. \tag{A.2}$$

Using this transformation, we can compute for any point $X \in D$ (Lagrangian coordinates) and for any $\lambda > 0$ a trajectory $x(\cdot)$ along which the point $x(\lambda) = T_\lambda(X)$ (Eulerian coordinates) moves with the velocity

$$\left| \frac{d}{d\lambda} x(\lambda) \right| = \left| \frac{\partial}{\partial \lambda} T_\lambda(X) \right|.$$

In this way, the given transformation induces a speed vector field

$$V(\lambda)(x) := V(\lambda, x) := \left(\frac{\partial}{\partial \lambda} T_\lambda \right) \circ T_\lambda^{-1}(x)$$

that has the smoothness

$$V \in C\big([0, \epsilon), C^k(\bar{D}; \mathbb{R}^d)\big). \tag{A.3}$$

Conversely, let $V \in C\big([0, \epsilon), C^k(\bar{D}; \mathbb{R}^d)\big)$ be a given speed vector field with

$$V(\lambda, x) \cdot n(x) = 0 \qquad \text{if } n(x) \text{ exists at } x \in \partial D, \tag{A.4a}$$
$$V(\lambda, x) = 0 \qquad \text{if } n(x) \text{ does not exist at } x \in \partial D, \tag{A.4b}$$

where $n(x)$ is the outward unit normal to ∂D at x. Note that condition (A.4a) holds almost everywhere on ∂D. The transformation T_λ can be obtained as

the solution to the system of ordinary differential equations

$$\left.\begin{array}{r}\dfrac{d}{d\lambda}x(\lambda,X) = V\big(\lambda,x(\lambda,X)\big), \\[2mm] x(0,X) = X. \end{array}\right\}\tag{A.5}$$

These observations are summarized in the following theorem.

Theorem A.1 (Equivalence Between Velocities and Transformations). *Let D be a bounded domain in $\mathbb{R}^d$ with piecewise smooth boundary ∂D and let V be a given speed vector field that satisfies* (A.3) *and* (A.4). *Then there exists a one-to-one transformation $T_\lambda(V) : \mathbb{R}^d \to \mathbb{R}^d$ that in particular maps $\bar{D}$ to $\bar{D}$ and satisfies the conditions* (A.1), (A.2), (A.5) *and*

$$V = \left(\frac{\partial}{\partial\lambda}\,T_\lambda\right)\circ T_\lambda{}^{-1}.\tag{A.6}$$

Conversely, if T_λ is a given transformation of $\bar{D}$ that satisfies (A.1) *and* (A.2), *and V is defined as in* (A.6) *then the compatibility conditions* (A.4) *and the smoothness property* (A.3) *hold. Moreover, the transformation $T_\lambda(X) = x(\lambda,X)$ can be obtained as the local solution of* (A.5).

Admissible Speed Vector Fields. As indicated above, the speed vector fields can not be chosen arbitrarily. Based on the set

$$\mathcal{D}^k(\mathbb{R}^d,\mathbb{R}^d) := \Big\{ f \in C^k(\mathbb{R}^d,\mathbb{R}^d) \mid f \text{ has compact support} \Big\},$$

we introduce the set of *admissible speed vector fields* [**151**, Section 2.10]

$$V^k(D) := \Big\{ V \in \mathcal{D}^k(\mathbb{R}^d,\mathbb{R}^d) \mid (\text{A.4}) \text{ is fulfilled} \Big\}.$$

For $V \in C\big([0,\epsilon), V^k(D)\big)$, D bounded, there exists $\delta \leq \epsilon$ and a one-to-one transformation $T_\lambda(V)$ such that Theorem A.1 is applicable for $\lambda < \delta$.

Shape Differentiability. We are now in the position to introduce the notion of *shape differentiability*. Assume that $D \subset \mathbb{R}^d$ is an open set and that $\Omega \subset D$ is measurable.

Definition A.2 (Eulerian Derivative [**151**, Definition 2.19]). *For $V \in C\big([0,\epsilon), V^k(D)\big)$ and the associated transformation $T_\lambda(V) : \bar{D} \to \bar{D}$, the Eulerian derivative of the domain functional $J(\Omega)$ at Ω in direction V is defined as the limit*

$$dJ(\Omega;V) = \lim_{\lambda\to 0}\frac{1}{\lambda}\big(J(\Omega_\lambda) - J(\Omega)\big),$$

where $\Omega_\lambda = T_\lambda(V)(\Omega)$.

Definition A.3 (Shape Differentiability [**151**, Definition 2.20])**.** *The functional $J(\Omega)$ is shape differentiable at Ω if*

    (1) *$dJ(\Omega; V)$ exists for all admissible directions V and*
    (2) *the mapping $V \mapsto dJ(\Omega; V)$ is linear and continuous.*

It remains to identify a gradient from this formula. The main result concerning the representation of shape gradients is the famous Hadamard formula which is sometimes also called the Hadamard-Zolesio structure theorem.

Theorem A.4 (The Hadamard Formula [**151**, Theorem 2.27])**.** *Let $J(\cdot)$ be a shape functional that is shape differentiable at each $\Omega \subset D$ of class C^k. If $\Omega \subset D$ has a boundary Γ of class C^{k-1} then there exists a scalar distribution $g(\Gamma) \in \mathcal{D}^{-k}(\Gamma)$ such that the gradient $G(\Omega) \in \mathcal{D}^{-k}(\Omega, \mathbb{R}^d)$ of the functional $J(\cdot)$ at Ω which is supported on Γ is given by*

$$G(\Omega) = \gamma_\Gamma^*(g \cdot n),$$

where γ_Γ^* is the transpose of the trace operator $\gamma_\Gamma : \mathcal{D}(\bar{D}, \mathbb{R}^d) \to \mathcal{D}(\Gamma, \mathbb{R}^d)$.

Under additional smoothness assumptions on the boundary of the domain, one can show [**40**, Chapter 8, Section 3.3] that there exists a scalar distribution $g(\Gamma) \in C^k(\Gamma)'$ such that

$$dJ(\Omega; V) = \langle g(\Gamma), \gamma_\Gamma(V) \cdot n \rangle_{C^k(\Gamma)}.$$

If this distribution is regular enough, e.g., $g(\Gamma) \in L^1(\Gamma)$, one can simply write

$$dJ(\Omega; V) = \int_\Gamma g\, V \cdot n\, ds.$$

A.2   Derivative of a Domain Integral

If $V \in \mathcal{D}^k(\mathbb{R}^d, \mathbb{R}^d)$, $k \geq 1$ and $f \in W^{1,1}(\mathbb{R}^d)$, the *domain functional*

$$J(\Omega) = \int_\Omega f\, dx$$

is shape differentiable for measurable Ω, and [**151**, Section 2.16]

$$dJ(\Omega; V) = \left(\frac{d}{d\lambda} \int_{\Omega_\lambda} f\, dx \right)\bigg|_{\lambda=0} = \int_\Omega \operatorname{div}\big(f\, V(0)\big)\, dx.$$

If Ω has a boundary Γ of class C^k, $k \geq 1$, then by virtue of Stokes' theorem

$$dJ(\Omega; V) = \int_\Gamma f\, \langle V(0), n \rangle\, ds. \tag{A.7}$$

In [**40**, Chapter 8, Section 4, pp. 352] one can find a somewhat more general statement under the smoothness conditions

$$\exists \delta > 0 \quad \forall x \in D: \quad V(\cdot, x) \in C([0, \delta], \mathbb{R}^d),$$

$$\exists c > 0 \quad \forall x, y \in D: \quad \|V(\cdot, y) - V(\cdot, x)\|_{C([0,\delta], \mathbb{R}^d)} \leq c\,|y - x|,$$

$$\forall c \in \partial D \quad \forall \lambda \in [0, \delta]: \quad V(\lambda, x) \in L_D(x)$$

on the velocity field V for bounded $D \subset \mathbb{R}^d$. Here, $L_D(x)$ is the linear tangent space to D at $x \in \partial D$.

Theorem A.5 (Theorem 4.2 (p. 352) in [**40**]). *Assume that there exists $\delta > 0$ such that $V \in C^0\big([0, \delta], C^1_{\mathrm{loc}}(\mathbb{R}^d, \mathbb{R}^d)\big)$ satisfies the above smoothness assumptions. For any $\varphi \in C\big([0, \delta), W^{1,1}_{\mathrm{loc}}(\mathbb{R}^d)\big) \cap C^1\big([0, \delta), L^1_{\mathrm{loc}}(\mathbb{R}^d)\big)$ and for any measurable domain Ω with boundary Γ, the Eulerian derivative of the functional*

$$J_V(\lambda) := \int_{\Omega_\lambda} \varphi(\lambda)\, dx$$

at $\lambda = 0$ is given by

$$dJ_V(0) = \int_\Omega \varphi'(0) + \mathrm{div}\big(\varphi(0)\, V(0)\big)\, dx,$$

where $\varphi'(0)(x) = \frac{\partial \varphi}{\partial \lambda}(0, x)$. If Ω is open with a Lipschitzian boundary Γ, then

$$dJ_V(0) = \int_\Omega \varphi'(0)\, dx + \int_\Gamma \varphi(0)\, V(0)\, n\, ds.$$

Application in the Context of Level Sets. For the application of the speed method in a level set context, we have to choose a proper velocity field V. If the transformed domains Ω_λ are defined by $\phi^{-1}(\lambda)$, the corresponding velocity field is autonomous [**151**, Section 2.9]:

$$V(\lambda, x) = \frac{\nabla \phi}{|\nabla \phi|^2}.$$

In contrast, if the transformed domains Ω_λ are defined by the level curves $\Phi_\lambda^{-1}(0)$ (or any other level curve), then the corresponding velocity field is non-autonomous and given by [**151**, Section 2.9]

$$V(\lambda, x) = -\Phi_\lambda'(x)\frac{\nabla \Phi_\lambda}{|\nabla \Phi_\lambda|^2}, \tag{A.8}$$

where Φ_λ' is the partial derivative of Φ_λ with respect to the parameter λ.

We describe the transformed domains Ω_λ via perturbations of a given level set function ϕ in the form

$$\Phi_\lambda = \phi + \lambda\,\delta\phi.$$

According to (A.8), the corresponding velocity field is

$$V(\lambda) = -\Phi_\lambda{}' \frac{\nabla\Phi_\lambda}{|\nabla\Phi_\lambda|^2} = -\delta\phi \frac{\nabla\phi + \lambda\,\nabla(\delta\phi)}{|\nabla\phi + \lambda\,\nabla(\delta\phi)|^2},$$

which implies

$$V(0) = -\delta\phi \frac{\nabla\phi}{|\nabla\phi|^2} = -\frac{\delta\phi}{|\nabla\phi|}\frac{\nabla\phi}{|\nabla\phi|}, \tag{A.9}$$

and (A.7) translates to

$$dJ(\Omega; V) = -\int_\Gamma f \frac{\delta\phi}{|\nabla\phi|}\frac{\nabla\phi}{|\nabla\phi|} \cdot n\,ds.$$

The expression

$$n = \frac{\nabla\phi}{|\nabla\phi|} \tag{2.9}$$

for the normal to the interface, n, in terms of the level set function ϕ admits the reformulation

$$dJ(\Omega; V) = -\int_\Gamma f \frac{\delta\phi}{|\nabla\phi|}\frac{\nabla\phi}{|\nabla\phi|} \cdot \frac{\nabla\phi}{|\nabla\phi|}\,ds = -\int_\Gamma f \frac{\delta\phi}{|\nabla\phi|}\,ds \tag{A.10}$$

of this formula for the shape derivative. The factor $-\frac{\delta\phi}{|\nabla\phi|}$ can be interpreted as the perturbation of Γ in normal direction that is introduced by perturbing ϕ.

Remark A.6. To ensure that the velocity field is admissible, we have to conform to (A.4), i.e., the conditions

$$\begin{cases} V(0) \cdot n = -\frac{\delta\phi}{|\nabla\phi|}\frac{\nabla\phi}{|\nabla\phi|} \cdot n \overset{!}{=} 0 & \text{if } n \text{ exists,} \\ V(0) = -\frac{\delta\phi}{|\nabla\phi|}\frac{\nabla\phi}{|\nabla\phi|} \overset{!}{=} 0 & \text{otherwise,} \end{cases}$$

have to be fulfilled. In both cases, we have to require $\delta\phi = 0$ on ∂D.

A.3 Derivative of a Boundary Integral

If $V \in C\big([0,\epsilon), \mathcal{D}^k(\mathbb{R}^d, \mathbb{R}^d)\big)$, $k \geq 1$, and $f \in W^{2,1}(\mathbb{R}^d)$, the *boundary functional*

$$J(\Omega) = \int_\Gamma f\,ds \tag{A.11}$$

is shape differentiable for measurable Ω, and [151, Section 2.18]

$$dJ(\Omega; V) = \left(\frac{d}{d\lambda} \int_{\Gamma_\lambda} f \, ds_\lambda \right) \Bigg|_{\lambda=0}$$
$$= \int_\Gamma \nabla f \cdot V(0) + f \big(\operatorname{div} V(0) - \langle DV(0) \cdot n, n \rangle \big) \, ds,$$

where $DV(0)$ denotes the Jacobian matrix of $V(0)$.

As for domain integrals, a more general statement is the following:

Theorem A.7 (Theorem 4.3 (p. 355) in [40]). *Let Γ be the boundary of a bounded open subset Ω of $\mathbb{R}^d$ of class C^2 and let $\psi \in C^1 \big([0, \delta), H^2_{\mathrm{loc}}(\mathbb{R}^d) \big)$. For $V \in C^0 \big([0, \delta], C^1_{\mathrm{loc}}(\mathbb{R}^d, \mathbb{R}^d) \big)$ consider the functional*

$$J_V(\lambda) := \int_{\Gamma_\lambda(V)} \psi(\lambda) \, ds_\lambda.$$

Then its derivative with respect to λ at $\lambda = 0$ is given by

$$dJ_V(0) = \int_\Gamma \psi'(0) + \nabla \psi \cdot V(0) + \psi \big(\operatorname{div} V(0) - \langle DV(0) \cdot n, n \rangle \big) \, ds$$
$$= \int_\Gamma \psi'(0) + \left(\frac{\partial \psi}{\partial n} + \kappa \, \psi \right) V(0) \cdot n \, ds, \tag{A.12}$$

where $\psi'(0)(x) = \frac{\partial \psi}{\partial \lambda}(0, x)$ and κ is the (mean) curvature of Γ.

Application in the Context of Level Sets. The velocity field V is constructed as in Section A.2. In particular, Remark A.6 applies here as well.

From (A.9) and (2.9) we infer

$$\operatorname{div} V(0) - \langle D V(0) \cdot n, n \rangle$$
$$= \operatorname{div} \left(-\frac{\delta\phi}{|\nabla\phi|} \frac{\nabla\phi}{|\nabla\phi|} \right) - \left\langle D \left(-\frac{\delta\phi}{|\nabla\phi|} \frac{\nabla\phi}{|\nabla\phi|} \right) \cdot n, n \right\rangle$$
$$= -\frac{\delta\phi}{|\nabla\phi|} \operatorname{div} \left(\frac{\nabla\phi}{|\nabla\phi|} \right) - \nabla \left(\frac{\delta\phi}{|\nabla\phi|} \right) \cdot \frac{\nabla\phi}{|\nabla\phi|}$$
$$+ \nabla \left(\frac{\delta\phi}{|\nabla\phi|} \right) \cdot \frac{\nabla\phi}{|\nabla\phi|} + \frac{\delta\phi}{|\nabla\phi|} \left\langle D \left(\frac{\nabla\phi}{|\nabla\phi|} \right) \cdot \frac{\nabla\phi}{|\nabla\phi|}, \frac{\nabla\phi}{|\nabla\phi|} \right\rangle.$$

A straightforward computation shows that

$$\left\langle D \left(\frac{\nabla\phi}{|\nabla\phi|} \right) \cdot \frac{\nabla\phi}{|\nabla\phi|}, \frac{\nabla\phi}{|\nabla\phi|} \right\rangle = 0,$$

and, thus, we have

$$\operatorname{div} V(0) - \langle D V(0) \cdot n, n \rangle = -\frac{\delta\phi}{|\nabla\phi|} \operatorname{div}\left(\frac{\nabla\phi}{|\nabla\phi|}\right).$$

Therefore, the Eulerian derivative of the boundary functional (A.11) is given by

$$dJ(\Omega; V) = -\int_\Gamma \frac{\delta\phi}{|\nabla\phi|} \nabla f \cdot \frac{\nabla\phi}{|\nabla\phi|} + \frac{\delta\phi}{|\nabla\phi|} f \operatorname{div}\left(\frac{\nabla\phi}{|\nabla\phi|}\right) ds$$

$$= -\int_\Gamma \frac{\delta\phi}{|\nabla\phi|}\left(\nabla f \cdot \frac{\nabla\phi}{|\nabla\phi|} + f \operatorname{div}\left(\frac{\nabla\phi}{|\nabla\phi|}\right)\right) ds.$$

Since

$$\nabla f \cdot \frac{\nabla\phi}{|\nabla\phi|} + f \operatorname{div}\left(\frac{\nabla\phi}{|\nabla\phi|}\right) = \operatorname{div}\left(f \frac{\nabla\phi}{|\nabla\phi|}\right),$$

this formula can be rewritten as

$$dJ(\Omega; V) = -\int_\Gamma \frac{\delta\phi}{|\nabla\phi|} \operatorname{div}\left(f \frac{\nabla\phi}{|\nabla\phi|}\right) ds.$$

Alternatively, we can make use of (2.9) and

$$\operatorname{div} \frac{\nabla\phi}{|\nabla\phi|} = \kappa \tag{2.10}$$

to derive the expression

$$dJ(\Omega; V) = -\int_\Gamma \frac{\delta\phi}{|\nabla\phi|}\left(\frac{\partial f}{\partial n} + f \kappa\right) ds. \tag{A.13}$$

Similarly, (A.12) translates to

$$dJ_V(0) = \int_\Gamma \psi'(0) - \left(\frac{\partial\psi}{\partial n} + \kappa\,\psi\right) \frac{\delta\phi}{|\nabla\phi|}\, ds. \tag{A.14}$$

A.4 Tangential Calculus

In this section, we give the definitions of the tangential gradient and the tangential divergence of smooth functions as they can be found in [151, Section 2.19]. The extension to functions in Sobolev spaces is possible by a density argument but not of interest here because we apply the tangential calculus only in a formal sense.

Definition A.8 (Tangential Divergence).

(1) *Let Ω be a given domain with its boundary Γ of class C^2 and let $V \in C^1(U, \mathbb{R}^d)$ be a vector field, where U is an open neighborhood of Γ. The tangential divergence of V is defined as*

$$\mathrm{div}_\Gamma V = \big(\mathrm{div}\, V - \langle D\,V \cdot n, n\rangle\big)|_\Gamma \in C(U).$$

(2) *If Ω has a boundary Γ of class C^2 and $V \in C^1(\Gamma, \mathbb{R}^d)$ is a vector field on Γ, the tangential divergence of V is defined as*

$$\mathrm{div}_\Gamma V = \big(\mathrm{div}\, \tilde{V} - \big\langle D\tilde{V} \cdot n, n\big\rangle\big)|_\Gamma \in C(\Gamma),$$

where $\tilde{V}$ is any C^1 extension of V to an open neighborhood of Γ.

It can be shown that for two admissible vector fields V_1, V_2 that satisfy $V_1|_\Gamma = V_2|_\Gamma$, the identity

$$\mathrm{div}\, V_1(x) - \langle DV_1(x) \cdot n(x), n(x)\rangle = \mathrm{div}\, V_2(x) - \langle DV_2(x) \cdot n(x), n(x)\rangle$$

holds for any $x \in \Gamma$. Hence the tangential divergence is independent of the choice of $\tilde{V}$ and, thus, well-defined.

Definition A.9 (Tangential Gradient). *Let $h \in C^2(\Gamma)$ be given and consider an extension $\tilde{h} \in C^2(U)$ to an open neighborhood U of Γ such that $\tilde{h}|_\Gamma = h$ on Γ. The tangential gradient of h is defined as*

$$\nabla_\Gamma h = \nabla\tilde{h}|_\Gamma - \frac{\partial \tilde{h}}{\partial n}\, n = \nabla\tilde{h}|_\Gamma - \big\langle \nabla\tilde{h}, n\big\rangle n.$$

It can be shown that such an extension exists and that the right hand side of this definition is independent of the choice of the extension $\tilde{h}$.

A.5   Transport Theorems

In addition to the shape calculus tools described in the preceding sections, the formal derivation of first-order optimality conditions for the control constrained optimal control problem in Chapter 3 requires characterizations of transport in moving domains and on moving interfaces. In particular, formulæ for integration by parts on variable domains are needed.

A proof of the following classical transport theorem can be found in [51, Section 5.4].

Theorem A.10 (Reynolds Transport Theorem). *The derivative of the quantity*

$$F(t) := \int_{\Omega(t)} f(x,t)\, dx$$

is given by

$$\frac{dF}{dt}(t) = \int_{\Omega(t)} \frac{\partial f}{\partial t} + \operatorname{div}(f\, V)\, dx \tag{A.15a}$$

$$= \int_{\Omega(t)} \frac{df}{dt} + f\, \operatorname{div}(V)\, dx \tag{A.15b}$$

$$= \int_{\Omega(t)} \frac{\partial f}{\partial t}\, dx + \int_{\partial\Omega(t)} f\, V \cdot n\, ds, \tag{A.15c}$$

where V is the velocity field in which the control volume $\Omega(t)$ moves.

From this theorem, we infer a formula for integration by parts in time in moving domains.

Corollary A.11 (Integration by Parts in Time in Moving Domains). *For $g = g(x,t)$ and $h = h(x,t)$, we have*

$$\int_0^T \int_{\Omega(t)} g\, h_t\, dx\, dt = \int_{\Omega(T)} g(x,T)\, h(x,T)\, dx - \int_{\Omega(0)} g(x,0)\, h(x,0)\, dx$$

$$- \int_0^T \int_{\Omega(t)} g_t\, h\, dx\, dt - \int_0^T \int_{\partial\Omega(t)} g\, h\, V \cdot n\, ds\, dt.$$

PROOF. By integrating (A.15c) over the time interval $[0,T]$ we derive the relation

$$F(T) - F(0) = \int_0^T \int_{\Omega(t)} \frac{\partial f}{\partial t}\, dx\, dt + \int_0^T \int_{\partial\Omega(t)} f\, V \cdot n\, ds\, dt.$$

Now, the assertion of Corollary A.11 follows by setting $f = g \cdot h$, applying the product rule and a simple rearrangement. $\qquad\square$

Transport across moving surfaces can be characterized as follows [**38**, **55**]:

Theorem A.12 (Surface Transport Theorem). *Let $f(\cdot, t) : \mathcal{S}_t \to \mathbb{R}$ be a scalar field defined on the moving surface $\mathcal{S}_t$. Then*

$$\frac{d}{dt} \int_{\mathcal{S}_t} f(x,t)\, d\mathcal{S}_t = \int_{\mathcal{S}_t} \dot{f}(x,t) + f(x,t)\, \operatorname{div}_{\mathcal{S}_t} \mathbf{w}(x,t)\, d\mathcal{S}_t, \tag{A.16}$$

where $\mathbf{w}$ *is the normal velocity of the moving surface* $\mathcal{S}_t$ *and* $\dot{f}$ *is the parameter-time derivative of* f. *If* $f(\cdot, t)$ *is the restriction of a function* $\hat{f}(\cdot, t)$ *to* $\mathcal{S}_t$, *then*

$$\dot{f}(x,t) = \mathbf{w}(x,t) \cdot \nabla \hat{f}(x,t) + \frac{\partial}{\partial t} \hat{f}(x,t).$$

Corollary A.13 (Integration by Parts in Time on a Moving Surface). *With the notation of Theorem A.12, we have*

$$\int_0^T \int_{\mathcal{S}_t} \hat{g}(x,t)\, \hat{h}_t(x,t)\, d\mathcal{S}_t\, dt = \int_{\mathcal{S}_T} g(x,T)\, h(x,T)\, d\mathcal{S}_T - \int_{\mathcal{S}_0} g(x,0)\, h(x,0)\, d\mathcal{S}_0$$

$$- \int_0^T \int_{\mathcal{S}_t} \hat{g}_t(x,t)\, \hat{h}(x,t) + \mathbf{w}(x,t) \cdot \nabla\big(\hat{g}(x,t)\, \hat{h}(x,t)\big)$$

$$+ g(x,t)\, h(x,t)\, \operatorname{div}_{\mathcal{S}_t} \mathbf{w}\, d\mathcal{S}_t\, dt,$$

where g *and* h *are restrictions of* $\hat{g}$ *and* $\hat{h}$ *to* $\mathcal{S}_t$.

PROOF. By integrating (A.16) over the time interval $[0, T]$ we derive the relation

$$\int_{\mathcal{S}_T} f(x,T)\, d\mathcal{S}_T - \int_{\mathcal{S}_0} f(x,0)\, d\mathcal{S}_0 = \int_0^T \int_{\mathcal{S}_t} \dot{f}(x,t) + f(x,t)\, \operatorname{div}_{\mathcal{S}_t} \mathbf{w}\, d\mathcal{S}_t\, dt.$$

After substituting $f = g \cdot h$, we infer

$$\int_{\mathcal{S}_T} g(x,T)\, h(x,T)\, d\mathcal{S}_T - \int_{\mathcal{S}_0} g(x,0)\, h(x,0)\, d\mathcal{S}_0$$

$$= \int_0^T \int_{\mathcal{S}_t} (g \cdot h)(x,t) + g(x,t)\, h(x,t)\, \operatorname{div}_{\mathcal{S}_t} \mathbf{w}\, d\mathcal{S}_t\, dt$$

$$= \int_0^T \int_{\mathcal{S}_t} \mathbf{w}(x,t) \cdot \nabla\big(\hat{g}(x,t)\, \hat{h}(x,t)\big) + \frac{\partial}{\partial t}\big(\hat{g}(x,t)\, \hat{h}(x,t)\big)$$

$$+ g(x,t)\, h(x,t)\, \operatorname{div}_{\mathcal{S}_t} \mathbf{w}\, d\mathcal{S}_t\, dt$$

$$= \int_0^T \int_{\mathcal{S}_t} \mathbf{w}(x,t) \cdot \nabla\big(\hat{g}(x,t)\, \hat{h}(x,t)\big) + \hat{g}_t(x,t)\, \hat{h}(x,t) + \hat{g}(x,t)\, \hat{h}_t(x,t)$$

$$+ g(x,t)\, h(x,t)\, \operatorname{div}_{\mathcal{S}_t} \mathbf{w}\, d\mathcal{S}_t\, dt,$$

and the above formula for integration by parts in time follows by a simple rearrangement. $\qquad\square$

B Theses

(1) This thesis is devoted to motion planning for the two-phase Stefan problem. The distinguishing feature of the proposed approach is the level set representation of the moving interface separating the fluid phases from the solid phases. In contrast to previous work in this direction which was based on representations of the interface as the graph of a function or on parameterizations, the level set formulation provides significantly more geometric flexibility.

(2) The resulting optimal control problems are solved by the "optimize-then-discretize" approach. This means that the optimality system is devised in a continuous framework. The coupled partial differential equations arising in this system are only discretized afterwards for the numerical solution.

(3) A major contribution of this thesis is the derivation of first-order necessary optimality conditions by the Lagrange formalism using tools from shape calculus. In the absence of control constraints, these conditions consist of the forward system modeling the physical problem, a structurally similar adjoint system, and the gradient equation.

(4) The gradient of the tracking-type cost functional can be computed efficiently on basis of the optimality conditions. Each gradient evaluation comes at the expense of one solution of the forward and the adjoint systems. This readily allows for the implementation of gradient-based optimization methods. The method of steepest descent and the limited memory BFGS (L-BFGS) method are discussed.

(5) In case of the steepest descent method, control constraints of box type are naturally included by applying a projection.

(6) The extended finite element approximation of the temperature in the forward system and the corresponding adjoint variable in the adjoint system constitutes a novel discretization approach in optimal control problems. Thanks to the dynamic local enrichment of

the underlying finite element spaces in the extended finite element method, costly remeshing is completely avoided. Thus, all computations can be carried out on a fixed triangular two-level grid.

(7) While the discretization of the level set method on the triangular grid necessitates only the reformulation of an existing discontinuous Galerkin scheme, the discretization of the corresponding adjoint equation requires the development of a novel solution strategy. The reason is that this adjoint level set equation can be interpreted as a first-order conservation law on the moving interface. Since this equation does not contain a diffusive flux, all available numerical schemes for conservation equations on moving surfaces exhibit stability problems. A narrow band embedding technique and a discontinuous Galerkin discretization are used to circumvent these difficulties.

(8) The implementations of the level set solver and the extended finite element method are tested on several benchmark examples. In all of these test cases, convergence of the implemented methods is observed. The typical order of convergence is linear. In addition, the scheme for the adjoint level set equation is validated on an example with known solution, showing linear convergence as well.

(9) The numerical examples for the motion planning problems highlight the potential of the proposed approach. They demonstrate that, in addition to the standard unidirectional solidification example in which the goal is to move a flat interface in one direction, closed interfaces and changes of topology are handled naturally. This geometric flexibility of the optimal control approach is inherited from the level set method.

(10) The unidirectional solidification example is the motivation for posing a constraint on the position of the interface. This state constraint is treated with the Moreau-Yosida regularization that converts the state constraint into a smooth penalty term which is added to the cost functional. The necessary modifications of the first-order optimality conditions and in the implementation are discussed. The numerical results demonstrate the efficacy of the state constraint.

C   Curriculum Vitæ

Personal Information

Full Name	DI Bernauer, Martin Karl
Date of Birth	January 19, 1981
Place of Birth	Schärding, Austria
Citizenship	Austrian
Marital Status	Married, one child

Education and Studies

- Master degree with distinction from Johannes Kepler University Linz   (2007-01)
- Study of Industrial Mathematics at Johannes Kepler University Linz   (2005-03/2007-01)
- Bachelor degree with distinction from Johannes Kepler University Linz   (2005-02)
- Study of Technical Mathematics at Johannes Kepler University Linz   (2001-10/2005-02)
- Study of Computer Sciences at Johannes Kepler University Linz   (1999-10/2001-06)
- High school in Schärding   (1991-09/1999-06)
- Elementary school in Wernstein am Inn   (1987-09/1991-07)

Community Service

- Upper Austrian Red Cross   (2000-02/2001-01)

Professional Record

- Research assistant in the group *Numerical Mathematics (Partial Differential Equations)* at Chemnitz University of Technology   (2008-08/2010-07)
- Research assistant at the *Johann Radon Institute for Computational and Applied Mathematics* (RICAM) in Linz   (2007-08/2008-07)
- Scientific employee at the *Institute for Design and Control of Mechatronical Systems* at Johannes Kepler University Linz   (2005-05/2007-07)

Teaching Experience

- Tutorial class *"Higher Mathematics I"*
  at Chemnitz University of Technology   (Fall 2009/10)
- Tutorial class *"Numerical Methods for Ordinary Differential Equations"*
  at Chemnitz University of Technology   (Fall 2009/10)
- Tutorial class *"Numerical Mathematics"*
  at Chemnitz University of Technology   (Spring 2009)
- Tutorial class *"Higher Mathematics III: Differential Equations"*
  at Chemnitz University of Technology   (Fall 2008/09)

Presentations

Presentations at Conferences and in Minisymposia

(1) *Optimal Control of the Two-Phase Stefan Problem in Level Set Formulation*, Oberwolfach workshop on "New Directions in Simulation, Control and Analysis for Interfaces and Free Boundaries", January 31–February 6, 2010, Mathematisches Forschungsinstitut Oberwolfach

(2) *XFEM for the Optimal Control of the Two-Phase Stefan Problem*, ECCOMAS thematic event: XFEM 2009, September 28–30, 2009, RWTH Aachen

(3) *Optimal Control of the Two-Phase Stefan Problem: Numerical Approximation Techniques*, The Mathematics of Finite Elements and Applications (MAFELAP) 2009, June 9–12, 2009, Brunel University, West London

(4) *Motion Planning for the Two-Phase Stefan Problem in Level Set Formulation*, Optimization with interfaces and free boundaries, March 23–27, 2009, University of Regensburg

(5) *Towards the Optimal Control of the One-Phase Stefan Problem*, Chemnitz FEM Symposium, September 22–24, 2008, Chemnitz University of Technology

(6) *Towards the Optimal Control of the One-Phase Stefan Problem*, DMV Annual Meeting, September 15–19, 2008, University of Erlangen-Nürnberg

Colloquium and Seminar Talks

(7) *Motion Planning for the Two-Phase Stefan Problem Subject to a State Constraint*, Research Seminar Numerics, July 13, 2010, Chemnitz University of Technology

(8) *Motion Planning for the Two-Phase Stefan Problem in Level Set Formulation*, 16th South-East-German Colloquium on Numerical Mathematics, April 30, 2010, TU Dresden

(9) *Optimal Control of the Classical Two-Phase Stefan Problem in Level Set Formulation*, Chemnitz Seminar on Optimal Control, March 6–13, 2010, Haus im Ennstal

(10) *Optimale Steuerung des klassischen Stefan Problems in zwei Phasen*, Seminar on Applied Mathematics, January 11, 2010, University of Bayreuth

(11) *Optimal Control of the Two-Phase Stefan Problem in Level Set Formulation*, Research Seminar Numerics, November 10, 2009, Chemnitz University of Technology

(12) *Optimal Control of the Two-Phase Stefan Problem Using Extended Finite Elements*, Radon Seminar, September 7, 2009, RICAM, Linz

(13) *Optimal Control of the Two-Phase Stefan Problem: Numerical Approximation Techniques*, Research Seminar Numerics, June 2, 2009, Chemnitz University of Technology

(14) *Motion Planning for the Two-Phase Stefan Problem in Level Set Formulation*, Chemnitz Seminar on Optimal Control, March 7–14, 2009, Gerlosberg

(15) *Techniques for the Optimal Control of the One-Phase Stefan Problem*, Research Seminar Numerics, November 11, 2008, Chemnitz University of Technology

Publications

Publications in Journals

(1) M. K. BERNAUER and R. HERZOG. *Optimal Control of the Classical Two-Phase Stefan Problem in Level Set Formulation.* Submitted to the SIAM Journal on Scientific Computing (SISC), 2010, currently in revision

(2) M. K. BERNAUER and R. GRIESSE. *Implementation of an X-FEM Solver for the Classical Two-Phase Stefan Problem.* Submitted, 2009

(3) M. K. BERNAUER and R. GRIESSE. *A Robustification Approach in Unconstrained Quadratic Optimization.* To appear in Mathematical Programming, Series A. doi:10.1007/s10107-009-0302-9

Conference Proceedings

(4) M. K. BERNAUER, R. HERZOG and K. KUNISCH. *Optimal Control of the Two-Phase Stefan Problem in Level Set Formulation*,

in: New Directions in Simulation, Control and Analysis for Interfaces and Free Boundaries, Oberwolfach Report No. 07/2010, 2010. `doi:10.4171/OWR/2010/07`

Other Publications

(5) *A Robustification Approach in Unconstrained Optimization and Its Applications in Optimal Control*, Master's Thesis supervised by Roland Griesse, RICAM and Johannes Kepler University Linz, 2007

Other Scientific Activities

- 15th South-Eastern German Colloquium on Numerical Mathematics, May 8, 2009, Chemnitz University of Technology
- Workshop: Advances in Shape and Topology Optimization, September 25–27, 2008, Karl-Franzens University Graz
- 4th Austrian Numerical Analysis Day, April 24–25, 2008, RICAM, Linz
- Lipschitz Lecture: "Semi-smooth Newton Methods for Non-differentiable Optimization Problems" by Prof. Karl Kunisch, November 26 – December 12, 2007, Hausdorff Research Institute for Mathematics, Bonn
- Short Course: "Dynamic Optimization in Engineering and Nonlinear Model Predictive Control" by Prof. Moritz Diehl, July 2–7, 2007, Linz

Bibliography

[1] D. Adalsteinsson and J. A. Sethian. A fast level set method for propagating interfaces. *Journal of Computational Physics*, 118(2):269–277, 1995. `doi:10.1006/jcph.1995.1098`. 61, 62

[2] D. Adalsteinsson and J. A. Sethian. Transport and diffusion of material quantities on propagating interfaces via level set methods. *Journal of Computational Physics*, 185(1):271 – 288, 2003. `doi:10.1016/S0021-9991(02)00057-8`. 81

[3] M. R. Albert and K. O'Neill. Moving boundary-moving mesh analysis of phase change using finite elements with transfinite mappings. *International Journal for Numerical Methods in Engineering*, 23(4):591–607, 1986. `doi:10.1002/nme.1620230406`. 52

[4] G. Allaire, F. Jouve, and A.-M. Toader. A level-set method for shape optimization. *Comptes Rendus Mathematique*, 334(12):1125–1130, 2002. `doi:10.1016/S1631-073X(02)02412-3`. 12

[5] R. Almgren. Variational algorithms and pattern formation in dendritic solidification. *Journal of Computational Physics*, 106(2):337–354, 1993. `doi:10.1016/S0021-9991(83)71112-5`. 75

[6] K. Anguige. Multi-phase Stefan problems for a non-linear one-dimensional model of cell-to-cell adhesion and diffusion. *European Journal of Applied Mathematics*, First View:1–28, 2010. `doi:10.1017/S0956792509990167`. 17

[7] N. Arada and J. P. Raymond. Optimal control problems with mixed control-state constraints. *SIAM Journal on Control and Optimization*, 39(5):1391–1407, 2000. `doi:10.1137/S0363012999357926`. 121

[8] A. Ayasoufi and T. Keith. Application of the conservation element and solution element method in numerical modeling of heat conduction with melting and/or freezing. *International Journal of Numerical Methods for Heat & Fluid Flow*, 13:448–472, 2003. `doi:10.1108/09615530310475902`. 77, 78

[9] M. Baines, M. Hubbard, and P. Jimack. A moving mesh finite element algorithm for the adaptive solution of time-dependent partial differential equations with moving boundaries. *Applied Numerical Mathematics*, 54(3-4):450–469, 2005. `doi:10.1016/j.apnum.2004.09.013`. 52

[10] V. Barbu, K. Kunisch, and W. Ring. Control and estimation of the boundary heat transfer function in Stefan problems. *RAIRO Modélisation Mathématique et Analyse Numérique*, 30(6):671–710, 1996. 23

[11] T. Barth and J. A. Sethian. Numerical schemes for the Hamilton-Jacobi and level set equations on triangulated domains. *Journal of Computational Physics*, 145:1–40, 1998. `doi:10.1006/jcph.1998.6007`. 52

[12] G. Beckett, J. A. Mackenzie, A. Ramage, and D. M. Sloan. Computational solution of two-dimensional unsteady pdes using moving mesh methods. *Journal of Computational Physics*, 182(2):478–495, 2002. `doi:10.1006/jcph.2002.7179`. 52

[13] G. Beckett, J. A. Mackenzie, and M. L. Robertson. A moving mesh finite element method for the solution of two-dimensional stefan problems. *Journal of Computational Physics*, 168(2):500–518, 2001. `doi:10.1006/jcph.2001.6721`. 52

[14] M. Bergounioux, K. Ito, and K. Kunisch. Primal-dual strategy for constrained optimal control problems. *SIAM Journal on Control and Optimization*, 37(4):1176–1194, 1999. 28

[15] M. Bergounioux and F. Tröltzsch. Optimal control of semilinear parabolic equations with state-constraints of bottleneck type. *ESAIM: Control, Optimisation and Calculus of Variations*, 4:595–608, 1999. `doi:10.1051/cocv:1999124`. 121

[16] M. A. Borodin. The existence of a classical solution in the multidimensional Stefan problem on a finite time interval. *Akademīya Nauk Ukraïni. Īnstitut Matematiki. Ukraïns′ kiĭ Matematichniĭ Zhurnal*, 44(12):1652–1657, 1992. doi:10.1007/BF01061277. 21

[17] M. A. Borodin. Existence of the global classical solution for a two-phase Stefan problem. *SIAM Journal on Mathematical Analysis*, 30(6):1264–1281 (electronic), 1999. doi:10.1137/S0036141097332530. 21

[18] B. M. Budak and M. Z. Moskal. On the classical solution of the Stefan multidimensional problem. *Soviet Math. Dokl.*, 10:219–222, 1969. 21

[19] M. Burger and S. Osher. A survey on level set methods for inverse problems and optimal design. *European Journal of Applied Mathematics*, 16(2):263–301, 2005. doi:10.1017/S0956792505006182. 12

[20] L. A. Caffarelli. The regularity of free boundaries in higher dimensions. *Acta Math.*, 139:155–184, 1977. doi:10.1007/BF02392236. 21

[21] G. Caginalp. An analysis of a phase field model of a free boundary. *Archive for Rational Mechanics and Analysis*, 92(3):2–245, 1986. doi:10.1007/BF00254827. 19

[22] G. Caginalp and X. Chen. Convergence of the phase field model to its sharp interface limits. *European Journal of Applied Mathematics*, 9(4):417–445, 1998. doi:10.1017/S0956792598003520. 19

[23] J. Caldwell and C.-C. Chan. Numerical solutions of the Stefan problem by the enthalpy method and the heat balance integral method. *Numerical Heat Transfer, Part B: Fundamentals: An International Journal of Computation and Methodology*, 33:99–117, 1998. doi:10.1080/10407799808915025. 52

[24] E. Casas. Control of an elliptic problem with pointwise state constraints. *SIAM Journal on Control and Optimization*, 24(6):1309–1318, 1986. doi:10.1137/0324078. 121

[25] H. Chen, C. Min, and F. Gibou. A numerical scheme for the Stefan problem on adaptive Cartesian grids with supralinear convergence rate. *Journal of Computational Physics*, 228(16):5803 – 5818, 2009. doi:10.1016/j.jcp.2009.04.044. 11, 51, 52, 75, 76, 77

[26] S. Chen, B. Merriman, S. Osher, and P. Smereka. A simple level set method for solving Stefan problems. *Journal of Computational Physics*, 135(1):8–29, 1997. doi:10.1006/jcph.1997.5721. 11, 12, 51, 75

[27] K. Cheng and T. Fries. Higher-order XFEM for curved strong and weak discontinuities. *International Journal for Numerical Methods in Engineering*, 82(5):564–590, 2010. doi:10.1002/nme.2768. 51, 66, 71

[28] T.-F. Cheng. Numerical analysis of nonlinear multiphase Stefan problems. *Computers & Structures*, 75(2):225–233, 2000. doi:10.1016/S0045-7949(99)00071-1. 17

[29] Y. Cheng and C.-W. Shu. A discontinuous Galerkin finite element method for directly solving the Hamilton-Jacobi equations. *Journal of Computational Physics*, 223(1):398–415, 2007. doi:10.1016/j.jcp.2006.09.012. 53, 55, 56, 63

[30] J. Chessa, P. Smolinski, and T. Belytschko. The extended finite element method (XFEM) for solidification problems. *International Journal for Numerical Methods in Engineering*, 53(8):1959–1977, 2002. doi:10.1002/nme.386. 2, 11, 51, 52, 60, 66, 72, 73, 77

[31] D. L. Chopp. Computing minimal surfaces via level set curvature flow. *Journal of Computational Physics*, 106(1):77–91, 1993. doi:10.1006/jcph.1993.1092. 61

[32] A. J. Chorin. Curvature and solidification. *Journal of Computational Physics*, 57(3):472–490, 1985. doi:10.1016/0021-9991(85)90191-3. 52

[33] D. M. Christopher. Comparison of interface-following techniques for numerical analysis of phase-change problems. *Numerical Heat Transfer, Part B: Fundamentals: An International Journal of Computation and Methodology*, 39(2):189–206, 2001. doi:10.1080/10407790150503503. 70

[34] B. Cockburn. Discontinuous Galerkin methods. *ZAMM*, 83(11):731–754, 2003. doi:10.1002/zamm.200310088. 52, 82

[35] M. G. Crandall and P.-L. Lions. Viscosity solutions of Hamilton-Jacobi equations. *Transactions of the American Mathematical Society*, 277(1):1–42, 1983. doi:10.2307/1999343. 14, 15

[36] M. G. Crandall and P.-L. Lions. Two approximations of solutions of Hamilton-Jacobi equations. *Mathematics of Computation*, 43:1–19, 1984. doi:10.2307/2007396. 14, 15

[37] A. B. Crowley. Numerical solution of Stefan problems. Technical report, Brunel University, 1976. Available from: http://bura.brunel.ac.uk/bitstream/2438/1979/1/TR_69.pdf. 52

[38] K. Deckelnick, G. Dziuk, and C. M. Elliott. Computation of geometric partial differential equations and mean curvature flow. *Acta Numerica*, 14:139–232, 2005. doi:10.1017/S0962492904000224. 145

[39] K. Deckelnick, G. Dziuk, C. M. Elliott, and C.-J. Heine. An *h*-narrow band finite-element method for elliptic equations on implicit surfaces. *IMA Journal of Numerical Analysis*, 30(2):351–376, 2010. doi:10.1093/imanum/drn049. 81

[40] M. Delfour and J.-P. Zolésio. *Shapes and Geometries. Analysis, Differential Calculus, and Optimization*. SIAM, Philadelphia, 2001. 136, 139, 140, 142

[41] D. A. Di Pietro, S. Lo Forte, and N. Parolini. Mass preserving finite element implementations of the level set method. *Applied Numerical Mathematics*, 56(9):1179–1195, 2006. doi:10.1016/j.apnum.2006.03.003. 52

[42] J. Dolbow. *An Extended Finite Element Method with Discontinuous Enrichment for Applied Mechanics*. PhD thesis, Northwestern University, 1999. Available from: http://dolbow.cee.duke.edu/phd.html. 66, 72

[43] Q. Du and L. Ju. Finite volume methods on spheres and spherical centroidal Voronoi meshes. *SIAM Journal on Numerical Analysis*, 43(4):1673–1692, 2005. doi:10.1137/S0036142903425410. 81

[44] Q. Du, L. Ju, and L. Tian. Analysis of a mixed finite-volume discretization of fourth-order equations on general surfaces. *IMA Journal of Numerical Analysis*, 29(2):376–403, 2009. doi:10.1093/imanum/drn021. 81

[45] R. Duddu, S. Bordas, D. L. Chopp, and B. Moran. A combined extended finite element and level set method for biofilm growth. *International Journal for Numerical Methods in Engineering*, 2007. doi:10.1002/nme.2200. 17

[46] W. Dunbar, N. Petit, P. Rouchon, and P. Martin. Motion planning for a nonlinear Stefan problem. *ESAIM: Control, Optimisation, and Calculus of Variations*, 9:275–296, 2003. doi:10.1051/cocv:2003013. 23

[47] G. Duvaut. Résolution d'un problème de Stefan (fusion d'un bloc de glace à zéro degré). *C. R. Acad. Sci. Paris Sér. A-B*, 276A:1461–1463, 1973. 19

[48] G. Duvaut. The solution of a two-phase Stefan problem by a variational inequality. In J. R. Ockendon and W. R. Hodgkins, editors, *Moving Boundary Problems in Heat Flow and Diffusion*. Clarendon Press, Oxford, 1975. 20

[49] G. Dziuk and C. M. Elliott. Finite elements on evolving surfaces. *IMA Journal of Numerical Analysis*, 27(2):262–292, 2007. doi:10.1093/imanum/drl023. 81

[50] G. Dziuk and C. M. Elliott. An Eulerian approach to transport and diffusion on evolving implicit surfaces. *Computing and Visualization in Science*, 13(1):17–28, 2008. doi:10.1007/s00791-008-0122-0. 32, 81

[51] C. Eck, H. Garcke, and P. Knabner. *Mathematische Modellierung*. Springer Lehrbuch. Springer-Verlag, Berlin Heidelberg, 2008. 6, 8, 16, 144

[52] C. M. Elliott and A. Gardiner. Double obstacle phase field computations of dendritic growth. Technical Report 1996-19, CMAIA University of Sussex Report, 1996. Available from: http://www.warwick.ac.uk/staff/C.M.Elliott/PAPERS/DoubleObstaclePhaseField/EllGar96.pdf. 52

[53] J. Escher, J. Prüss, and G. Simonett. Analytic solutions for a Stefan problem with Gibbs-Thomson correction. *Journal für die Reine und Angewandte Mathematik*, 563:1–52, 2003. doi:10.1515/crll.2003.082. 21

[54] A. Esen and S. Kutluay. A numerical solution of the Stefan problem with a Neumann-type boundary condition by enthalpy method. *Applied Mathematics and Computation*, 148(2):321–329, 2004. doi:10.1016/S0096-3003(02)00846-9. 52

[55] R. Fosdick and H. Tang. Surface transport in continuum mechanics. *Mathematics and Mechanics of Solids*, 14(6):587–598, 2009. doi:10.1177/1081286507087316. 145

[56] F. Frank. Radially symmetric phase growth controlled by diffusion. *Proceedings of the Royal Society of London. Series A. Mathematical and Physical Sciences*, 201(1067):586–599, 1950. doi:10.1098/rspa.1950.0080. 75

[57] M. Fremond. Variational formulation of the Stefan problem–coupled Stefan problem–frost propagation problem in porous media. In J. T. Oden, E. B. Becker, R. R. Craig, R. S. Dunham, C. P. Johnson, and W. L. Oberkampf, editors, *Computational Methods in Nonlinear Mechanics*, pages 341–349. Texas Institute for Computational Mechanics, Austin, 1974. 19

[58] M. Fried. *Niveauflächen zur Berechnung zweidimensionaler Dendrite*. PhD thesis, Universität Freiburg, 1999. Available from: http://www.mathematik.uni-freiburg.de/IAM/homepages/micha/publications/diss.pdf. 51, 70, 71, 83, 84

[59] A. Friedman. Free boundary problems for parabolic equations. *Bulletin of the American Mathematical Society*, 76:934–941, 1970. doi:10.1090/S0002-9904-1970-12508-3. 17

[60] A. Friedman. Free boundary problems in science and technology. *Notices of the AMS*, 47(8):854–861, 2000. 17

[61] A. Friedman and D. Kinderlehrer. A one-phase Stefan problem. *Ind. Univ. Math.*, 24:1005–1035, 1975. doi:10.1512/iumj.1975.24.24086. 19

[62] T. Fries. A corrected XFEM approximation without problems in blending elements. *International Journal for Numerical Methods in Engineering*, 75(5):503–532, 2008. doi:10.1002/nme.2259. 68

[63] T. Fries and A. Zilian. On time integration in the XFEM. *International Journal for Numerical Methods in Engineering*, 79(1):69–93, 2009. doi:10.1002/nme.2258. 68, 69

[64] P. Frolkovič and K. Mikula. Flux-based level set method: a finite volume method for evolving interfaces. *Applied Numerical Mathematics. An IMACS Journal*, 57:436–454, 2007. doi:10.1016/j.apnum.2006.06.002. 52, 63

[65] T. Fukao, N. Kenmochi, and I. Pawłow. Transmission-Stefan problems arising in Czochralski process of crystal growth. In *Free boundary problems (Trento, 2002)*, volume 147 of *International Series of Numerical Mathematics*, pages 151–165. Birkhäuser, Basel, 2004. 17

[66] F. Gibou and R. Fedkiw. A fourth order accurate discretization for the Laplace and heat equations on arbitrary domains, with applications to the Stefan problem. *Journal of Computational Physics*, 202(2):577–601, 2005. doi:10.1016/j.jcp.2004.07.018. 51, 77

[67] F. Gibou, R. Fedkiw, R. Caflisch, and S. Osher. A level set approach for the numerical simulation of dendritic growth. *Journal of Scientific Computing*, 19(1–3):183–199, 2003. doi:10.1023/A:1025399807998. 11, 51, 75

[68] N. L. Gol'dman. Solving an optimal multiphase Stefan problem. *Computational Mathematics and Modeling*, 2(2):138–148, 1991. doi:10.1007/BF01128924. 17

[69] S. Gottlieb and C.-W. Shu. Total variation diminishing Runge-Kutta schemes. *Mathematics of Computation*, 67(221):73–85, 1998. doi:10.1090/S0025-5718-98-00913-2. 52

[70] S. Gottlieb, C.-W. Shu, and E. Tadmor. Strong stability-preserving high-order time discretization methods. *SIAM Review*, 43(1):89–112, 2001. doi:10.1137/S003614450036757X. 53, 56, 57

[71] S. Groß, V. Reichelt, and A. Reusken. A finite element based level set method for two-phase incompressible flows. *Computing and Visualization in Science*, 9:239–257, 2006. doi:10.1007/s00791-006-0024-y. 12, 71

[72] S. Gupta. *The Classical Stefan Problem. Basic Concepts, Modelling and Analysis*, volume 45 of *Applied Mathematics and Mechanics*. North-Holland, Amsterdam, 2003. 6, 8, 9, 13, 15, 16, 17, 20, 98

[73] M. Heinkenschloss and E. W. Sachs. Numerical solution of a constrained control problem for a phase field model. In *Control and estimation of distributed parameter systems: nonlinear phenomena (Vorau, 1993)*, volume 118 of *International Series of Numerical Mathematics*, pages 171–187. Birkhäuser, Basel, 1994. 24

[74] M. Heinkenschloss and F. Tröltzsch. Analysis of the Lagrange-SQP-Newton method for the control of a phase-field equation. *Control and Cybernetics*, 28:177–211, 1998. 24

[75] J. M. Hill and Y.-H. Wu. On a nonlinear Stefan problem arising in the continuous casting of steel. *Acta Mechanica*, 107(1–4):183–198, 1994. doi:10.1007/BF01201828. 17

[76] M. Hintermüller and K. Kunisch. Path-following methods for a class of constrained minimization problems in function space. *SIAM Journal on Optimization*, 17(1):159–187, 2006. doi:10.1137/040611598. 122

[77] M. Hintermüller and W. Ring. A level set approach for the solution of a state-constrained optimal control problem. *Numerische Mathematik*, 98(1):135–166, 2004. doi:10.1007/s00211-004-0531-z. 12

[78] M. Hinze and K. Kunisch. Second order methods for optimal control of time-dependent fluid flow. *SIAM Journal on Control and Optimization*, 40(3):925–946, 2001. doi:10.1137/S0363012999361810. 45

[79] M. Hinze and S. Ziegenbalg. Optimal control of the free boundary in a two-phase Stefan problem. *Journal of Computational Physics*, 223(2):657–684, 2007. doi:10.1016/j.jcp.2006.09.030. 11, 23, 28, 52, 116

[80] M. Hinze and S. Ziegenbalg. Optimal control of the free boundary in a two-phase Stefan problem with flow driven by convection. *ZAMM*, 87(6):430–448, 2007. doi:10.1002/zamm.200610326. 11, 23

[81] K.-H. Hoffmann and L. S. Jiang. Optimal control of a phase field model for solidification. *Numerical Functional Analysis and Optimization*, 13(1-2):11–27, 1992. doi:10.1080/01630569208816458. 24

[82] K.-H. Hoffmann, M. Niezgódka, and J. Sprekels. Feedback control via thermostats of multidimensional two-phase Stefan problems. *Nonlinear Analysis*, 15(10):955–976, 1990. doi:10.1016/0362-546X(90)90078-U. 22

[83] K.-H. Hoffmann and J. Sprekels. Real-time control of the free boundary in a two-phase Stefan problem. *Numerical Functional Analysis and Optimization*, 5(1):47–76, 1982. doi:10.1080/01630568208816131. 22

[84] R. H. W. Hoppe. A globally convergent multi-grid algorithm for moving boundary problems of two-phase Stefan type. *IMA Journal of Numerical Analysis*, 13(2):235–253, 1993. doi:10.1093/imanum/13.2.235. 52

[85] K. Ito and K. Kunisch. Semi-smooth Newton methods for state-constrained optimal control problems. *Systems and Control Letters*, 50:221–228, 2003. doi:10.1016/S0167-6911(03)00156-7. 121

[86] H. Ji, D. Chopp, and J. Dolbow. A hybrid extended finite element/level set method for modeling phase transformations. *International Journal for Numerical Methods in Engineering*, 54(8):1209–1233, 2002. doi:10.1002/nme.468. 11, 51, 66

[87] H. Ji and J. Dolbow. On strategies for enforcing interfacial constraints and evaluating jump conditions with the extended finite element method. *International Journal for Numerical Methods in Engineering*, 61:2508–2535, 2004. doi:10.1002/nme.1167. 72, 73, 74

[88] S. L. Kamenomostskaja. On Stefan's problem. *Mat. Sb. (N.S.)*, 53 (95):489–514, 1961. 19

[89] S. Kang and N. Zabaras. Control of the freezing interface motion in two-dimensional solidification processes using the adjoint method. *International Journal for Numerical Methods in Engineering*, 38:63–80, 1995. doi:10.1002/nme.1620380105. 22, 23

[90] A. Karma and W.-J. Rappel. Numerical simulation of three-dimensional dendritic growth. *Physical Review Letters*, 77(19):4050–4053, 1996. doi:10.1103/PhysRevLett.77.4050. 52

[91] C. T. Kelley. *Iterative Methods for Optimization*, volume 18 of *Frontiers in Applied Mathematics*. Society for Industrial and Applied Mathematics (SIAM), Philadelphia, PA, 1999. 45, 47, 49

[92] R. Kimmel and J. A. Sethian. Computing geodesic paths on manifolds. *Proceedings of the National Academy of Sciences of the United States of America*, 95(15):8431–8435, 1998. 60

[93] P. Knabner. Control of Stefan problems by means of linear-quadratic defect minimization. *Numerische Mathematik*, 46(3):429–442, 1985. doi:10.1007/BF01389495. 22

[94] R. Kobayashi. Modeling and numerical simulations of dendritic crystal growth. *Physica D: Nonlinear Phenomena*, 63(3–4):410–423, 1993. doi:10.1016/0167-2789(93)90120-P. 52

[95] G. Kossioris, C. Makridakis, and P. Souganidis. Finite volume schemes for Hamilton-Jacobi equations. *Numerische Mathematik*, 83(3):427–442, 1999. doi:10.1007/s002110050457. 52

[96] K. Krumbiegel and A. Rösch. A virtual control concept for state constrained optimal control problems. *Computational Optimization and Applications*, 43(2):213–233, 2009. doi:10.1007/s10589-007-9130-0. 121

[97] E. Kubatko, C. Dawson, and J. Westerink. Time step restrictions for Runge-Kutta discontinuous Galerkin methods on triangular grids. *Journal of Computational Physics*, 227:9697–9710, 2008. doi:10.1016/j.jcp.2008.07.026. 58

[98] K. Kunisch, K. Murphy, and G. Peichl. Estimation of the conductivity in the one-phase Stefan problem: Numerical results. *Mathematical Modelling and Numerical Analysis*, 27(5):613–650, 1993. 22

[99] K. Kunisch, K. Murphy, and G. Peichl. Estimation of the conductivity in the one-phase Stefan problem: Basic results. *Unione Matematica Italiana. Bolletino B. Serie VII*, 9(1):77–103, 1995. 22

[100] W. Kurz and D. Fisher. *Fundamentals of Solidification*. Trans Tech Publications Inc., Stafa-Zurich, fourth edition, 1998. 17

[101] D. Kuzmin. A vertex-based hierarchical slope limiter for *p*-adaptive discontinuous Galerkin methods. *Journal of Computational and Applied Mathematics*, 233(12):3077–3085, 2010. doi:10.1016/j.cam.2009.05.028. 58, 59, 82, 85

[102] G. Lamé and B. Clapeyron. Mémoire sur la solidification par refroidissement d'un globe liquide. *Annales de chimie et de physique*, 47:250–256, 1831. 17

[103] A. Lazaridis. A numerical solution of the multidimensional solidification (or melting) problem. *International Journal of Heat and Mass Transfer*, 13(9):1459–1477, 1970. doi:10.1016/0017-9310(70)90180-8. 77

[104] M. Lenz, S. F. Nemadjieu, and M. Rumpf. Finite volume method on moving surfaces. Technical report, Institute for Numerical Simulation, University of Bonn, 2008. Available from: http://numod.ins.uni-bonn.de/research/papers/public/LeNeRu08.pdf. 81

[105] R. J. LeVeque. High-resolution conservative algorithms for advection in incompressible flow. *SIAM Journal on Numerical Analysis*, 33:627–665, 1996. doi:10.1137/0733033. 63

[106] R. J. LeVeque. *Finite volume methods for hyperbolic problems*. Cambridge Texts in Applied Mathematics. Cambridge University Press, Cambridge, 2002. 52

[107] J. L. Lions. *Optimal Control of Systems Governed by Partial Differential Equations*. Springer, New York, 1971. 27

[108] E. Marchandise, J.-F. Remacle, and N. Chevaugeon. A quadrature-free discontinuous Galerkin method for the level set equation. *Journal of Computational Physics*, 212(1):338–357, 2006. doi:10.1016/j.jcp.2005.07.006. 52

[109] A. M. Meïrmanov. *The Stefan Problem*. de Gruyter, Berlin, 1992. 21

[110] R. Merle and J. Dolbow. Solving thermal and phase change problems with the eXtended finite element method. *Computational Mechanics*, 28:339–350, 2002. doi:10.1007/s00466-002-0298-y. 66

[111] C. Meyer, U. Prüfert, and F. Tröltzsch. On two numerical methods for state-constrained elliptic control problems. *Optimization Methods and Software*, 22(6):871–899, 2007. doi:10.1080/10556780701337929. 121

[112] C. Meyer, A. Rösch, and F. Tröltzsch. Optimal control of PDEs with regularized pointwise state constraints. *Computational Optimization and Applications*, 33(2–3):209–228, 2005. doi:10.1007/s10589-005-3056-1. 121

[113] L. V. Miegroet and P. Duysinx. Stress concentration minimization of 2D filets using X-FEM and level set description. *Structural and Multidisciplinary Optimization*, 33(4-5):425–438, 2007. doi:10.1007/s00158-006-0091-1. 51

[114] L. V. Miegroet and P. Duysinx. 3D shape optimization with X-FEM and a level set constructive geometry approach. In T.-P. Fries and A. Zilian, editors, *Proceedings of the International Conference on Extended Finite Element Methods - Recent Developments and Applications*, pages 225–228. RWTH Aachen University, 2009. 51

[115] N. Moës, J. Dolbow, and T. Belytschko. A finite element method for crack growth without remeshing. *International Journal for Numerical Methods in Engineering*, 46:131–150, 1999. doi:10.1002/(SICI)1097-0207(19990910)46:1<131:: AID-NME726>3.0.CO;2-J. 72

[116] W. Mulder, S. Osher, and J. A. Sethian. Computing interface motion in compressible gas dynamics. *Journal of Computational Physics*, 100(2):209–228, 1992. doi:10.1016/0021-9991(92)90229-R. 12

[117] R. Müller. *Numerische Simulation dendritischen Kristallwachstums*. PhD thesis, Otto-von-Guericke-Universität Magdeburg, 2005. Available from: http://diglib.uni-magdeburg.de/Dissertationen/2005/ruemueller.pdf. 51, 70

[118] D. Mumford and J. Shah. Optimal approximations by piecewise smooth functions and associated variational problems. *Communications on Pure and Applied Mathematics*, 42(5):577–685, 1989. doi:10.1002/cpa.3160420503. 32

[119] P. Neittaanmäki. On the optimal cooling of the steel during continuous casting. In *System Modelling and Optimization*, volume 84 of *Lecture Notes in Control and Information Sciences*, pages 637–646. Springer, Berlin/Heidelberg, 1986. doi:10.1007/BFb0043889. 17

[120] P. Neittaanmäki, J. Sprekels, and D. Tiba. *Optimization of Elliptic Systems*. Springer, New York, 2006. 27

[121] P. Neittaanmäki and D. Tiba. On the finite element approximation of the boundary control for two-phase Stefan problems. In *Analysis and Optimization of Systems, Part 1 (Nice, 1984)*, volume 62 of *Lecture Notes in Computational Science and Engineering*, pages 356–370. Springer, Berlin, 1984. doi:10.1007/BFb0004966. 25

[122] P. Neittaanmäki and D. Tiba. On the approximation of the boundary control in two-phase Stefan problems. *Control and Cybernetics*, 16(3–4):33–44, 1987. 25

[123] P. Neittaanmäki and D. Tiba. A steepest descent method for the approximation of the boundary control in two-phase Stefan problem. *Mathematica–Revue d'Analyse Numérique et the Théorie de l'Approximation*, 29(2):157–167, 1987. 25

[124] P. Neittaanmäki and D. Tiba. Optimal control for state constrained two-phase Stefan problems. In *Numerical Methods for Free Boundary Problems (Jyväskylä 1990)*, volume 99 of *Internationale Schriftenreihe Numerische Mathematik*, pages 309–316. Birkhäuser, Basel, 1991. 25

[125] M. Niezgódka and I. Pawłow. Optimal control for parabolic systems with free boundaries. Existence of optimal controls, approximation results. In *Optimization Techniques (Proceedings of the Ninth IFIP Conference, Warsaw, 1979), Part 1*, volume 22 of *Lecture Notes in Computational Science and Engineering*, pages 412–420. Springer, Berlin, 1980. doi:10.1007/BFb0036420. 22

[126] M. Niezgódka and I. Pawłow. A generalized Stefan problem in several space variables. *Applied Mathematics and Optimization*, 9(3):193–224, 1982/83. doi: 10.1007/BF01460125. 20, 22

[127] J. Nocedal and S. Wright. *Numerical Optimization*. Springer, New York, second edition, 2006. 45, 46, 47, 48

[128] R. H. Nochetto, A. Schmidt, and C. Verdi. Adapting meshes and time-steps for phase change problems. *Atti della Accademia Nazionale dei Lincei. Classe di Scienze Fisiche, Matematiche e Naturali. Rendiconti Lincei. Serie IX. Matematica e Applicazioni*, 8(4):273–292, 1997. 52

[129] O. A. Oleĭnik. A method of solution of the general Stefan problem. *Soviet Mathematics. Doklady*, 1:1350–1354, 1960. 18

[130] S. Osher and R. Fedkiw. *Level Set Methods and Dynamic Implicit Surfaces*, volume 153 of *Applied Mathematical Sciences*. Springer, Berlin, 2003. 12, 32

[131] S. Osher and J. A. Sethian. Fronts propagating with curvature-dependent speed. *Journal of Computational Physics*, 79:12–49, 1988. doi:10.1016/0021-9991(88)90002-2. 12

[132] S. Osher and C.-W. Shu. High-order essentially nonoscillatory schemes for Hamilton-Jacobi equations. *SIAM Journal on Numerical Analysis*, 28(4):907–922, 1991. doi:10.1137/0728049. 52

[133] I. Pawłow. A variational inequality approach to generalized two-phase Stefan problem in several space variables. *Annali di Matematica Pura ed Applicata. Serie Quarta*, 131:333–373, 1982. doi:10.1007/BF01765160. 20

[134] I. Pawłow. Optimal control of two-phase Stefan problems—numerical solutions. In *Optimal Control of Partial Differential Equations, II (Oberwolfach, 1986)*, volume 78 of *Internationale Schriftenreihe Numerische Mathematik*, pages 179–206. Birkhäuser, Basel, 1987. 22

[135] D. Peng, B. Merriman, H. Zhao, S. Osher, and M. Kang. A PDE-based fast local level set method. *Journal of Computational Physics*, 155:410–438, 1999. doi:10.1006/jcph.1999.6345. 61, 64

[136] O. Pironneau. *Optimal Shape Design for Elliptic Systems*. Springer, New York, 1984. 136

[137] B. Protas and W. Liao. Adjoint-based optimization of PDEs in moving domains. *Journal of Computational Physics*, 227:2707–2723, 2008. doi:10.1016/j.jcp.2007.11.014. 23

[138] J. Prüss, J. Saal, and G. Simonett. Existence of analytic solutions for the classical Stefan problem. *Mathematische Annalen*, 338(3):703–755, 2007. doi:10.1007/s00208-007-0094-2. 21

[139] S. Repke, N. Marheineke, and R. Pinnau. On adjoint-based optimization of a free surface Stokes flow. Technical Report 186(2010), Fraunhofer-Institut für Techno-und Wirtschaftsmathematik, 2010. 23

[140] J.-F. Rodrigues and F. H. Yi. On a two-phase continuous casting Stefan problem with nonlinear flux. *European Journal of Applied Mathematics*, 1(3):259–278, 1990. doi:10.1017/S0956792500000218. 17

[141] T. Roubíček and C. Verdi. A stable approximation of a constrained optimal control for continuous casting. *Numerical Functional Analysis and Optimization. An International Journal*, 13(5-6):487–494, 1992. doi:10.1080/01630569208816494. 24

[142] T. Roubíček. Optimal control of a Stefan problem with state-space constraints. *Numerische Mathematik*, 50(6):723–744, 1987. doi:10.1007/BF01398381. 24

[143] L. Rubinstein. The Stefan problem: Comments on its present state. *Journal of the Institute of Mathematics and its Applications*, 24(3):259–277, 1979. doi:10.1093/imamat/24.3.259. 21

[144] A. Schiela. Convergence of the control reduced interior point method for pde constrained optimal control with state constraints. Technical Report 06–16, Zuse Institute Berlin, 2006. Available from: http://opus.kobv.de/zib/volltexte/2006/910/pdf/ZR-06-16.pdf. 121

[145] A. Schiela. Barrier methods for optimal control problems with state constraints. *SIAM Journal on Optimization*, 20(2):1002–1031, 2009. `doi:10.1137/070692789`. 121

[146] A. Schmidt. *Die Berechnung dreidimensionaler Dendriten mit Finiten Elementen*. PhD thesis, Universität Freiburg, 1993. `http://www.mathematik.uni-freiburg.de/IAM/homepages/alfred/paper_diss.html`. 11, 51, 52

[147] J. A. Sethian. *Level Set Methods and Fast Marching Methods*, volume 3 of *Cambridge Monographs on Applied and Computational Mathematics*. Cambridge University Press, second edition, 1999. 12

[148] J. A. Sethian and J. Strain. Crystal growth and dendritic solidification. *Journal of Computational Physics*, 98(2):231–253, 1992. `doi:10.1016/0021-9991(92)90140-T`. 51

[149] J. A. Sethian and A. Vladimirsky. Fast methods for the eikonal and related Hamilton-Jacobi equations on unstructured meshes. *Proceedings of the National Academy of Sciences of the United States of America*, 97:5699–5703, 2000. `doi:10.1073/pnas.090060097`. 64

[150] C.-W. Shu and S. Osher. Efficient implementation of essentially nonoscillatory shock-capturing schemes. *Journal of Computational Physics*, 77(2):439–471, 1988. `doi:10.1016/0021-9991(88)90177-5`. 57

[151] J. Sokołowski and J.-P. Zolésio. *Introduction to Shape Optimization*. Springer, New York, 1992. 136, 137, 138, 139, 140, 142, 143

[152] R. J. Spiteri and S. J. Ruuth. A new class of optimal high-order strong-stability-preserving time discretization methods. *SIAM Journal on Numerical Analysis*, 40(2):469–491 (electronic), 2002. `doi:10.1137/S0036142901389025`. 57, 58

[153] J. Stefan. Über die Theorie der Eisbildung, insbesondere über die Eisbildung im Polarmeere. *Annalen der Physik*, 278(2):965–983, 1891. `doi:10.1002/andp.18912780206`. 16, 17

[154] J. M. Sullivan Jr., D. R. Lynch, and K. O'Neill. Finite element simulation of planar instabilities during solidification of an undercooled melt. *Journal of Computational Physics*, 69(1):81–111, 1987. `doi:10.1016/0021-9991(87)90157-4`. 52

[155] D. Tarzia. A bibliography on moving-free boundary problems for the heat-diffusion equation. the Stefan and related problems. *MAT. Serie A: Conferencias, Seminarios y Trabajos de Mathemática*, 2, 2000. 17

[156] D. Tiba and M. Tiba. Approximation for control problems with pointwise state constraints. In *Control and estimation of distributed parameter systems (Vorau, 1988)*, volume 91 of *International Series of Numerical Mathematics*, pages 379–390. Birkhäuser, Basel, 1989. 25

[157] F. Tröltzsch. *Optimale Steuerung partieller Differentialgleichungen*. Vieweg, Wiesbaden, 2005. 27, 28

[158] Y.-H. Tsai and S. Osher. Total variation and level set methods in image science. *Acta Numerica*, 14:509–573, 2005. `doi:10.1017/S0962492904000273`. 12

[159] A. Voigt and K.-H. Hoffmann. Control of Czochralski crystal growth. In *Optimal control of complex structures (Oberwolfach, 2000)*, volume 139 of *International Series of Numerical Mathematics*, pages 259–265. Birkhäuser, Basel, 2002. 17

[160] A. Voigt, C. Weichmann, and K.-H. Hoffmann. Multiscale simulation of industrial crystal growth. In A. H. et al., editor, *ALGORITMY 2002*, Proceedings of ALGORITMY, pages 1–13, 2002. 17

[161] O. Volkov, B. Protas, W. Liao, and D. Glander. Adjoint-based optimization of thermo-fluid phenomena in welding processes. *Journal of Engineering Mathematics*, 65(3):201–220, 2009. `doi:10.1007/s10665-009-9292-0`. 17, 24

[162] V. R. Voller, C. R. Swaminathan, and B. G. Thomas. Fixed grid techniques for phase change problems: A review. *International Journal for Numerical Methods in Engineering*, 30:875–898, 1990. `doi:10.1002/nme.1620300419`. 52

[163] P. Wei, M. Y. Wang, and X. Xing. A study on X-FEM in continuum structural optimization using a level set model. *Computer-Aided Design*, In Press, Corrected Proof:–, 2009. `doi:10.1016/j.cad.2009.12.001`. 51

[164] D. G. Wilson. Lagrangian coordinates for moving boundary problems. *SIAM Journal on Applied Mathematics*, 42(6):1195–1201, 1982. doi:10.1137/0142083. 17

[165] J.-J. Xu and H.-K. Zhao. An Eulerian formulation for solving partial differential equations along a moving interface. *Journal of Scientific Computing*, 19(1-3):573–594, 2003. doi:10.1023/A:1025336916176. 81

[166] J. Yan and S. Osher. A new discontinuous Galerkin method for Hamilton-Jacobi equations. Technical Report 10-08, UCLA Computational and Applied Mathematics, 2010. Available from: ftp://ftp.math.ucla.edu/pub/camreport/cam10-08.pdf. 53, 134

[167] Z. Yang. *The Adjoint Method for the Inverse Design of Solidification Processes with Convection*. PhD thesis, Cornell University, 1997. Available from: http://mpdc.mae.cornell.edu/Publications/PDFiles/THESES/Yang.pdf. 22, 116

[168] N. Zabaras, B. Ganapathysubramanian, and L. Tan. Modelling dendritic solidification with melt convection using the extended finite element method. *Journal of Computational Physics*, 218:200–227, 2006. doi:10.1016/j.jcp.2006.02.002. 11, 51, 52, 66, 72, 73, 77, 133

[169] N. Zabaras, Y. Ruan, and O. Richmond. Design of two-dimensional Stefan processes with desired front motions. *Numerical Heat Transfer, Part B*, 21:307–325, 1992. doi:10.1080/10407799208944907. 22

[170] Y.-T. Zhang and C.-W. Shu. High-order WENO schemes for Hamilton-Jacobi equations on triangular meshes. *SIAM Journal on Scientific Computing*, 24(3):1005–1030, 2002. doi:10.1137/S1064827501396798. 52

[171] H.-K. Zhao, T. Chan, B. Merriman, and S. Osher. A variational level set approach to multiphase motion. *Journal of Computational Physics*, 127(1):179–195, 1996. doi:10.1006/jcph.1996.0167. 60

[172] S. Ziegenbalg. *Kontrolle freier Ränder bei der Erstarrung von Kristallschmelzen*. PhD thesis, Technische Universität Dresden, 2008. Available from: http://www.qucosa.de/fileadmin/data/qucosa/documents/248/1212521184972-5583.pdf. 23

Nomenclature

Constants

ρ	density	$\left[kg/m^3\right]$
y_M	equilibrium temperature at $\Gamma_I(t)$	$[K]$
$c_{S/F}$	heat capacity in the solid/fluid phase	$[J/(kg\,K)]$
$k_{S/F}$	heat conductivity in the solid/fluid phase	$[J/(m\,s\,K)]$
L	latent heat per unit mass	$[J/kg]$
ϵ_κ	regularization parameter for the discrete curvature	
γ	penalty parameter in the Moreau-Yosida regularization	
μ	penalty parameter for interface conditions in the X-FEM	
τ^σ	tolerance for the step length in the Armijo rule	
τ_a^u, τ_r^u	absolute and relative tolerance on the control	
τ_a^∇, τ_r^∇	absolute and relative tolerance on the gradient	
$\gamma_1,\,\ldots,\,\gamma_5$	weights in the cost functional J	

Domains

D	hold-all, $D = \Omega_S(t) \cup \Omega_F(t)$
∂D	boundary of D
$\Omega_F(t)$	fluid phase
$\Omega_S(t)$	solid phase
Γ_C	the controled part of ∂D, $\Gamma_C = \Gamma_C^S \cup \Gamma_C^F$
Γ_C^F	boundary of $\Omega_F(t)$ on which the control u is active
Γ_C^S	boundary of $\Omega_S(t)$ on which the control u is active
Γ_N	the uncontroled part of ∂D, $\Gamma_N = \Gamma_N^S(t) \cup \Gamma_N^F(t)$
$\Gamma_N^F(t)$	boundary of $\Omega_F(t)$ on which a prescribed heat flux is active
$\Gamma_N^S(t)$	boundary of $\Omega_S(t)$ on which a prescribed heat flux is active
$\Gamma_I(t)$	moving interface
NB	narrow band

Functionals

J	cost functional
$\widehat{J}$	reduced cost functional
$\mathcal{L}$	Lagrange functional

$\mathcal{P}_{[a,b]}(\cdot)$	projection to the interval $[a,b]$
$D[\![g;\,\delta g]\!]$	variation of the functional g in direction δg
$\mathcal{V}(\gamma)$	measure of the constraint violation in dependence on the Moreau-Yosida penalty parameter
E	enthalpy
$\mathcal{F}$	Ginzberg-Landau free energy
H	Hamiltonian
$[g]_F^S$	jump of the quantity g across $\Gamma_I(t)$ from fluid to solid
$\mathfrak{K}$	Kirchhoff transformation

Differential Operators

div, $\nabla\cdot$	divergence
∇	gradient
Δ	Laplace operator

Sets

$\mathcal{T}$	triangulation
$\mathrm{BUC}(\Omega)$	set of bounded and uniformly continuous functions on Ω
$C^k(\Omega)$	set of k times continuously differentiable functions on Ω
$P^k(\Omega)$	set of all polynomials of degree k on Ω
$\mathcal{U}$	control space
$\mathcal{U}_{\mathrm{ad}}$	set of admissible controls, $\mathcal{U}_{\mathrm{ad}} \subset \mathcal{U}$
$\mathcal{Y}$	state space
$\mathbb{R}$	the real numbers

Variables

ψ	adjoint level set function
p	adjoint temperature (the adjoint state variable in Section 3.1)
u	control (the control variable in Section 3.1) $\left[J/(s\,m^2)\right]$,
ϕ	level set function
y	temperature (the state variable in Section 3.1) $[K]$
δu	direction of variation of the control u
$\delta\phi$	direction of variation of the level set function ϕ
δy	direction of variation of the temperature y
$\mathbf{v}$	velocity in the modeling of the heat equation
$\vec{V}$	velocity with which $\Gamma_I(t)$ moves
κ	curvature of $\Gamma_I(t)$
n	outward unit normal vector
$n_{S/F}$	outward unit normal vector to the solid/fluid phase

x_1, x_2	coordinates
T	terminal time
Δt^j	time step for the heat equation and its adjoint
$\Delta t^j_{\mathrm{CFL}}$	time step for the level set equation and its adjoint
$\mathbf{M}$	mass matrix for the temperature equation and its adjoint
$\mathcal{M}$	mass matrix for the level set equation and its adjoint
$\mathbf{Q}$	penalty matrix for the interface condition in the forward problem
$\mathbf{K}$	stiffness matrix for the temperature equation and its adjoint
$\mathcal{K}$	system matrix for the level set equation and its adjoint

Index